THIOREDOXIN IN NEUTROPHIL INFLAMMATION AND GROWTH OF NEOPLASTIC CELLS *IN VIVO*

By

Benjamin Korte

A dissertation submitted in partial fulfillment

of the requirements for the degree of

Doctor of Philosophy

(Cancer Biology)

at the

UNIVERSITY OF WISCONSIN – MADISON

2021

Date of final oral examination: 4/20/2021

The dissertation is approved by the following members of the Final Oral Committee:

William Sugden, Professor, Oncology
Paul Lambert, Professor, Oncology
JD Sauer, Associate Professor, Medical Microbiology and Immunology
Peter Lewis, Associate Professor, Biomolecular Chemistry
Anna Huttenlocher, Professor, Pediatrics and Medical Microbiology and Immunology

Table of Contents

Acknowledgements

The page that follows is woefully inadequate at expressing the depth of my gratitude for everyone who's helped me through the last five and half years – alas, I'll do my best. Firstly, I want to thank my wonderful Huttenlocher lab family who have kept me (mostly) sane through the trials and tribulations of grad school. To my postdoc mentors, Sofia and Emily, your help and guidance was invaluable in shaping my projects and trajectory as a scientist. To my officemates Youtao, Morgan, and Taylor, you made coming into lab fun and hilarious every day – I don't know what I would have done without you. To my mentor Anna, I grew tremendously from your advice and direction and you've taught me how to be a better scientist.

Secondly, I have my wonderful, supportive friends to thank for giving balance to my life. To my "nerd" friends Keith, Kaylin, Alex, Ani, Marissa, Isaac, Stef, and Vin, thank you for making my Dungeons and Dragons fantasies a reality. To Megan and Spencer, thanks for all the meals and Murphy slobber and paddle trips on beautiful lakes. And to Taner, my kindred German friend, your patient listening and all-around compassion are the best gifts a friend could ask for.

Lastly, but certainly not least, my wonderful family has always been there to offer encouragement and support. Lydia and Cole, my favorite and only siblings, thank you for giving me nothing but love. To my cousin and de facto brother, Matt, thank you for supporting me even when we both knew I was in the wrong. To my Dad, I've learned from all your wisdom and perspective – you've helped me see the spiritual side of life, and the peace that's always around me. And to my Mom, thank you for always encouraging my interest in science, for all your questions about the health of my "glowy fish", and your perpetual and unconditional love.

I love you all more than I can say.

Abstract

Neutrophils are motile in the tumor microenvironment and regulate tumor progression from the onset of transformation. However, the mechanisms that regulate neutrophil motility during tumor initiation remain largely unknown. To investigate cues that modulate neutrophil dynamics near $KRas^{G12V}$-transformed keratinocytes, we conducted tissue-specific RNA sequencing of transformed keratinocytes in zebrafish larvae. We found the antioxidant, thioredoxin (*txn*), a small thiol that regulates reduction-oxidation (redox) balance, is upregulated in transformed cells. We generated a thioredoxin mutant and observed increased neutrophil recruitment and retention around transformed cells in *txn* null larvae. Additionally, in the $txn^{-/-}$ background we observed a neutrophil-dependent increase in proliferation of transformed cells. Injection of *txn*-sufficient melanoma cells into the hindbrain ventricle of *txn* wildtype and mutant larvae did not recapitulate results from *txn*-null transformed cell experiments, suggesting transformed-cell *txn* drives neutrophil and proliferative changes. Taken together, our findings indicate thioredoxin is a tumor suppressor during early tumor initiation acting to inhibit neutrophil recruitment and retention and thereby limit neutrophil-mediated proliferation.

Chapter One

Introduction

Inflammation: a Hallmark of Cancer

Inflammation, in the broadest sense, is the attempt by an organism to clear damaged tissues of microbes and then to promote wound healing. It engages many defense mechanisms including recruitment of phagocytic cells from the vasculature to clear bacteria and fungi, vascular leakage to allow complement and antibody diffusion into tissues, and stimulation of powerful adaptive responses if infection persists [1, 2]. More recently, inflammation has been associated with many forms of cancer [3] and it is now readily accepted to be a driving force in tumorigenesis and as such, a Hallmark of Cancer [4, 5].

Correlations between inflammation and cancer

The link between cancer and inflammation was first hypothesized by the physician Rudolf Virchow in 1863 [6]. He observed substantial leukocyte infiltration into tumors and first postulated tumors to be inherently inflammatory. Since then, the body of literature supporting this link has expanded significantly. Many studies indicate inflammation often precedes cancer onset. Chronic infection with *Helicobacter pylori* in the gut, HBV or HCV virus in the liver, or commensal *Bacteroides spp.* in the colon are associated with gastric cancer, hepatocellular carcinoma (HCC), and colon cancer, respectively [7-9]. Inflammatory bowel disease (IBD) is similarly associated with increased colorectal cancer risk [10]. Irritants such as tobacco smoke, asbestos, and silica particles cause inflammation in the lung and are each risk factors for lung cancer development [11, 12]. Additionally, obesity is reported to increase basal inflammation and risk of HCC [13].

Anti-inflammatory drugs in cancer prevention

In addition to the correlation between inflammation and cancer, many reports indicate that inhibiting inflammatory signaling often decreases cancer risk or recurrence. Epidemiologic studies have demonstrated that regular aspirin use decreases risk of colorectal, esophageal, prostate, breast, and gastric cancer [14-18]. Interestingly, aspirin use was not correlated with risk of lung cancer development in men [19]. The primary molecular targets of aspirin are cyclooxygenase enzymes, COX-1 and COX-2, responsible for producing the inflammatory precursor lipid prostaglandin H_2 (PGH_2) from arachidonic acid [20]. Two controlled studies on the effects of aspirin in preventing recurrence in colorectal cancer patients found aspirin use decreased frequency of adenoma formation and increased time to adenoma recurrence [21, 22].

Tumors are similar to unhealed wounds

In the context of a wound, inflammation proceeds in a series of orchestrated steps to first eliminate potentially infectious agents and then promote tissue repair [1, 2]. This process, particularly the wound-healing effects of inflammation, are found in cancer as well and led to the proposal that tumors behave like unhealed wounds [23]. The foundation for this hypothesis was based on the finding that tumors and wounds both stimulate vascular permeability via vascular endothelial growth factor (VEGF) [24]. VEGF was shown to stimulate coating of tumor cells with the clotting factor, fibrin, further supporting the similarity between wounds and cancer [25].

More recently, infiltrating innate immune cells including neutrophils and macrophages have been implicated in both processes [26]. Neutrophils and macrophages are cellular responders to injury and function to clear the wounded site of microbes via phagocytosis, secretion of cytotoxic molecules, and induction of an adaptive response [27]. Recent studies have determined that neutrophils play a role in wound healing though a number of mechanisms including secretion of growth factors and removal of damaged cellular debris through phagocytosis [28, 29]. Macrophages also support wound healing via phagocytosis of apoptotic cells which stimulates the production of VEGF and the anti-inflammatory cytokine, IL-10 [30, 31]. Macrophages help remodel the extracellular matrix (ECM), an important phase in wound healing, via matrix metalloproteinase degradation of collagen [32]. Notably, both neutrophils and macrophages are found in the tumor microenvironment (discussed below) where they appear to adopt the pro-resolution phenotypes observed at wounds.

Immune cells in the tumor microenvironment: a causal link

Until recently, the association between cancer and inflammation has been correlative. In the last 20 years, extensive studies have been conducted on the role immune cells play in cancer development [3, 4]. The overwhelming consensus is that infiltrating immune cells are powerful, contributing factors to tumorigenesis, with both pro- and anti-tumor functions described for many of the cell types present [33-35]. These tumor-infiltrating leukocytes, most notably CD8+ T cells, have been used to combat tumor growth through checkpoint blockade and tumor-targeting chimeric antigen receptor (CAR) expression [36, 37]. While lymphocytes (B cells, T cells, NK cells) and other innate immune cell types (dendritic cells and mast cells) are

important in regulating tumor growth, the summary that follows is concerned with the functions of two myeloid cells: macrophages and neutrophils.

Tumor-associated macrophages (TAMs)

Macrophages, as stated above, are a common component of the tumor microenvironment [38]. Their presence has been associated with poor prognosis of several cancers such as Hodgkin's lymphoma and pancreatic cancer [39, 40]. Within the tumor microenvironment, macrophages seem to polarize toward one of two defined states: M1 which are classified as pro-inflammatory and induced by TLR stimulation and IFN-γ, and M2 which are deemed "alternatively activated" and induced by Il-4, IL-10, and IL-13 [41]. M1 polarized macrophages produce high levels of pro-inflammatory cytokines IL-1β, TNFα, and IL-6; increase production of reactive oxygen species (ROS); and generally are associated with tumoricidal and bactericidal functions [42]. M2 polarized macrophages produce IL-4, IL-10, and IL-13 and are most commonly associated with tissue repair and supporting cancer progression [42, 43]. Due to their role in promoting tumor growth, M2-polarized macrophages are the most common subtype found in tumors [44].

Functionally, M2 TAMs support a number of processes that promote tumor growth. In a mouse mammary tumor model, macrophages were shown to promote the angiogenic switch, in which blood density dramatically increases within the tumor [45]. Macrophages likely induce vessel growth by secreting a number of angiogenic factors including VEGF, TNFα, MMP9, and IL-1β [46]. Additionally, macrophages can support tumor growth by stimulating EGFR-signaling in tumor cells [47]. CSF-1, a macrophage-targeted cytokine and growth factor, was shown to

induce macrophage-dependent tumor cell invasion into a collagen matrix [48]. Finally, macrophages can inhibit adaptive mechanisms that would otherwise participate in tumor cell killing. T cell killing in a mouse 4T1 mammary cancer model was inhibited by macrophage-derived CCL2 [49]. In human patients with ovarian cancer, macrophage-derived IL-10 was shown to inhibit T cell proliferation [50]. Together, these reports indicate macrophages play an important role in promoting tumor progression.

Tumor-associated neutrophils (TANs)

As mentioned above, neutrophils are a common immune cell infiltrate observed in the tumor microenvironment [51, 52]. Many epidemiologic studies have correlated high intratumoral neutrophil burden with poor prognosis. This association has been demonstrated for renal cell carcinoma, hepatocellular carcinoma, head and neck cancer, and melanoma [53, 54]. Similar to macrophages, neutrophils display phenotypic plasticity and exist in several polarization states. Fridlender *et al.* demonstrated differential neutrophil polarization in cancer describing N1 and N2 neutrophils as anti- and pro-tumor, respectively [55]. Polarization toward the tumor-promoting N2 phenotype was shown to be driven by TGF-β, as TGF-β inhibition lead to N1-dependent tumor size reduction. While pro- and anti-tumor neutrophils have been well documented, TANs appear to primarily assume the N2 phenotype when present in the tumor microenvironment.

<u>Anti-tumor neutrophil functions</u>

Anti-tumor neutrophil functions were first described in 1972 as having cytotoxic effects *in vitro* and *in vivo* on rat ascites-derived tumors [56]. Since then, neutrophil-mediated tumor

cell killing has been documented in a number of studies. Neutrophils co-cultured with bladder carcinoma or melanoma cells induced tumor cell death in a protease-independent manner [57]. One interesting study observed that intraperitoneal injection of gastric cancer patients with *Streptococcus pyogenes* induced neutrophil recruitment and adenocarcinoma clearance [58]. Patient-derived neutrophils were subsequently shown to inhibit gastric tumor growth *in vitro*. Additionally, neutrophils express several F_c receptors and can therefore respond to antibody-coated pathogens and cells. Indeed, neutrophil cytotoxicity is reportedly increased with anti-tumor Ab application [59]. A recent study found neutrophils mediate antibody-dependent cellular cytotoxicity (ADCC) of antibody-opsonized breast cancer cells by mechanically damaging tumor cell plasma membranes [60].

Neutrophils also have the capacity to promote anti-tumor immune function, most notably killing by CD8+ T cells. N1-polarized neutrophils release pro-inflammatory cytokines including IL-12, TNFα, and GM-CSF to recruit M1 macrophages and CCL3, CXCL9, and CXCL10, potent T cell chemoattractants [61]. IL-2 expression in mouse mammary carcinoma cells prompted neutrophil infiltration and subsequent tumor rejection, though these studies were primarily correlative [62]. Neutrophils have also been shown to cross-present antigen to CD8+ T cells, thus stimulating their activation [63]. This study demonstrated prolonged presentation of ovalbumin fragments on neutrophil MHCI molecules after intraperitoneal ovalbumin injection. However, the ramifications of cross-presentation on neutrophil-mediated tumor clearance have yet to be determined.

Pro-tumor neutrophil functions

N2 TANs promote tumor growth by a number of mechanisms, the most well-studied being angiogenesis and invasion. Neutrophils produce high levels of MMP9, a metalloproteinase that can degrade components of the ECM and thus release sequestered VEGF [64]. VEGF association with its receptor was shown to be neutrophil-dependent [65]. This study goes on to demonstrate neutrophil-depletion prevents angiogenesis, and a similar study observed neutrophil-depletion dramatically reduced tumor growth in mice [66]. Neutrophil-derived MMP9, in addition to promoting angiogenesis, can stimulate tumor cell migration and invasion [67]. Hepatocyte growth factor (HGF) derived from neutrophils similarly induces bronchioloalveolar carcinoma migration *in vitro* [68]. Macrophage-derived migration inhibitory factor (MIF) also induced a neutrophil-dependent increase in head and neck cancer migration [69]. Neutrophil-mediated tumor migration may be contact dependent, as the intercellular adhesion molecule (ICAM-1) was shown to be necessary for breast cancer migration in this context [70].

Neutrophils have also been implicated in promoting metastasis, in part by infiltrating distant organs and priming pre-metastatic sites for tumor seeding [71]. One exciting observation demonstrated that neutrophil extracellular traps (NETs), extruded neutrophil chromatin embedded with a number of proteases, coat circulating tumor cells and aided in metastatic seeding [72].

Apart from stimulating invasion and metastasis, N2 TANs have been shown to directly stimulate tumor cell proliferation. In a spheroid model of lung adenocarcinoma, neutrophil

infiltration enhanced spheroid growth [73]. Further studies have identified neutrophil elastase (NE) as having inherent growth promoting properties. Exogenous NE promoted growth of esophageal cancer cells [74]. The authors went on to show NE induced EGFR phosphorylation as well as release of the growth factor PDGF. *In vivo*, NE-depleted mice had reduced lung carcinoma tumor burden [75]. In this model, NE inhibited tumor growth by degrading insulin receptor substrate-1 (IRS-1) promoting PI3K-PDGFR association and subsequent tumor proliferation.

One final process by which neutrophils promote tumor growth is via suppressing effector T cell functions. TANs produce CCL2 and CCL17 and therefore stimulate recruitment of macrophages and Tregs into the TME [76]. These recruited cells were found to contribute to tumor growth likely by inhibiting cytotoxic CD8+ T cell function. TANs can also inhibit T cell proliferation by secreting arginase-1 (Arg-1)[77]. Arg-1 degrades arginine, an important factor in T cell proliferation, and thus may inhibit T cell killing of non-small cell lung cancer (NSCLC)[77]. Neutrophils similarly have been shown to induce CD8+ T cell apoptosis in three mammary thoracic tumor models *in vitro* [78]. T cell apoptosis was shown to require nitric oxide (NO) as well as direct neutrophil-T cell contact, as soluble factors could not mediate neutrophil-induced apoptosis [78].

Clearly, the conflicting functions of neutrophils in the TME require further investigation to determine exactly when and where N1 and N2 TANs exist. Pro- versus anti-tumor neutrophils may be tumor- or stage-specific and little is currently understood about the timeline of neutrophil engagement throughout tumor development.

Reactive oxygen species (ROS) and antioxidants in tumor inflammation

Reactive oxygen species (ROS) are a diverse family of labile oxygen molecules that play important roles in many cellular processes including inflammation and cancer. Hydrogen peroxide (H_2O_2), a cell-permeable ROS isoform, is a potent neutrophil chemoattractant produced by Ras-transformed cells and tumors [79, 80]. Likely in response to elevated ROS levels, antioxidant proteins are more active in some human tumors including non-small-cell lung cancer [81] and colorectal cancer [82]. Below, I describe the cellular sources of ROS and the antioxidants that catalyze their clearance.

Reactive oxygen species

Mitochondrial ROS

Generally considered to be a byproduct of oxidative phosphorylation, mitochondria are the primary source of ROS produced in non-phagocytic cells. Electrons shuttling through the electron transport chain can pass through Complex I or Complex III and interact with O_2 and produce superoxide anion (O_2^-) [83]. O_2^- is highly reactive, capable of oxidizing and damaging proteins and DNA (Benov 2001). Roughly 80% of O_2^- produced by mitochondria accumulates in the intermembrane space [83]. The mitochondrial permeability transition pore (MPTP) allows for passage of O_2^- into the cytoplasm, where it can interact with the cytoplasmic superoxide dismutase (SOD1) to generate H_2O_2 [84]. Cytoplasmic transfer of O_2^- is thought to prevent accumulation to levels that would impair mitochondrial function [85].

Phagocyte ROS

Phagocytes, namely neutrophils and macrophages, deliberately produce O_2^- as a means of killing engulfed pathogens in a phenomenon termed the oxidative burst [86]. Superoxide is produced by the NADPH oxidase (NOX2) complex composed of six proteins that assemble on the membrane of the phagolysosome: $gp91^{phox}$, $gp22^{phox}$, $gp40^{phox}$, $gp47^{phox}$, $gp67^{phox}$, and the small GTPase Rac1/2 [87, 88]. $gp91^{phox}$ is the core enzymatic subunit, stabilized by $gp22^{phox}$, catalyzing the transfer of electrons from NADPH to O_2 [86, 88]. One additional ROS-generating enzyme produced primarily by neutrophils is myeloperoxidase, which generates the highly toxic hypochlorous acid (HOCl) from H_2O_2 and halides [89]. Other NOX isoforms (NOX1, NOX3, NOX4, NOX5) exist in many tissue types and appear to play signaling functions as opposed to inducing pathogen clearance [87].

Injury-induced ROS

In the NOX family of enzymes are two unique members, dual oxidase 1 and 2 (DUOX1 and DUOX2) [87]. Duox enzymes are unique in that, in addition to oxidizing NADPH to produce O_2^-, they also contain a peroxidase domain capable of oxidizing target proteins via H_2O_2 [90]. Duox enzymes are expressed in mucosa and epithelia, where their primary function appears to be in barrier protection after injury. In support of this claim, DUOX1/2 were shown to be active in salivary glands and necessary for H_2O_2 production in bronchial epithelial cells *in vitro* [91]. Depletion of *duox* mRNA in zebrafish larvae impaired wound-induced production of H_2O_2 and recruitment of leukocytes [92]. Additionally, dominant-negative Duox expression, in which the

NADPH-binding domain was excised, reduced H_2O_2 production in response to tail transection [93].

Antioxidants

Cellular antioxidants

All organisms produce a battery of antioxidant enzymes and small molecules to combat buildup of ROS to toxic levels. Mitochondrially-derived O_2^- is converted to H_2O_2 and O_2 by a family of superoxide dismutase enzymes [94]. Three such enzymes have been identified with differing localizations: the Cu/Zn superoxide dismutase 1 (SOD1) in the cytoplasm, Mn superoxide dismutase 2 (SOD2) in the mitochondrial matrix, and Cu/Zn superoxide dismutase (SOD3) in the extracellular space [95]. *Sod1*$^{-/-}$ mice develop symptoms of premature aging and oxidative damage in a number of tissues, phenotypes which can be ameliorated with antioxidant supplementation [96].

To detoxify H_2O_2, cells utilize a number of enzymes including catalase, peroxidases, and peroxiredoxins. Catalase is a cytoplasmic and peroxisomal protein that converts 2 H_2O_2 into 2 $H_2O + O_2$ and does not require subsequent reduction to regenerate [97]. Peroxidases similarly catalyse the reduction of H_2O_2 but typically use a xenobiotic molecule as an electron donor [98]. Peroxiredoxins contain redox-active dithiols that serve as electron donors to H_2O_2 [99]. They therefore require subsequent reduction from another source, typically thioredoxin, to regenerate their reducing power [100].

In addition to enzymatic antioxidants, cells contain a number of small molecules that assist in keeping the intracellular environment in a reduced state. Glutathione, and vitamins A,

C, and E are notable examples [101]. Glutathione (GSH) is a tripeptide composed of glutamate, cysteine, and glycine [102]. GSH is highly abundant at intracellular concentrations between 1-10mM [103]. The cysteine residue is redox sensitive and therefore the molecule can exist in the reduced (GSH) or oxidized (GSSG) state [102]. GSH is a substrate for several reductases including glutathione peroxidases (GPx) which reduce H_2O_2 [104]. GSH is also involved in eliminating toxic lipophilic molecules through conjugation, which improves solubility, and subsequent excretion [105].

Thioredoxin

Thioredoxin (Txn) is a ubiquitous ~12kDa antioxidant enzyme found in all cells from bacteria to humans first purified from *E. coli* in 1964 [106, 107]. Txn contains a dithiol active site (cys-gly-pro-cys) that can exist in the reduced (Txn-$(SH)_2$) or oxidized (Txn-S_2) state. Txn catalyzes the reduction of many oxidized intracellular proteins (R-S_2). Thioredoxin reductase (TR) subsequently catalyzes the regeneration of Txn-$(SH)_2$ using NADPH as a substrate [106].

Reduction of substrate proteins

$$\text{Txn-(SH)}_2 + \text{R-S}_2 \rightarrow \text{Txn-S}_2 + \text{R-(SH)}_2$$

Regeneration of reduced Txn

$$\text{Txn-S}_2 + \text{NADPH} + \text{H}^+ \xrightarrow{\text{TR}} \text{Txn-(SH)}_2 + \text{NADP}^+$$

Functionally, Txn is a pleiotropic enzyme involved in many cellular processes. As a disulfide reductant, it donates electrons to a number of other reductase enzymes. Txn has been shown to reduce ribonucleotide reductase essential for generating dNTPs and thus newly-synthesized DNA [108]. As mentioned above, Txn can serve as a cofactor for peroxiredoxins and therefore assist in the elimination of H_2O_2 [109]. In addition to cysteine, methionine contains a redox-sensitive sulfur moiety which can become oxidized, reducing its activity [110]. Oxidized methionine is reduced by methionine sulfoxide reductases which themselves are reduced by Txn [110].

Txn plays additional supportive and inhibitory roles in inflammation and tumorigenic processes, which will be discussed in subsequent sections. Briefly, Txn regulates NF-κB activity [111], apoptosis [112], and chemotaxis of leukocytes when secreted [113]. That said, its role in these processes is incompletely understood, especially at early stages of tumorigenesis. We therefore set out to identify the function of Txn in inflammatory signaling, neutrophil recruitment, and oncogene-transformed cell growth in the work that follows.

Chapter Two

Effects of ROS and antioxidants on neutrophil recruitment to neoplastic cells

Benjamin Korte, Morgan Giese, Gayathri Ramakrishnan, Veronika Miskolci, Stella Ma, David Bennin, Colin Dewey, Melissa Skala, Anna Huttenlocher

This manuscript will be sent to the Journal of Cell Science following co-author review.

Author contributions: BK designed and performed experiments, analyzed data, and wrote the manuscript. DB purified thioredoxin protein and performed Western blots. MG and CD assisted in analyzing RNA-seq results and preparing figures. SM and GR performed neutrophil abundance assays in unwounded and wounded larvae. VM and MS assisted in metabolic imaging experiments and analysis. AH designed experiments and edited manuscript.

Introduction

Neutrophils, in the majority of instances, appear to promote tumor growth; however, when this occurs during the process of tumorigenesis is understudied and largely unknown. Recent work, primarily in zebrafish larvae, has determined that neutrophils are recruited to and promote the growth of oncogene-transformed cells. The main purpose of the work presented below is to identify signaling molecules that mediate changes in neutrophil behavior and ultimately affect transformed-cell fate.

Evidence, both *in vitro* and *in vivo*, suggest that the process of oncogene-induced transformation is sufficient to induce an inflammatory response. One common family of oncogenes activated in human cancer are the Ras proteins with mutations in KRas, NRas, and HRas reported in 22%, 8%, and 3% of human tumors [114]. Up to 89 percent of KRas mutations in human cancers are reported at codon twelve [115], including the glycine to valine mutant $KRas^{G12V}$. This substitution renders the GTPase insensitive to GTPase activating protein (GAP)-mediated GTP hydrolysis [114]. Thus Ras^{G12V} is constitutively active, continuously delivering mitogenic and anti-apoptotic signals to the cell via MAP kinase and PI3K pathways, respectively [116].

When $HRas^{G12V}$ was exogenously introduced into HeLa cells, lung carcinoma cells (H125), or immortalized human mammary epithelial cells (MCF-10A); expression of the pro-inflammatory cytokine and neutrophil chemoattractant cxcl8 (IL-8) was highly upregulated [117]. The authors went on to show through pharmacological inhibition that cxcl8 expression induced by $HRas^{G12V}$ required the ERK-MAPK and PI3K pathways. Therefore, the mitogenic and

anti-apoptotic signaling pathways stimulated by Ras activation are intimately linked with Ras-induced inflammatory signaling.

Additionally, $HRas^{G12V}$ and $KRas^{G12V}$ overexpression in ovarian cells *in vitro* upregulated expression of a number of inflammatory cytokines including IL-1α, IL-1β, IL-6, cxcl8 (IL-8), and IL-11 [118]. Antibodies targeting IL-1β or cxcl8 induced Ras-transformed cell apoptosis and elicited minimal cell death in control cell lines devoid of constitutively active Ras [118]. Interestingly, these inflammatory cytokines appear to support autocrine cell survival. The authors go on to demonstrate the necessity of the inflammatory transcription factor NF-κB in mediating Ras-induced cxcl8 expression [118]. Thus, constitutive Ras activation through ERK-MAPK, PI3K, and ultimately NF-κB stimulates expression of inflammatory cytokines, including the neutrophil chemoattractant cxcl8.

In vivo in zebrafish larvae, $KRas^{G12V}$ expression in glial cells increased expression of the two zebrafish cxcl8 isoforms (*cxcl8a* and *cxcl8b.1*) as well as *il1b* expression [119]. Neutrophil recruitment to $KRas^{G12V}$-transformed glial cells required the chemokine receptor, Cxcr2, thus demonstrating that oncogene-induced transformation *in vivo* stimulates chemokine-dependent neutrophil recruitment.

Apart from inflammatory cytokines, reactive oxygen species (ROS) such as superoxide (O_2^-) and hydrogen peroxide (H_2O_2), have been demonstrated to play a pro-inflammatory and pro-survival role in a variety of contexts. Firstly, H_2O_2 is produced at high levels *in vitro* in several human melanoma, colon carcinoma, and neuroblastoma cell lines [120]. This H_2O_2 appears to originate from superoxide (O_2^-) produced in mitochondria as a byproduct of

oxidative phosphorylation, as inhibition of superoxide dismutase reduces H_2O_2 abundance [120]. Interestingly, $HRas^{G12V}$ expression alone in NIH 3T3 fibroblasts was sufficient to induce mitochondrial ROS (mROS) production [121, 122]. $HRas^{G12V}$ expression in zebrafish goblet cells within the skin induced H_2O_2 production in both transformed cells and neighboring non-transformed cells [123]. Additionally, extracellular mitogens including epidermal growth factor (EGF) and platelet-derived growth factor (PDGF) were also able to stimulate ROS production [124, 125]. Therefore, activation of growth signals from a variety of sources all seem to upregulate ROS production, likely as a byproduct of increased anabolic pressure on mitochondria to produce ATP.

Reactive oxygen species promote inflammatory signaling both directly and indirectly. H_2O_2 is a well-established neutrophil chemoattractant, guiding neutrophils to sites of tissue damage and infection via the redox-sensitive Src family kinase, Lyn [126]. In the context of a wound, H_2O_2 is largely produced by the enzyme dual oxidase (Duox) which is necessary for early neutrophil recruitment to the wounded tissue [127]. In contrast, in cancer cells H_2O_2 appears to be generated primarily by mitochondria, as mentioned above. Mitochondrially-derived H_2O_2 has been shown to be necessary for LPS-induced expression of pro-IL-1β and secretion of mature IL-1β in mouse bone-marrow derived macrophages (BMDMs) [128, 129]. This necessity for mROS on IL-1β secretion was demonstrated to be dependent on the potent, pro-inflammatory signaling complex, the inflammasome [130]. Additionally, mitochondrial ROS is necessary for LPS-stimulated expression of inflammatory cytokines IL6, Cxcl8, and Tnfα [131]. Thus, oncogene-expressing cells produce H_2O_2 from a mitochondrial source, which has the capacity to induce neutrophil recruitment directly or indirectly through upregulation of

inflammatory cytokines. Therefore, one aim of the work conducted below was to assess the role of mROS in neutrophil recruitment to neoplastic cells *in vivo.*

In *vivo* studies in zebrafish modeling tumor initiation have shown that neutrophils are recruited shortly after Ras^{G12V}-induced transformation of epithelial cells [123, 132]. These recruited neutrophils make frequent, direct cell-cell contact with Ras^{G12V}-transformed cells, occasionally forming long membrane tethers between cells [132]. At these early stages, neutrophils support proliferation of transformed epithelial and glial cells [79, 119], the former likely via production of prostaglandin E_2. Neutrophils also upregulate the epithelial-mesenchymal transition (EMT)-associated genes *mmp9* and *slug* within transformed cells [132]. These observations suggest neutrophils promote tumorigenic processes early in the process of tumor development. Additionally, recent evidence suggests neutrophil migratory behavior changes during the course of tumor development, with early stage tumors inducing elevated, albeit random, migration of bone marrow-derived neutrophils and late stage tumors inducing slower, immunosuppressive neutrophil migration [133].

Therefore, constitutive oncogene activation alone, an event that commonly occurs early in tumor development, is sufficient to activate a number of inflammatory processes including cytokine expression and ROS production. These inflammatory cues then recruit neutrophils which appear to promote transformed cell growth at these early stages. However, the signaling events that mediate neutrophil recruitment and retention are incompletely characterized and are the focus of the work presented below. Studying neutrophil migratory behavior early in tumorigenesis may provide insight into how these cells elicit their tumor-supporting effects.

To study neutrophil recruitment to oncogene-transformed cells early in the process of tumorigenesis, we utilized transparent zebrafish larvae. Previous efforts in the lab have generated transgenic zebrafish lines harboring stably-integrated fluorescent proteins under the neutrophils specific promoter LyzC (*Tg(LyzC:H2B-mcherry)*). Fluorescently-labeled HRas control (pTol2-krt4-RFP-HRas) or $HRas^{G12V}$ oncogenic (pTol2-krt4-RFP-$HRas^{G12V}$) plasmids were then injected into 1-cell stage *Tg(LyzC:H2B-mcherry)* embryos in conjunction with Tol2 transposase mRNA [132] (Fig. 1a). The gene of interest was subsequently inserted into the developing zebrafish genomic DNA via the action of transposase. Ras expression is directed to the superficial keratinocyte layer via the action of the krt4 promoter. By three days post-fertilization (3dpf), neutrophils have developed and are readily recruited to the immediate vicinity of $HRas^{G12V}$- but not HRas-expressing keratinocytes. Time-lapse microscopy revealed neutrophils remain in the vicinity of $HRas^{G12V}$-expressing cells for minutes to hours, indicating oncogene expression induces sustained inflammatory signaling (Fig. 1b).

Fig.1

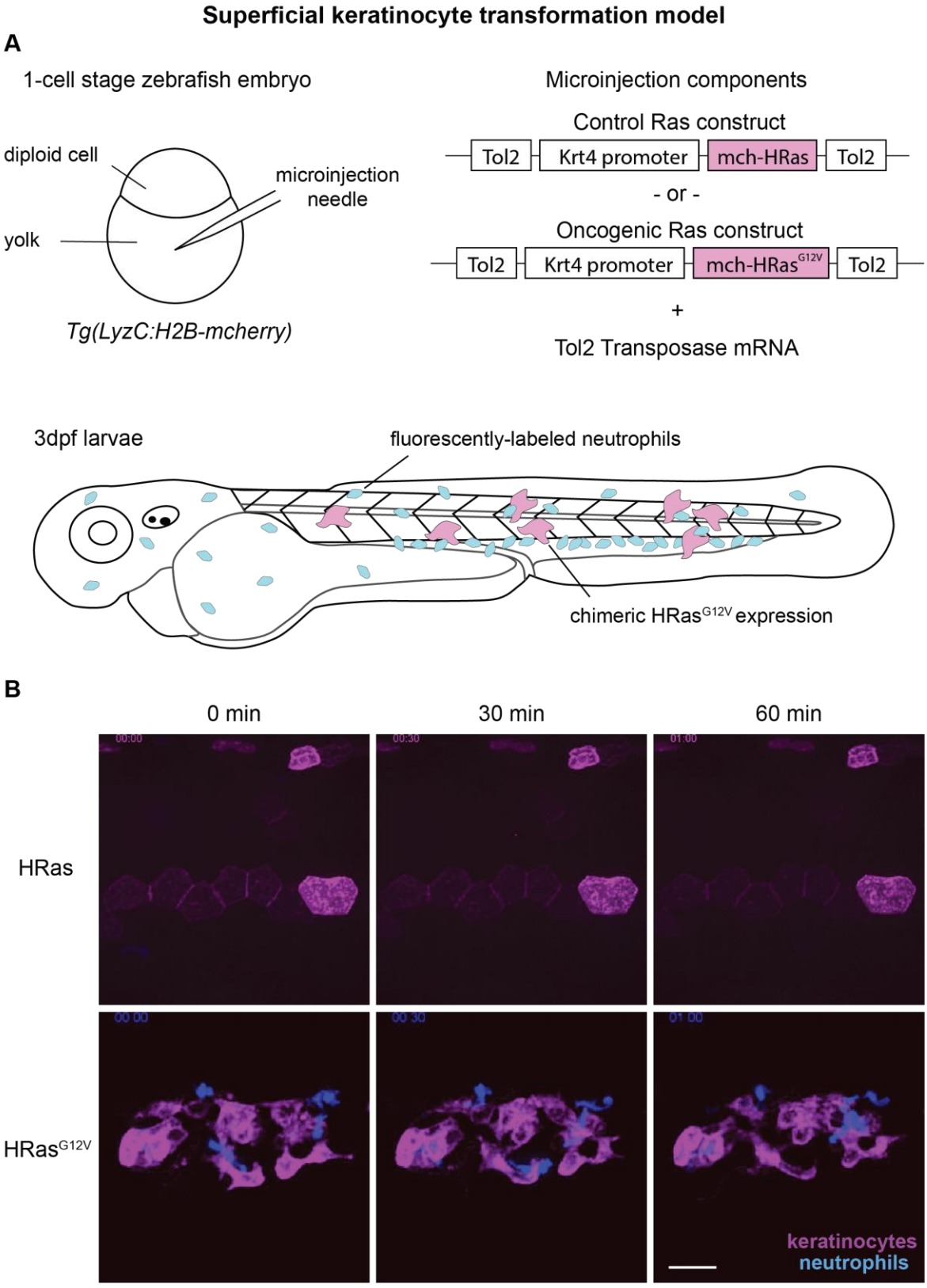
Superficial keratinocyte transformation model
A
1-cell stage zebrafish embryo
diploid cell
microinjection needle
yolk
Tg(LyzC:H2B-mcherry)
Microinjection components
Control Ras construct
Tol2
Krt4 promoter
mch-HRas
Tol2
- or -
Oncogenic Ras construct
Tol2
Krt4 promoter
mch-HRasG12V
Tol2
+
Tol2 Transposase mRNA
3dpf larvae
fluorescently-labeled neutrophils
chimeric HRasG12V expression
B
0 min
30 min
60 min
HRas
HRasG12V
keratinocytes
neutrophils

Fig. 1 – **Superficial keratinocyte Ras^{G12V}-transformation model** A) Schematic of microinjection procedure. One cell stage *Tg(LyzC:H2B-mcherry)* embryos are injected with control (pTol2-Krt4-HRas-mcherry) or transformation (pTol2-Krt4-HRas^{G12V}-mcherry) constructs. 3dpf larvae present with chimeric expression of HRas variant in superficial keratinocytes. B) Neutrophil (blue) recruitment around wildtype- or constitutively active Ras^{G12V}-expressing cells (magenta) at relative T=0min, T=30min, T=60min.

Results

Mitochondrial ROS mediates neutrophil retention around Ras^{G12V}-transformed cells

Neutrophils migrate toward elevated concentrations of reactive oxygen species (ROS), a phenomenon common to many inflammatory situations. We therefore set out to identify sources of ROS produced by oncogene-transformed cells and subsequently determine their role in neutrophil recruitment and retention. Krt4-KRas or Krt4-KRas^{G12V}-expressing larvae were treated with the intracellular ROS probe CellRox, a proprietary reagent with enhanced fluorescence following oxidation. We observe an increase in intracellular ROS abundance with KRas^{G12V} expression in superficial keratinocytes over KRas control keratinocytes (Fig. 2a,b). Interestingly, the intracellular ROS appeared to localize primarily to the cytoplasm, suggesting a mitochondrial source. We therefore probed control or oncogenic Krt4-KRas expressing larvae with the mitochondrial-targeted redox reagent, mitoSOX. Similar to the CellRox result, we observed an increase in mROS signal within KRas^{G12V}-expressing cells (Fig. 2c,d).

Fig.2

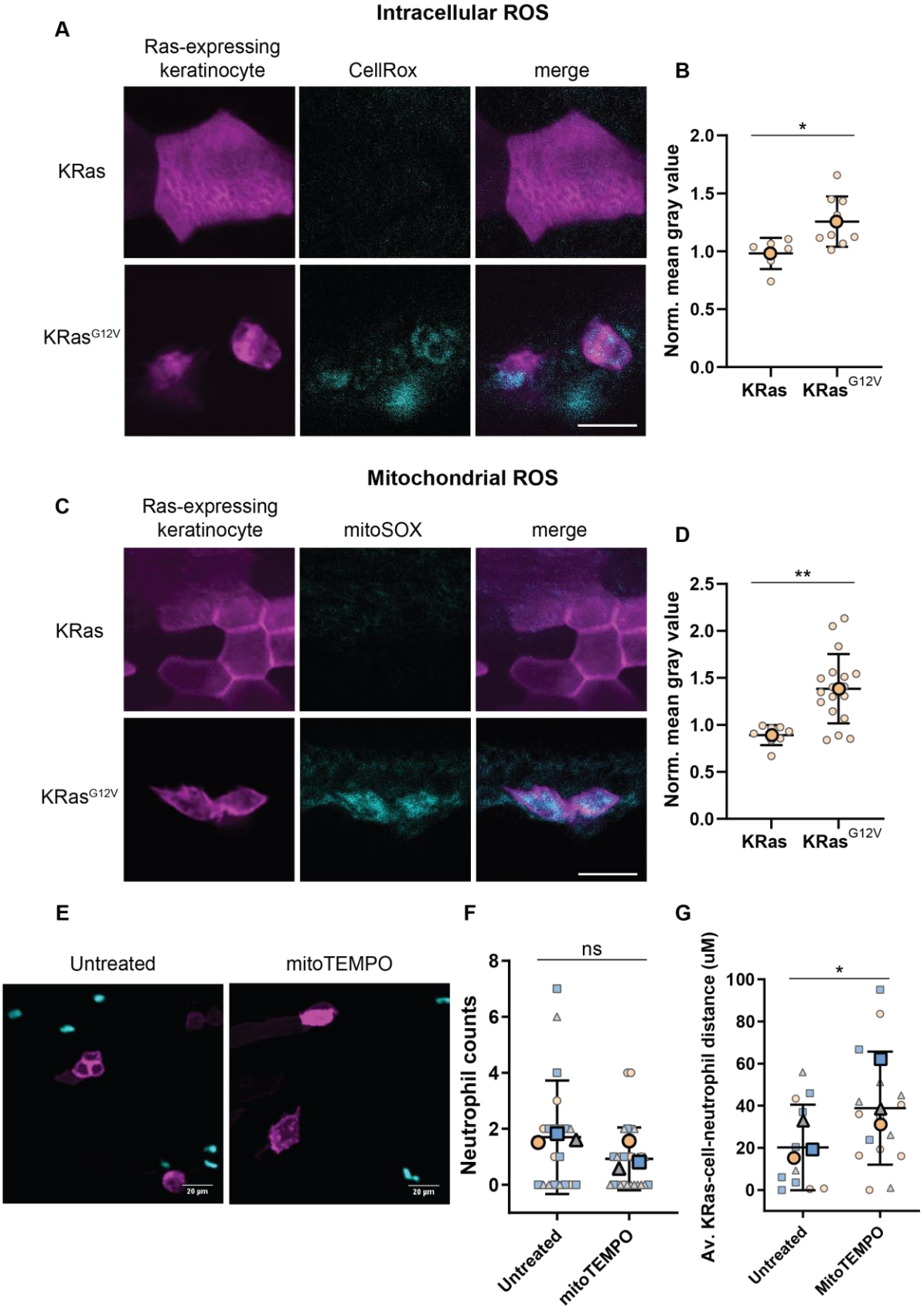
Intracellular ROS
A
Ras-expressing keratinocyte
CellRox
merge
KRas
KRasG12V
B
Norm. mean gray value
2.0
1.5
1.0
0.5
0.0
*
KRas
KRasG12V
Mitochondrial ROS
C
Ras-expressing keratinocyte
mitoSOX
merge
KRas
KRasG12V
D
Norm. mean gray value
2.5
2.0
1.5
1.0
0.5
0.0
**
KRas
KRasG12V
E
Untreated
mitoTEMPO
20 µm
20 µm
F
Neutrophil counts
8
6
4
2
0
ns
Untreated
mitoTEMPO
G
Av. KRas-cell-neutrophil distance (uM)
100
80
60
40
20
0
*
Untreated
MitoTEMPO

Fig. 2 – Mitochondrial ROS mediates neutrophil retention around Ras^{G12V}-transformed superficial keratinocytes A) CellRox probe for intracellular ROS (1uM) in KRas wt (n=6) and KRas^{G12V} (n=9) expressing larvae. B) Quantification of CellRox intracellular mean gray value normalized to wt average. C) MitoSOX probe for mitochondrial ROS (1uM) in KRas wt (n=8) and KRas^{G12V} (n=18) expressing larvae. D) Quantification of MitoSox intracellular mean gray value normalized to wt average. E) mitoTEMPO treatment (50uM) of KRas^{G12V}. F) Quantification of neutrophil abundance around transformed cells in untreated (n=20) and mitoTEMPO treated (n=28) larvae. G) Quantification of average KRas cell-neutrophil distance in untreated (n=12) and mitoTEMPO treated (n=17) larvae. Scale bar, 20uM. Bolded shapes indicate average value per technical replicate, with shaded values representing data points from independent larvae. Samples were analyzed for statistical significance via t-test ($p<0.05$ *, $p<0.01$**, $p<0.001$***,$p<0.0001$****).

After confirming increased intracellular mROS in oncogene-transformed cells, we assessed the role of mROS in neutrophil recruitment. To this end, the mitochondrially-targeted superoxide dismutase mimetic, mitoTEMPO, was utilized to reduce mROS burden. mitoTEMPO treatment did not significantly alter neutrophil abundance around transformed superficial keratinocytes, though a trend toward decreased recruitment was observed (Fig. 2e,f). Scavenging mROS did however increase the average distance between transformed cells and the nearest neutrophil, suggesting mROS is necessary in mediating recruitment to the immediate vicinity of KRas^{G12V}-expressing cells (Fig. 2g).

<u>Thioredoxin expression is upregulated in Ras^{G12V}-transformed cells and human cancers</u>

As innate immune cells can affect tumor development, we looked for changes in gene expression in response to Ras^{G12V}-induced transformation that might regulate leukocyte

behavior in zebrafish larvae. We thus conducted translating ribosome affinity purification (TRAP) [134] and subsequent RNA sequencing of three cell-types in the transformed-cell microenvironment: Ras^{G12V}-expressing keratinocytes, neutrophils, and macrophages. Briefly, constructs expressing either control HRas (pTol2-Krt4-RFP-HRas) or oncogenic $HRas^{G12V}$ (pTol2-Krt4-RFP-$HRas^{G12V}$) under the superficial keratinocyte promoter Krt4 were microinjected into 1 cell-stage embryos. To identify gene expression changes within transformed cells, plasmid expressing the ribosomal subunit L10a-GFP (pTol2-Krt4-EGFP-L10a) was co-injected with either the HRas control or oncogenic $HRas^{G12V}$ construct. GFP-tagged ribosomes were isolated via immunoprecipitation and their associated transcripts sequenced yielding cell type-specific gene expression information (Fig. 3a). Neutrophil and macrophage ribosomes were isolated from transgenic lines, *Tg(Lyzc:EGFP-L10a)* and *Tg(mpeg:EGFP-L10a)* respectively, injected with control or oncogenic HRas plasmids (Fig. 3b,c).

Selected cell-type specific genes were enriched in TRAP samples from their respective tissue, thus reinforcing the tissue-specificity of the TRAP-seq dataset (Fig. 4a). Gene set enrichment analysis (GSEA) revealed enrichment of several inflammatory pathways within all three cell-types, including IL6-Jak-Stat3-signaling, Tnfα-signaling-via-NF-κB, and reactive-oxygen-species-pathways (Fig. 4b).

Fig.3

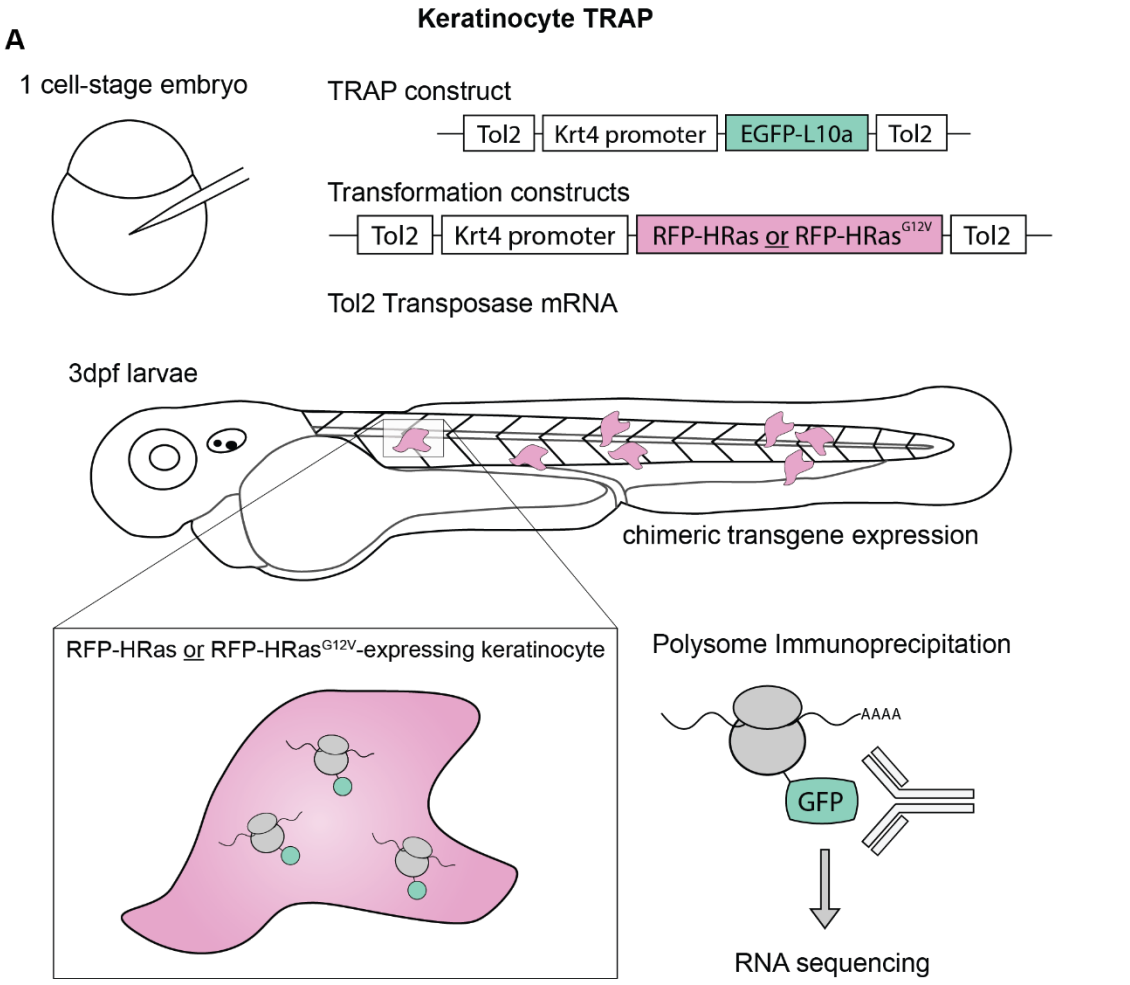
Keratinocyte TRAP
A
1 cell-stage embryo
TRAP construct
Tol2
Krt4 promoter
EGFP-L10a
Tol2
Transformation constructs
Tol2
Krt4 promoter
RFP-HRas or RFP-HRasG12V
Tol2
Tol2 Transposase mRNA
3dpf larvae
chimeric transgene expression
RFP-HRas or RFP-HRasG12V-expressing keratinocyte
Polysome Immunoprecipitation
AAAA
GFP
RNA sequencing
B
Neutrophil TRAP
Tg(LyzC:EGFP-L10a)
HRas or HRasG12V-expressing keratinocyte
EGFP-L10a-expressing neutrophils
C
Macrophage TRAP
Tg(mpeg:EGFP-L10a)
HRas or HRasG12V-expressing keratinocyte
EGFP-L10a-expressing macrophage

Fig. 3 – **Translating Ribosome Affinity Purification (TRAP)-seq** A) Schematic of TRAP procedure. Wildtype embryos are injected with the TRAP plasmid (pTol2-Krt4-EGFP-L10a) and either control (pTol2-Krt4-HRas-mcherry) or transformation (pTol2-Krt4-HRas^{G12V}-mcherry) constructs. Immunoprecipitation and sequencing was conducted 3dpf on batches of ~50 larvae collected on three separate days (n=3). B) *Tg(LyzC:EGFP-L10a)* larvae were injected with either control (pTol2-Krt4-HRas-mcherry) or transformation (pTol2-Krt4-HRas^{G12V}-mcherry) constructs for neutrophil-targeted L10a expression. C) *Tg(mpeg:EGFP-L10a)* larvae were injected with either control (pTol2-Krt4-HRas-mcherry) or transformation (pTol2-Krt4-HRas^{G12V}-mcherry) constructs for macrophage-targeted L10a expression.

Fig. 4 – **TRAP-seq validation and preliminary pathway analysis** A) Select genes expressed in keratinocytes (*krt17, krt15, krt97, krt91, krt8, krt92, krt18,* krt94), neutrophils (*mpx,lyz*), and macrophages (*mpeg1.1, irf8, csf1rb, spi1a, mfap4, irg1, csf1ra, spi1b, ncf1, cyba*) and their expression profiles in TRAP samples from keratinocyte, neutrophils, and macrophages. *B*) Analysis of Hallmark pathways enriched in the context of oncogene transformation in neutrophils, keratinocytes, and macrophages.

Fig.4

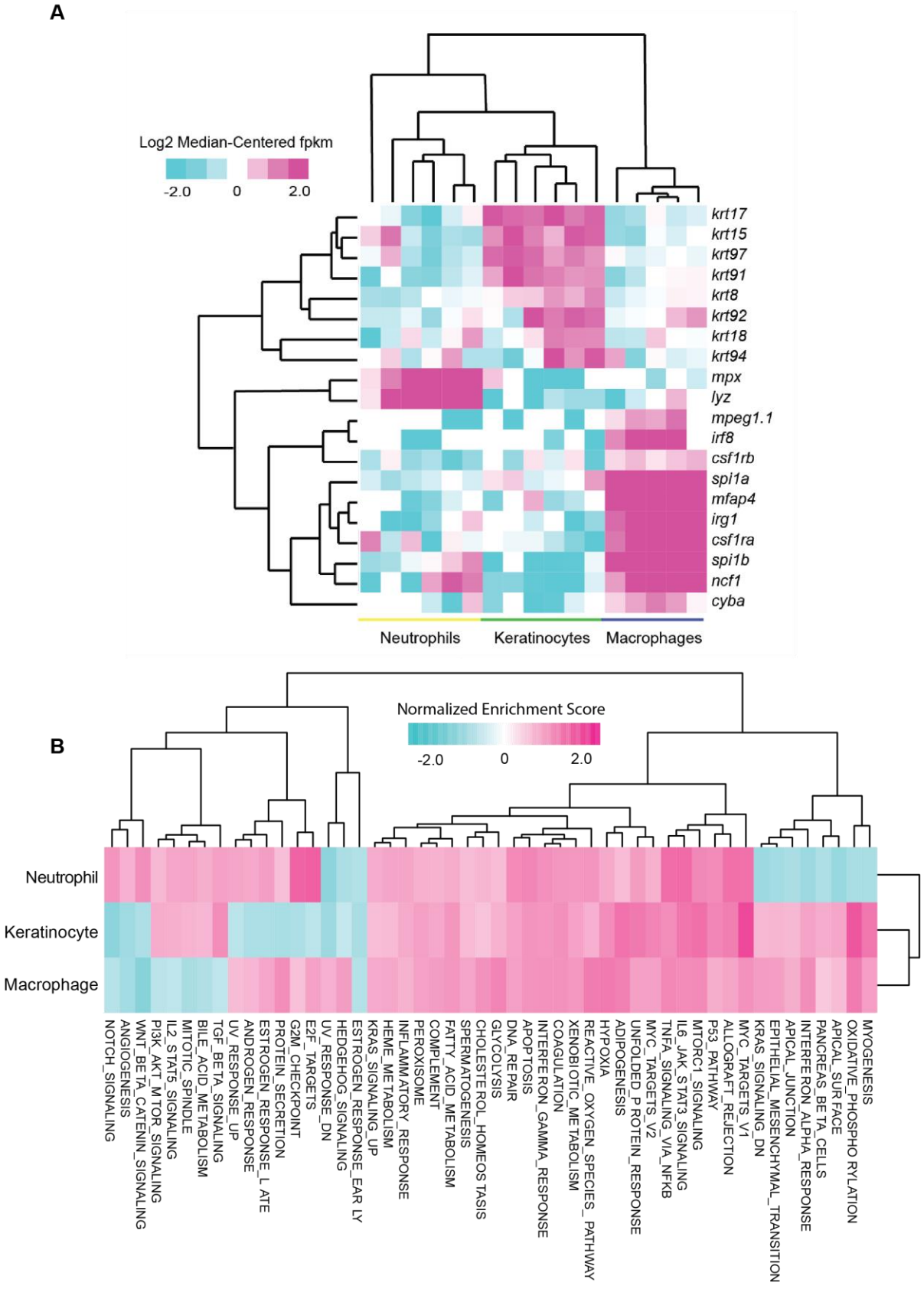
A
Log2 Median-Centered fpkm
-2.0
0
2.0
krt17
krt15
krt97
krt91
krt8
krt92
krt18
krt94
mpx
lyz
mpeg1.1
irf8
csf1rb
spi1a
mfap4
irg1
csf1ra
spi1b
ncf1
cyba
Neutrophils
Keratinocytes
Macrophages
B
Normalized Enrichment Score
-2.0
0
2.0
Neutrophil
Keratinocyte
Macrophage
NOTCH_SIGNALING
ANGIOGENESIS
WNT_BETA_CATENIN_SIGNALING
PI3K_AKT_MTOR_SIGNALING
IL2_STAT5_SIGNALING
MITOTIC_SPINDLE
BILE_ACID_METABOLISM
TGF_BETA_SIGNALING
UV_RESPONSE_UP
ANDROGEN_RESPONSE
ESTROGEN_RESPONSE_LATE
PROTEIN_SECRETION
G2M_CHECKPOINT
E2F_TARGETS
UV_RESPONSE_DN
HEDGEHOG_SIGNALING
ESTROGEN_RESPONSE_EARLY
KRAS_SIGNALING_UP
HEME_METABOLISM
INFLAMMATORY_RESPONSE
PEROXISOME
COMPLEMENT
FATTY_ACID_METABOLISM
SPERMATOGENESIS
CHOLESTEROL_HOMEOSTASIS
GLYCOLYSIS
DNA_REPAIR
APOPTOSIS
INTERFERON_GAMMA_RESPONSE
COAGULATION
XENOBIOTIC_METABOLISM
REACTIVE_OXYGEN_SPECIES_PATHWAY
HYPOXIA
ADIPOGENESIS
UNFOLDED_PROTEIN_RESPONSE
MYC_TARGETS_V2
TNFA_SIGNALING_VIA_NFKB
IL6_JAK_STAT3_SIGNALING
MTORC1_SIGNALING
P53_PATHWAY
ALLOGRAFT_REJECTION
MYC_TARGETS_V1
KRAS_SIGNALING_DN
EPITHELIAL_MESENCHYMAL_TRANSITION
APICAL_JUNCTION
INTERFERON_ALPHA_RESPONSE
PANCREAS_BETA_CELLS
APICAL_SURFACE
OXIDATIVE_PHOSPHORYLATION
MYOGENESIS

Fig.5

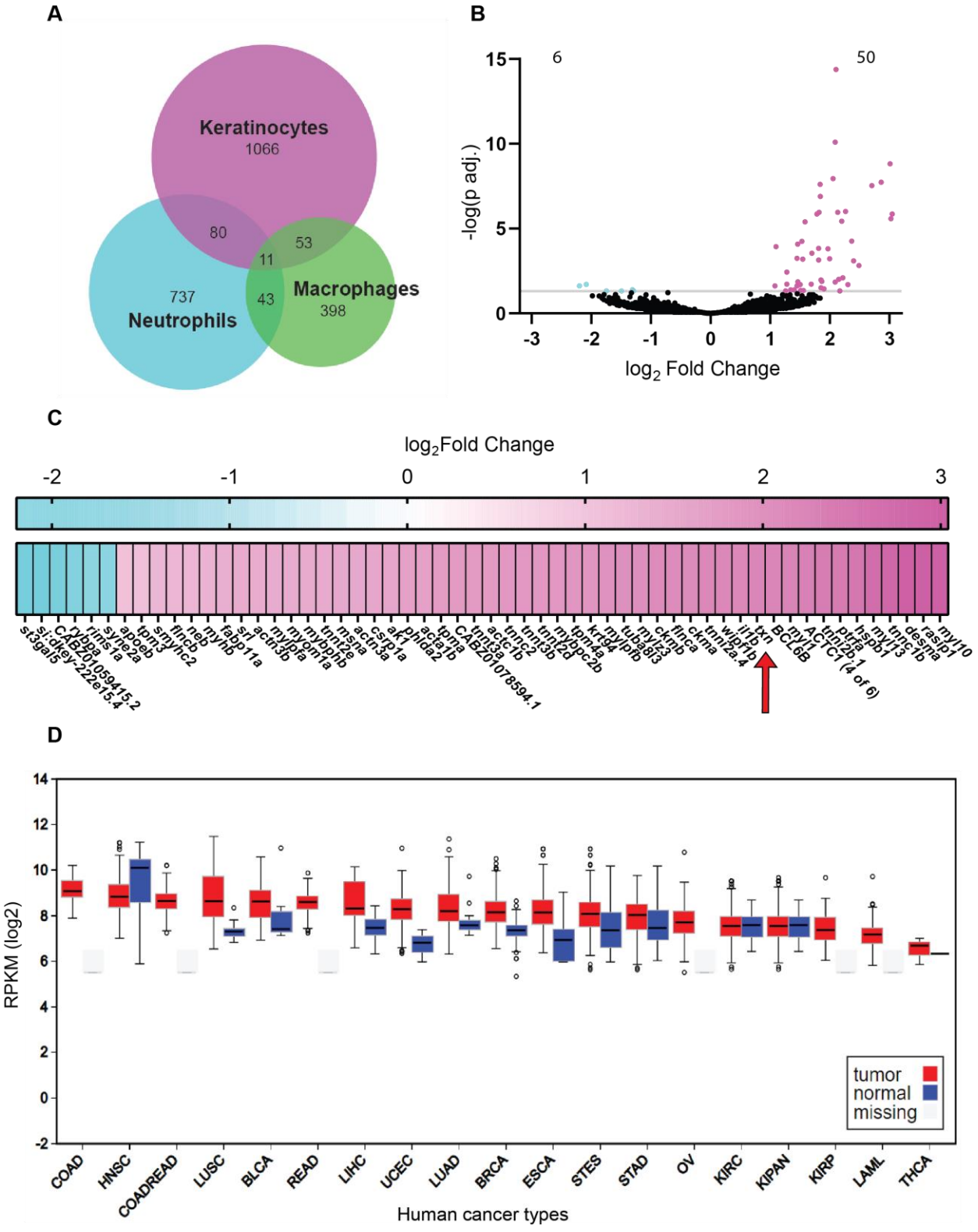
A
Keratinocytes
1066
80
53
11
737
Neutrophils
43
Macrophages
398
B
6
50
-log(p adj.)
log2 Fold Change
C
log2Fold Change
D
RPKM (log2)
tumor
normal
missing
COAD
HNSC
COADREAD
LUSC
BLCA
READ
LIHC
UCEC
LUAD
BRCA
ESCA
STES
STAD
OV
KIRC
KIPAN
KIRP
LAML
THCA
Human cancer types

Fig. 5 – **Thioredoxin expression is upregulated in Ras^{G12V}-transformed cells and human cancers** A) Venn diagram showing distribution of genes altered >2fold by TRAP-seq in response to HRas^{G12V} expression in superficial keratinocytes. *B*) Volcano plot displaying number of significantly ($p<0.05$) downregulated (6) and upregulated (50) genes in HRas^{G12V}-expressing keratinocytes relative to HRas-expressing keratinocytes. C) Heat map showing gene symbols for significantly ($p<0.05$) changed genes in HRas^{G12V}-expressing keratinocytes. D) mRNA expression profile of *txn* in human cancer and normal tissue. Firebrowse was used to extract expression profiles of human tumors from The Cancer Genome Atlas (TCGA).

In response to oncogenic HRas^{G12V}-expression, 1210 genes in keratinocytes, 871 genes in neutrophils, and 505 genes in macrophages were altered >2fold (Fig. 5a). Specifically within keratinocytes, 50 genes were found to be significantly upregulated ($p.adj < 0.05$) and 6 genes significantly downregulated in HRas^{G12V}-expressing cells over control HRas-expressing cells (Fig. 5b). Thioredoxin (*txn*) was among the most highly upregulated genes in response to transformation with expression levels roughly five-fold higher in HRas^{G12V}-transformed cells over HRas controls (Fig. 5c). Importantly, thioredoxin expression was upregulated in ten of thirteen human carcinoma samples based on bulk sequencing available through The Cancer Genome Atlas (TCGA)(Fig. 5d).

<u>Generation of thioredoxin mutant zebrafish line via CRISPR; Tail wounds are more inflammatory in *txn*$^{-/-}$ larvae</u>

Despite its known role as an antioxidant, the role thioredoxin plays in inflammatory processes is controversial with both pro- and anti-inflammatory functionalities described. To dissect the effects of *txn* on inflammation and growth of transformed cells, *txn* mutant

zebrafish were generated via CRISPR-Cas9. The mutant harbors a 1bp insertion and codes for a premature stop codon predicted to yield a truncated protein (Fig. 6a). Western blotting of 3dpf extracts in *txn* wildtype and mutant backgrounds confirmed loss of full length Txn protein in the mutant (Fig. 6b). Inflammatory cytokine expression (*il1b*, *cxcl8a*, *cxcl8b.1*, *tnfa*) was unchanged in whole larval extracts of wildtype and *txn* mutants (Fig. 6c). Additionally, $txn^{-/-}$ larvae appear morphologically normal and develop similar total neutrophil numbers compared to wildtype larvae (Fig. 6d,e).

H_2O_2 is rapidly produced in response to injury by the enzyme dual oxidase (Duox) ultimately establishing a chemotactic gradient to promote neutrophil migration to the wound site [92]. To assess the effect of *txn* on sterile wound inflammation, larval tails were transected and H_2O_2 and neutrophil abundance in the wounded region was quantified, the former using the fluorescent H_2O_2 sensor, pentafluorobenzene sulphonyl fluorescein (pfbs-f) (Fig. 7a). *txn* mutant larvae displayed increased H_2O_2 abundance at the wound site 30 minutes post-wound (mpw) and 4 hours post-wound (hpw) (Fig. 7b,c) as well as increased neutrophil abundance 2hpw but not 6hpw (Fig. 7d,e). Our findings thus suggest thioredoxin assists in the turnover of H_2O_2 produced at a wound thus dampening chemotactic signaling to neutrophils.

Fig.6

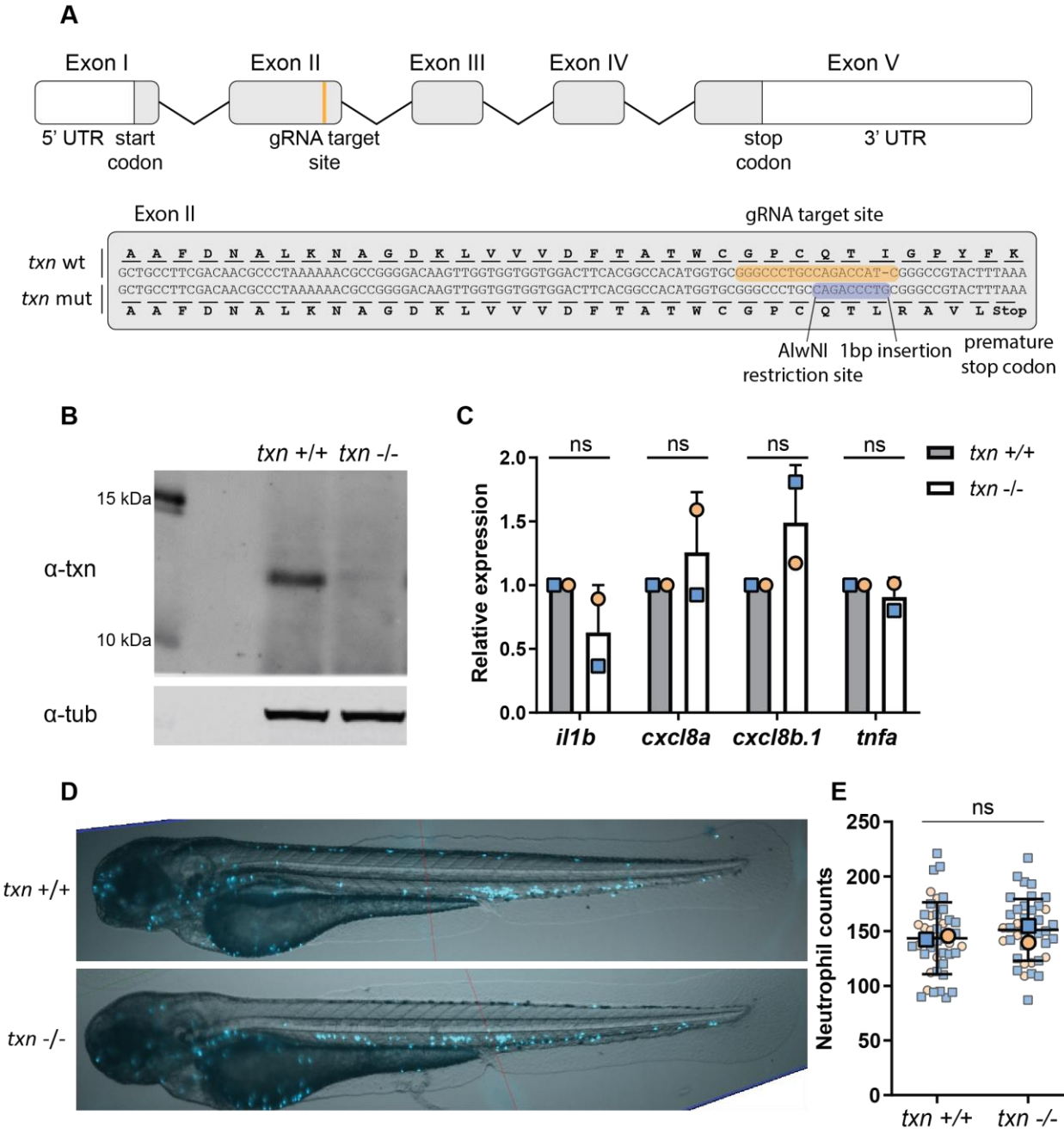
A
Exon I
Exon II
Exon III
Exon IV
Exon V
5' UTR
start codon
gRNA target site
stop codon
3' UTR
Exon II
gRNA target site
txn wt
txn mut
A A F D N A L K N A G D K L V V V D F T A T W C G P C Q T I G P Y F K
GCTGCCTTCGACAACGCCCTAAAAAACGCCGGGGACAAGTTGGTGGTGGTGGACTTCACGGCCACATGGTGCGGGCCCTGCCAGACCAT-CGGGCCGTACTTTAAA
GCTGCCTTCGACAACGCCCTAAAAAACGCCGGGGACAAGTTGGTGGTGGTGGACTTCACGGCCACATGGTGCGGGCCCTGCCAGACCCTGCGGGCCGTACTTTAAA
A A F D N A L K N A G D K L V V V D F T A T W C G P C Q T L R A V L Stop
AlwNI restriction site
1bp insertion
premature stop codon
B
txn +/+
txn -/-
15 kDa
α-txn
10 kDa
α-tub
C
ns
txn +/+
txn -/-
Relative expression
2.0
1.5
1.0
0.5
0.0
il1b
cxcl8a
cxcl8b.1
tnfa
D
txn +/+
txn -/-
E
ns
Neutrophil counts
250
200
150
100
50
0
txn +/+
txn -/-

Fig. 6 – **Generation of *txn* mutant zebrafish line** A) Schematic of *txn* gene with annotations of gRNA target site and 1bp insertion identified in mutant. B) Western blot of Txn and Tubulin on whole lysate from *txn* wildtype and mutant larvae. C) qPCR of inflammatory cytokines *il1b*, *cxcl8a*, *cxcl8b.1*, *tnfa* in whole larval lysates (pooled, 30 larvae) from *txn* wildtype (n=2) or mutant (n=2) larvae 3dpf. D) Neutrophil distribution and abundance in unstimulated $txn^{+/+}$ Tg(*LyzC*:*H2B-mcherry*) or $txn^{-/-}$Tg(*LyzC*:*H2B-mcherry*) larvae 3dpf. E) Quantification of total neutrophil number in unstimulated larvae, wildtype (n=41) and mutant (n=40). Bolded shapes indicate average value per technical replicate, with shaded values representing data points from independent larvae. Samples were analyzed for statistical significance via t-test.

Fig. 7 – **Tail wounds are more inflammatory in $txn^{-/-}$ larvae** A) Schematic of tail transection assay to measure neutrophil recruitment and H_2O_2 abundance conducted on $txn^{+/+}$ Tg(*LyzC*:*H2B-mcherry*) or $txn^{-/-}$Tg(*LyzC*:*H2B-mcherry*) larvae 3dpf. B) pfbs-f probe for H_2O_2 (1uM) in response to tail transection 30 minutes post-wound (mpw) (wt n=56, mut n=54) and 4 hours post-wound (hpw) (wt n=51, mut n=51) with C) quantification of signal density in region posterior to notochord. D) Neutrophil recruitment in response to tail transection 2hpw (wt n=79, mut n=85) and 6hpw (wt n=87, mut n=90) with E) quantification of neutrophil abundance in region posterior to notochord. Scale bar, 50um. Bolded shapes indicate average value per technical replicate, with shaded values representing data points from independent larvae. Samples were analyzed for statistical significance by Mann-Whitney U test ($p<0.05$ *, $p<0.01$**, $p<0.001$***,$p<0.0001$****).

Fig.7

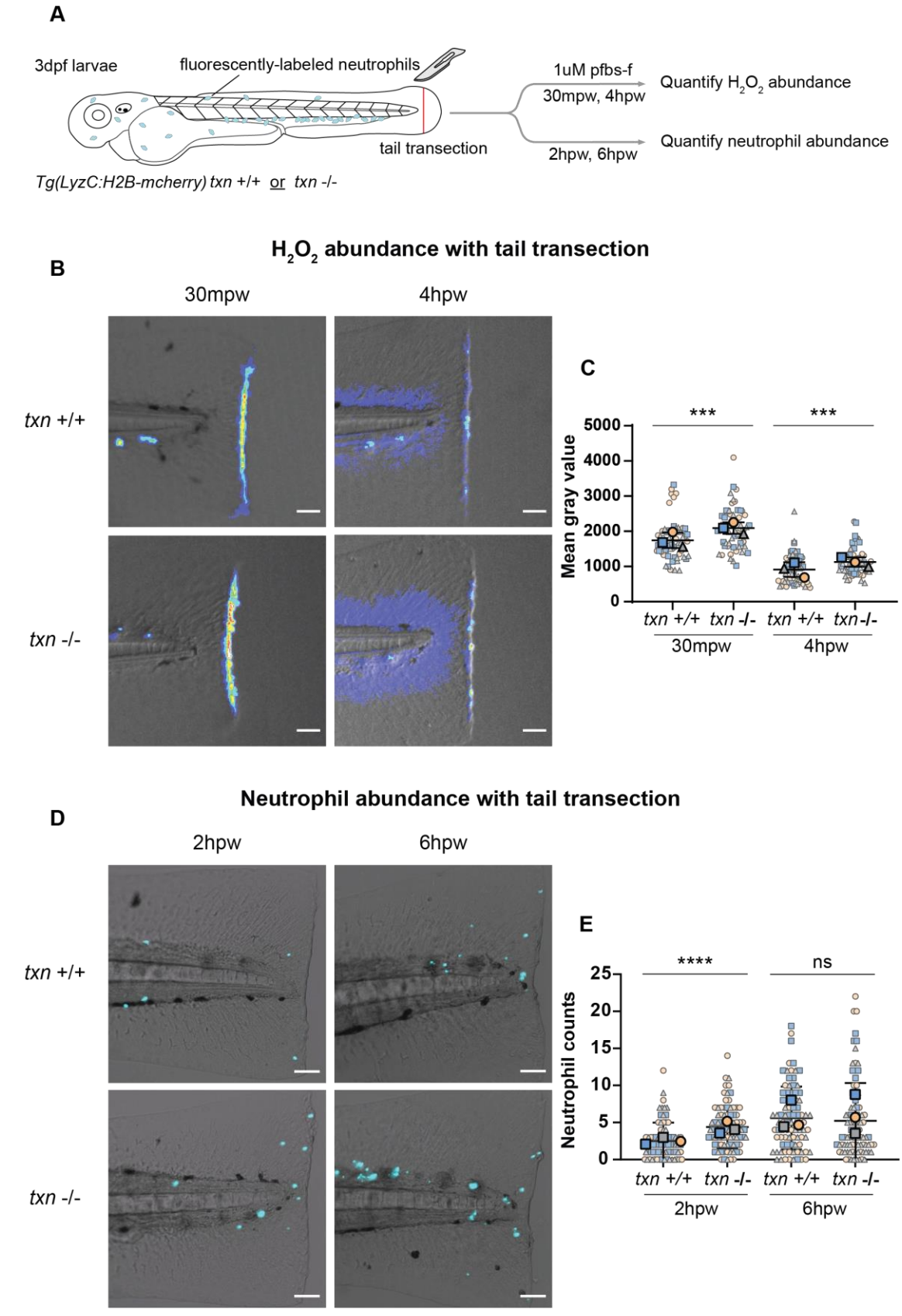
A
3dpf larvae
fluorescently-labeled neutrophils
tail transection
1uM pfbs-f
30mpw, 4hpw
Quantify H2O2 abundance
2hpw, 6hpw
Quantify neutrophil abundance
Tg(LyzC:H2B-mcherry) txn +/+ or txn -/-
H2O2 abundance with tail transection
B
30mpw
4hpw
txn +/+
txn -/-
C
Mean gray value
5000
4000
3000
2000
1000
0
***
***
txn +/+
txn -/-
txn +/+
txn -/-
30mpw
4hpw
Neutrophil abundance with tail transection
D
2hpw
6hpw
txn +/+
txn -/-
E
Neutrophil counts
25
20
15
10
5
0
****
ns
txn +/+
txn -/-
txn +/+
txn -/-
2hpw
6hpw

Thioredoxin inhibits neutrophil recruitment and retention around transformed keratinocytes

We next assessed the role of thioredoxin in inflammatory signaling and neutrophil recruitment to transformed cells. In an attempt to improve larval survival and increase sample size, a variation of the HRas model (Fig. 1a) was adopted in which the constitutively-active $KRas^{G12V}$ is driven under the basal keratinocyte promoter, krtt1c19e (Fig. 8a). Similar to the HRas model in superficial, krt4-expressing keratinocytes; neutrophils were more abundant around $KRas^{G12V}$-expressing basal keratinocytes and made frequent contact with transformed cells (Fig. 8b,c).

Fig. 8 – **Basal keratinocyte Ras^{G12V}-transformation model** A) Schematic of microinjection procedure. One cell stage *Tg(LyzC:H2B-mcherry)* embryos are injected with control (pTol2-krtt1c19e-KRas-mcherry) or transformation (pTol2-krtt1c19e-$KRas^{G12V}$-mcherry) constructs. 3dpf larvae present with chimeric expression of KRas variant in basal keratinocytes. B) Neutrophil (blue) recruitment around wildtype- or constitutively active $KRas^{G12V}$-expressing cells (magenta). Quantification of neutrophil abundance in KRas wt-injected (n=14) and $KRas^{G12V}$-injected (n=31) larvae. Scale bar, 20uM. Bolded shapes indicate average value per technical replicate, with shaded values representing data points from independent larvae. Samples were analyzed for statistical significance via t-test ($p<0.05$ *).

Fig.8

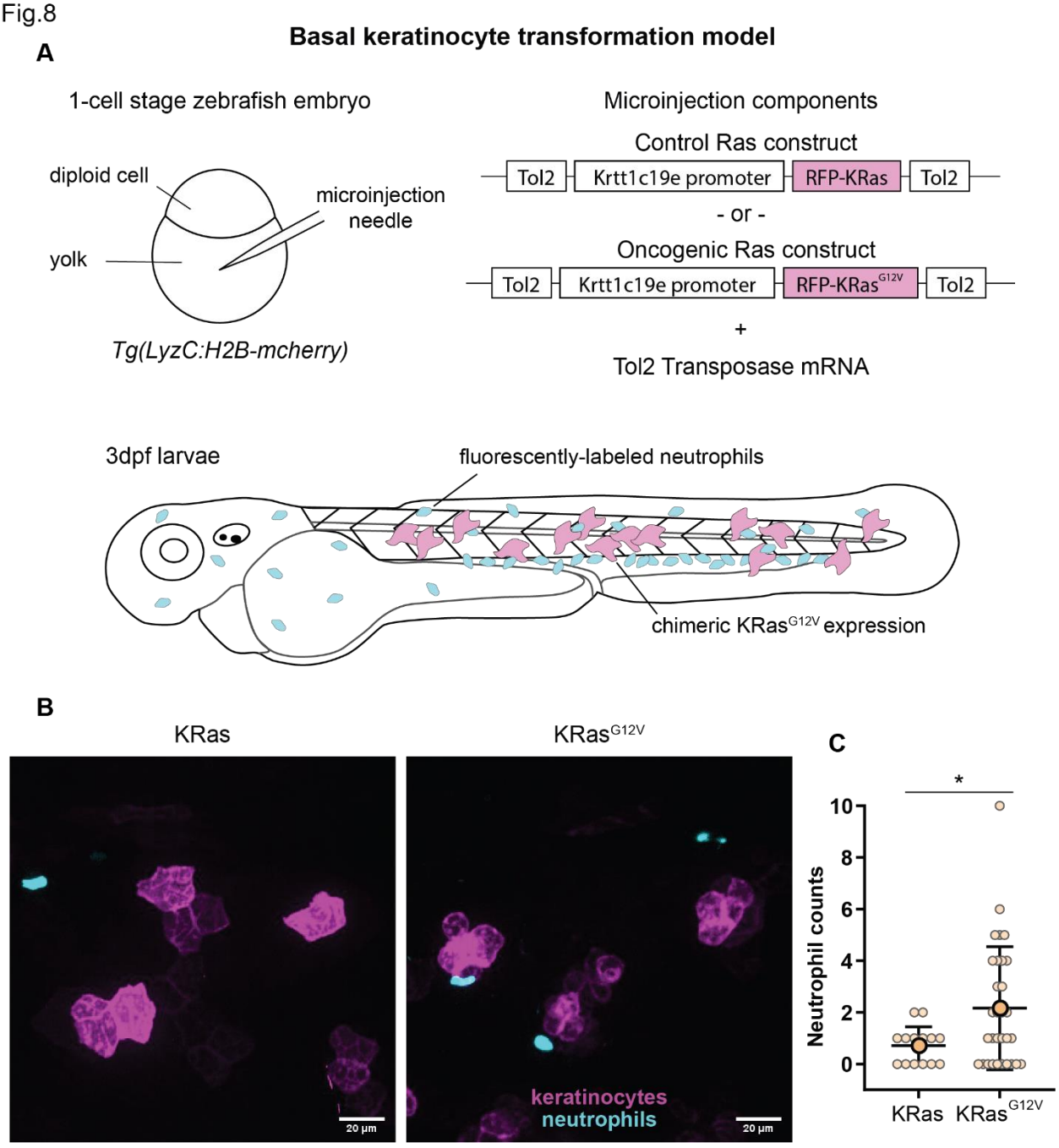

We observed basal transformed keratinocytes recruited more neutrophils in the *txn* mutant background, with neutrophil abundance increased by roughly 60% (Fig. 9a,b). In wildtype larvae, neutrophils migrate faster on average when not in direct contact with transformed cells, often accelerating as they leave and decelerating as they enter physical

contact distance (Fig. 9c,d). In *txn* mutant larvae, neutrophil speed on average is unchanged between the contact and non-contact states (Fig. 9c,d). The average speed of all neutrophils in *txn* mutant larvae, regardless of contact status, was similar in magnitude to the reduced neutrophil speed observed in wildtype larvae with direct transformed cell contact. (Fig. 9d). Therefore, neutrophil retention around transformed cells is likely enhanced in *txn* mutant larvae.

To assess changes in transformed cell gene expression that might explain this increase in neutrophil retention, TRAP was employed to isolate transcripts from transformed cells in the *txn* wildtype and mutant backgrounds. While no change in expression was observed for inflammatory cytokines *il1b*, *cxcl8a*, or *cxcl8b.1*; *tnfa* expression was elevated more than two fold in *txn*-deficient transformed cells (Fig. 9e). This finding suggests thioredoxin inhibits expression of at least one potent inflammatory cytokine within oncogene-expressing cells.

While we observed a statistically significant change in neutrophil speed when stratified by direct transformed cell contact (Fig. 9d), unstratified average neutrophil speed across was not significantly altered with *txn* loss-of-function, though a trend toward decreased average speed was observed in *txn*-deficient larvae (Fig. 10a,b). Additionally, neutrophil random migration speed in untreated larvae was not significantly altered between *txn* mutants and wildtype, though a trend toward an increase in average basal speed was observed (Fig. 10c,d).

Fig.9

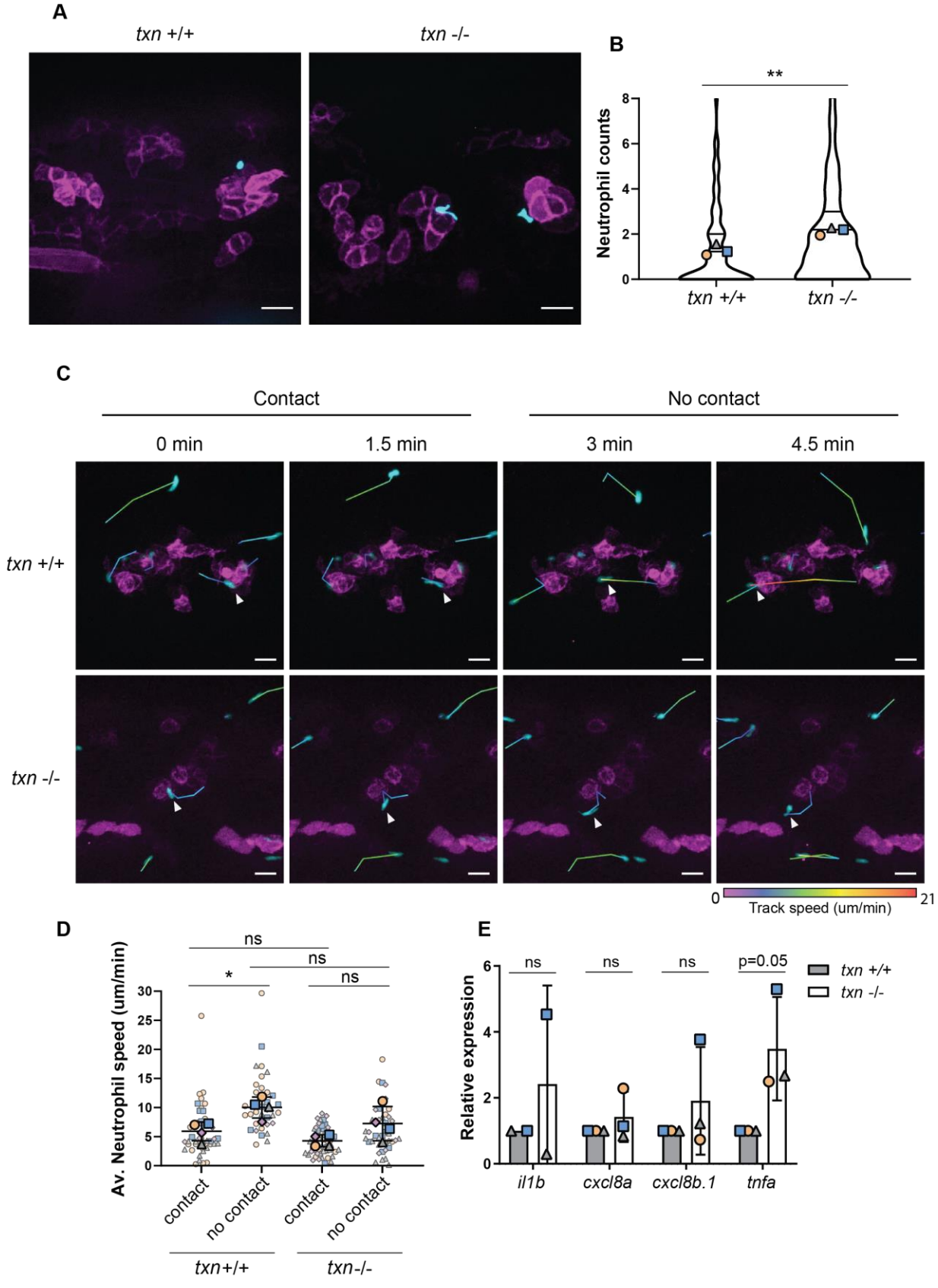
A
txn +/+
txn -/-
B
**
Neutrophil counts
txn +/+
txn -/-
C
Contact
No contact
0 min
1.5 min
3 min
4.5 min
txn +/+
txn -/-
0
Track speed (um/min)
21
D
ns
ns
*
ns
Av. Neutrophil speed (um/min)
contact
no contact
contact
no contact
txn+/+
txn-/-
E
ns
ns
ns
p=0.05
txn +/+
txn -/-
Relative expression
il1b
cxcl8a
cxcl8b.1
tnfa

Fig. 9 – **Thioredoxin inhibits neutrophil recruitment and retention around transformed keratinocytes** A) Neutrophil (blue) recruitment around $KRas^{G12V}$-expressing basal keratinocytes (magenta) in *txn*$^{+/+}$ Tg(*LyzC*:*H2B-mcherry*) or *txn*$^{-/-}$Tg(*LyzC*:*H2B-mcherry*) larvae 3dpf. B) Quantification of neutrophil abundance in *txn* wt (n=74) and mutant (n=116) larvae. C) Stills from live imaging of neutrophil behavior around $KRas^{G12V}$-expressing cells in *txn* wt and mutant larvae. Arrows track the same neutrophil across frames (1.5min/frame) and track color delineates instantaneous neutrophil velocity. D) Quantification of average neutrophil speed when in contact or not in contact with $KRas^{G12V}$-expressing basal cells (wt n=4, mut n=4). E) TRAP-qPCR of $KRas^{G12V}$-expressing genes assessing inflammatory cytokines *il1b*, *cxcl8a*, *cxcl8b.1*, *tnfa* (pool, 30 larvae/replicate, wt n=3, mut n=3). Scale bar, 10uM. Bolded shapes indicate average value per technical replicate, with shaded values representing data points from independent larvae. Samples were analyzed for statistical significance by Mann-Whitney U test (B) and t-test (D,E) ($p<0.05$ *, $p<0.01$ **).

Fig. 10 – **Thioredoxin loss may reduce average neutrophil speed and does not affect random migration speed in unstimulated larvae** A) Neutrophil average migration speed around $KRas^{G12V}$-expressing basal keratinocytes (magenta) in *txn*$^{+/+}$ Tg(*LyzC*:*H2B-mcherry*) or *txn*$^{-/-}$Tg(*LyzC*:*H2B-mcherry*) larvae 3dpf. Track color indicates average velocity per neutrophil tracked. B) Quantification of average neutrophil speed in *txn* wt (n=4) and *txn* mut (n=4) larvae. C) Neutrophil random migration speed in the head region in unstimulated *txn*$^{+/+}$ Tg(*LyzC*:*H2B-mcherry*) or *txn*$^{-/-}$Tg(*LyzC*:*H2B-mcherry*) larvae 3dpf. Track color indicates average velocity per neutrophil tracked. D) Quantification of average neutrophil speed in *txn* wt (n=4) and *txn* mut (n=4) larvae. Scale bar, 10uM (A), 50uM (C). Bolded shapes indicate average value per technical replicate, with shaded values representing data points from independent larvae. Samples were analyzed for statistical significance via t-test.

Fig.10

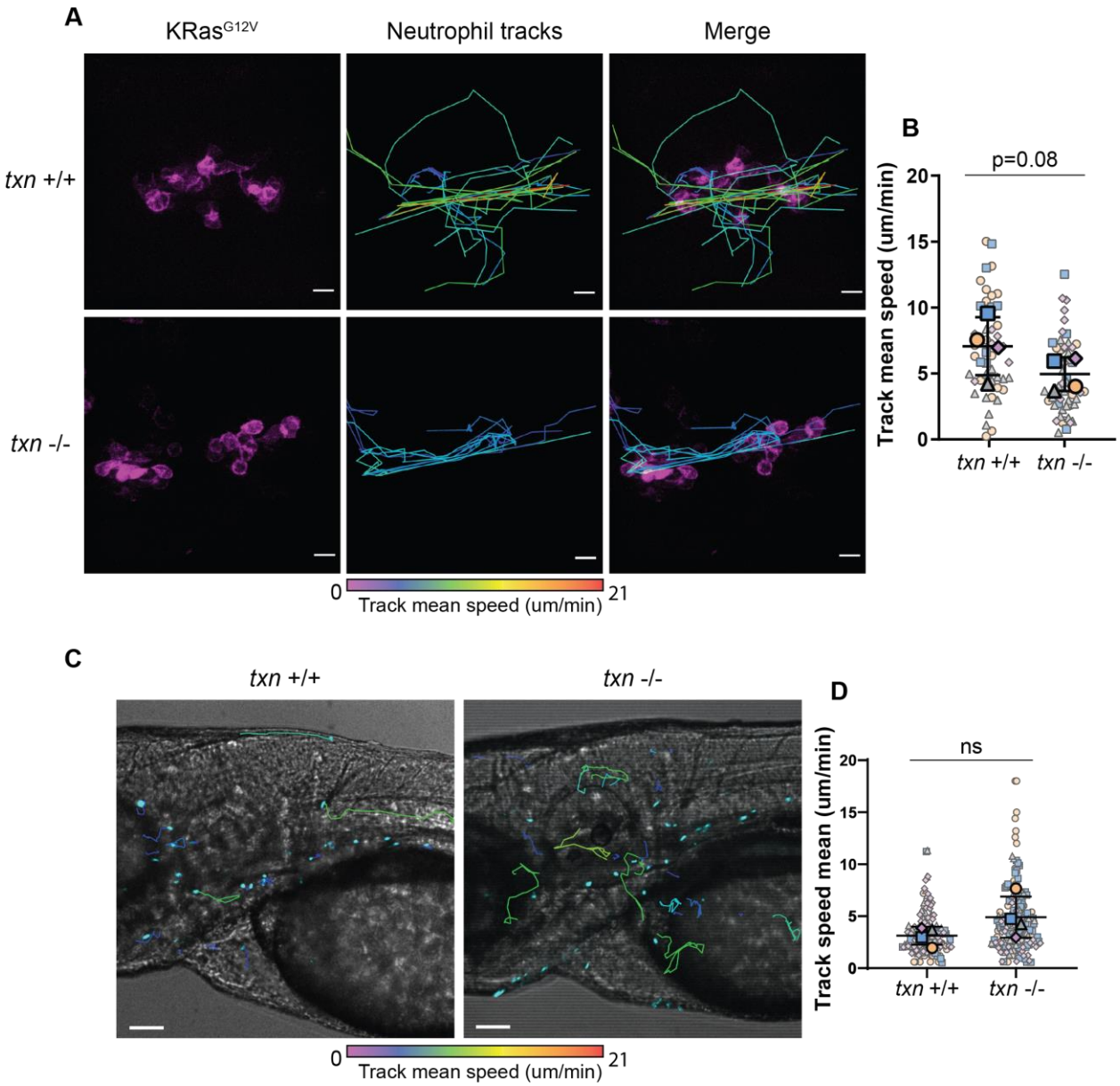

Thioredoxin does not significantly affect NF-κB reporter activity or intracellular redox status

With an increase in *tnfa* expression observed within transformed cells in *txn* mutant larvae, we sought to identify additional, transformed-cell intrinsic changes in inflammatory processes that may explain augmented neutrophil retention in *txn* mutants. To this end, we first utilized the NF-κB transgenic reporter model *Tg(NF-kB RE:GFP)* in which six NF-κB binding

sites are placed upstream of EGFP [135]. NF-κB reporter expression is strongly induced by infection with the filamentous fungus *Aspergillus fumigatus* [136] and within $KRas^{G12V}$-expressing basal keratinocytes (Fig. 11a). There was however no observable difference in EGFP expression level between *txn* wildtype and mutant larvae (Fig. 11a,b).

Another indicator of mitochondrial stress and inflammation is redox status which can be measured using the autofluorescent properties of cofactors FAD and NAD(P)H by two-photon excitation microscopy [137]. The ratio of reduced NAD(P)H to oxidized FAD yields the optical redox ratio (optical redox ratio = NAD(P)H/NAD(P)H + FAD) where values closer to one indicate a more reduced intracellular environment and values closer to zero indicate a more oxidized intracellular environment. Using this approach, we did not observe a significant change in intracellular transformed cell redox status with *txn* ablation (Fig. 11c,d). However, the data trend toward a slight decrease with *txn*-deficient transformed cells and further replicates are in order to determine the role of *txn* in regulating intracellular redox balance.

Fig. 11 – Thioredoxin does not significantly affect NF-κB reporter activity or intracellular redox status A) NF-κB reporter activity (white) in $KRas^{G12V}$-expressing basal keratinocytes (magenta) in $txn^{+/+}$ or $txn^{-/-}$ larvae 3dpf. B) Quantification of intracellular mean gray value txn wt (n=16) and mut (n=13) larvae normalized to wt average. C) Redox ratio of cofactors NAD(P)H and FAD within $KRas^{G12V}$-transformed basal keratinocytes in $txn^{+/+}$ or $txn^{-/-}$ larvae 3dpf. D) Quantification of average intracellular redox ratio per larvae in *txn* wt (n=18) and mut (n=19) larvae. Scale bar, 10um. Bolded shapes indicate average value per technical replicate, with shaded values representing data points from independent larvae. Samples were analyzed for statistical significance via t-test.

Fig.11

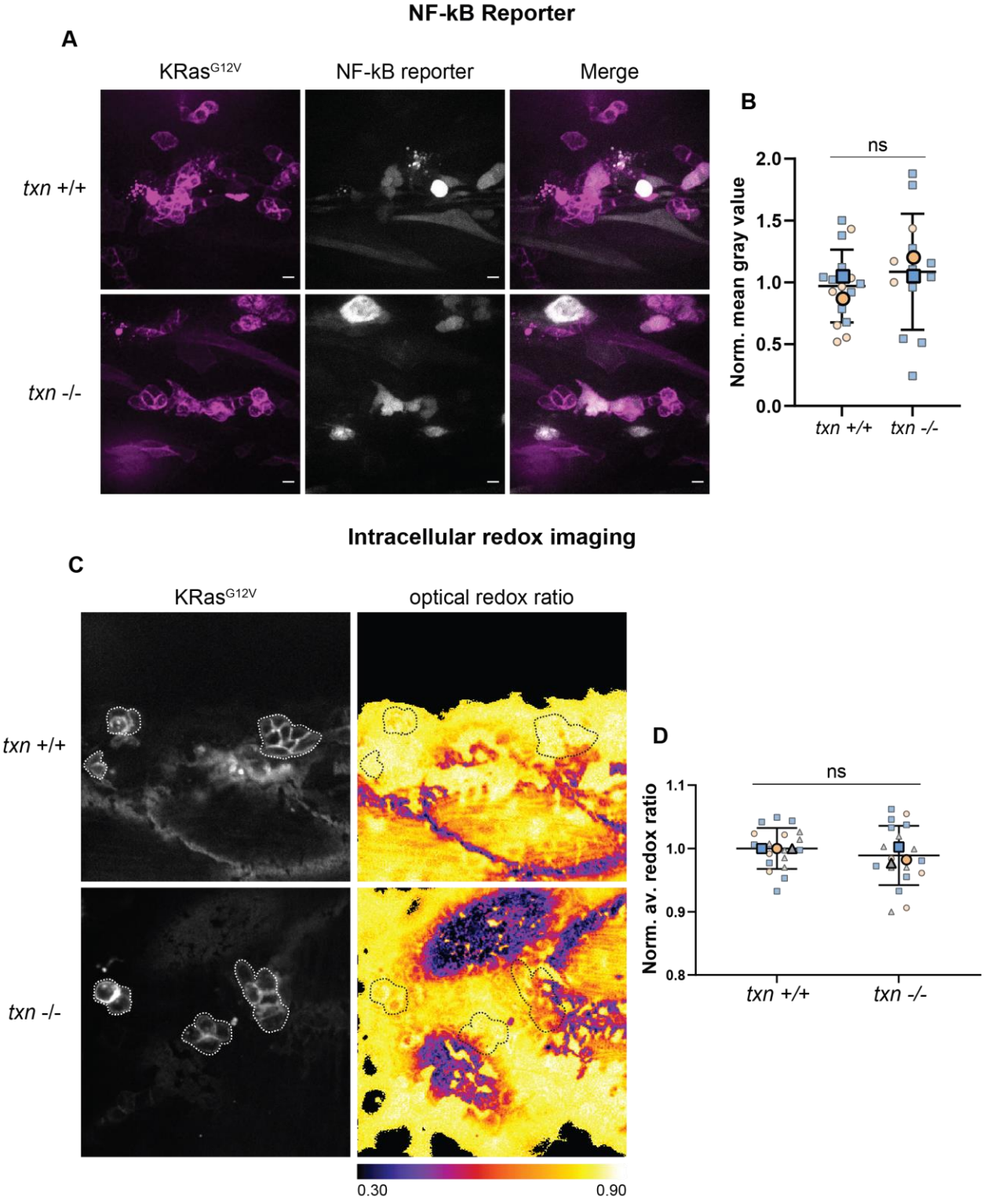
NF-kB Reporter
A
KRasG12V
NF-kB reporter
Merge
txn +/+
txn -/-
B
ns
Norm. mean gray value
2.0
1.5
1.0
0.5
0.0
txn +/+
txn -/-
Intracellular redox imaging
C
KRasG12V
optical redox ratio
txn +/+
txn -/-
0.30
0.90
D
ns
Norm. av. redox ratio
1.1
1.0
0.9
0.8
txn +/+
txn -/-

Thioredoxin promotes transformed cell apoptosis

With changes in neutrophil behavior observed in the *txn* mutant background, we wanted to assess the effect of *txn* on transformed cell fate, including apoptosis and proliferation. To assess apoptosis, immunofluorescence was employed targeting cleaved caspase-3. *txn* mutant transformed cells showed reduced caspase-3 staining compared to wildtype controls (Fig. 12a,b). These findings suggest thioredoxin promotes transformed cell apoptosis during tumor initiation.

Fig.12

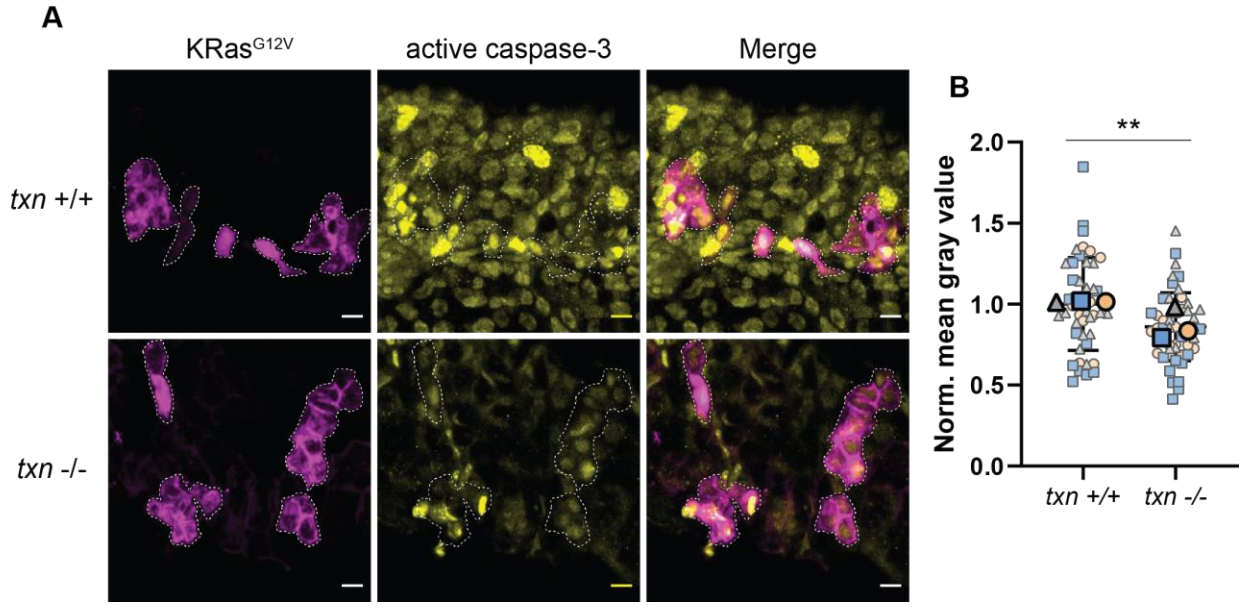

Fig. 12 –Thioredoxin promotes transformed cell apoptosis A) Cleaved caspase-3 immunofluorescence (yellow) in *txn*$^{+/+}$ or *txn*$^{-/-}$ larvae with KRas^{G12V}-expressing basal keratinocytes (magenta) 3dpf. B) Quantification of cleaved caspase-3 mean gray value in *txn* wt (n=45) and mutant (n=51) larvae normalized to wt average. Scale bar, 10um. Bolded shapes indicate average value per technical replicate, with shaded values representing data points from independent larvae. Samples were analyzed for statistical significance via t-test ($p<0.05$ *, $p<0.01$**, $p<0.001$***,$p<0.0001$****).

Neutrophils mediate increased transformed cell proliferation in the thioredoxin mutant

To determine the effect of *txn* on transformed cell fate, transformed cell proliferation was measured in *txn* wildtype and mutant backgrounds via Edu, a thymidine analog and probe for newly synthesized DNA. We observed transformed cells were more frequently Edu-positive in *txn* mutant larvae suggesting thioredoxin inhibits transformed cell proliferation *in vivo* (Fig. 13a,b).

We next sought to determine the role of neutrophils in this increased proliferation phenotype observed in *txn* mutant transformed cells. We utilized Tg(*mpx:Rac2*^{D57N}) larvae to inhibit neutrophil migration out of the vasculature and thus severely limit neutrophil migration to the transformed cell vicinity [132]. In this background, we observed a comparable frequency of Edu-positive transformed cells between *txn* wildtype and mutant larvae (Fig. 13c,d). Thus, neutrophils are responsible for mediating increased transformed cell proliferation in the *txn* mutant background.

Fig. 13 – **Neutrophils mediate increased transformed cell proliferation in the thioredoxin mutant** A) Edu staining (white) of neutrophil-sufficient *txn*$^{+/+}$ or *txn*$^{-/-}$ larvae with KRas^{G12V}-expressing basal keratinocytes (magenta) 3dpf. B) Quantification of frequency of Edu-positive KRas^{G12V}-expressing basal cells 3dpf in *txn* wt (n=35) and mutant (n=35) larvae. C) Edu staining (white) of neutrophil-deficient Tg(*mpx:Rac2*^{D57N}*-mcherry*) *txn*$^{+/+}$ and Tg(*mpx:Rac2*^{D57N}*-mcherry*) *txn*$^{-/-}$ larvae with KRas^{G12V}-expressing basal keratinocytes (magenta) 3dpf. D) Quantification of frequency of Edu-positive KRas^{G12V}-expressing basal cells 3dpf in *Rac2*^{D57N} *txn* wt (n=21) and *Rac2*^{D57N} *txn* mutant (n=22) larvae. Scale bar, 10um. Bolded shapes indicate average value per technical replicate, with shaded values representing data points from independent larvae. Samples were analyzed for statistical significance via t-test ($p<0.05$ *, $p<0.01$**, $p<0.001$***,$p<0.0001$****).

Fig.13

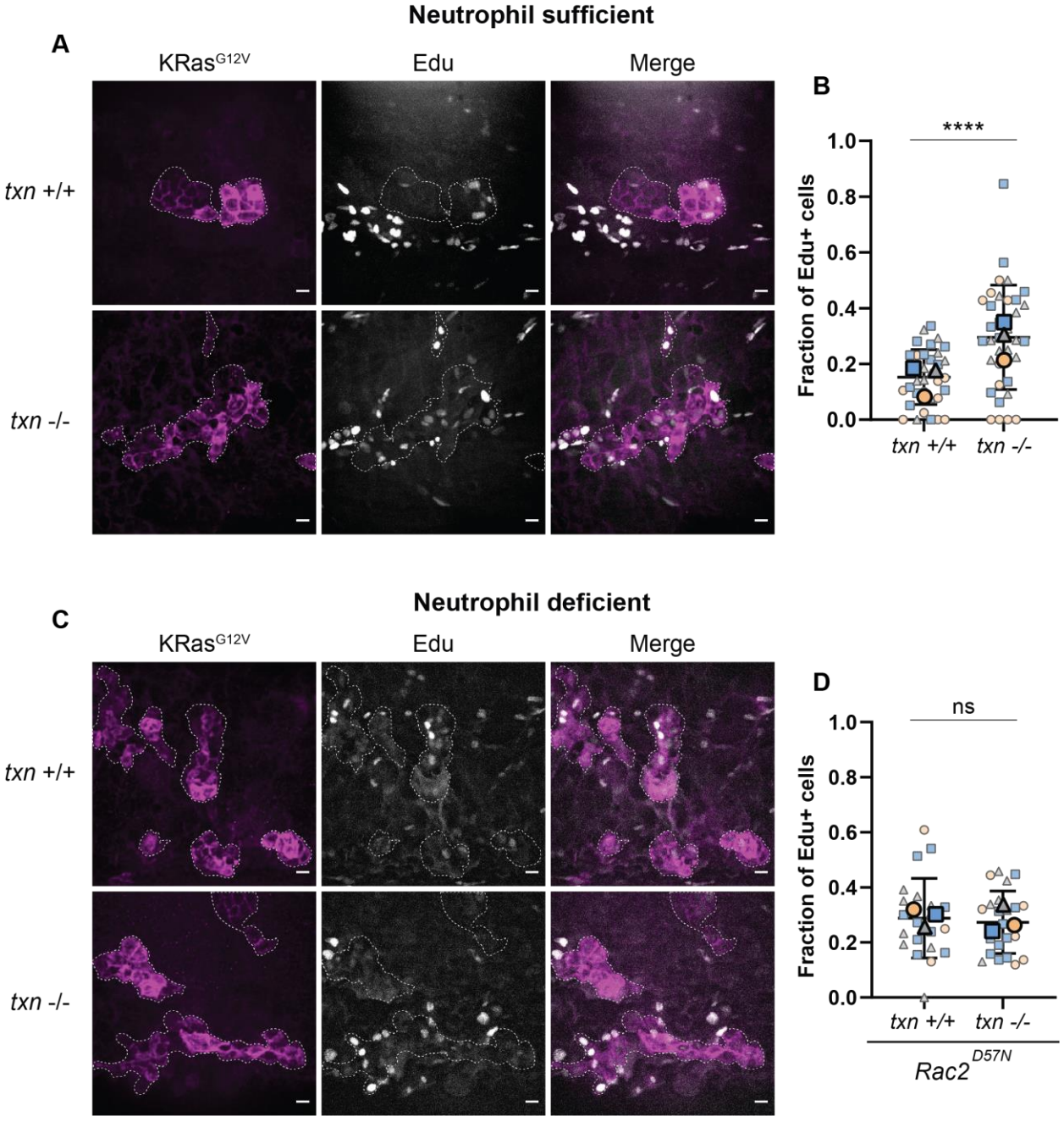
Neutrophil sufficient
A
KRasG12V
Edu
Merge
txn +/+
txn -/-
B
****
Fraction of Edu+ cells
1.0
0.8
0.6
0.4
0.2
0.0
txn +/+
txn -/-
Neutrophil deficient
C
KRasG12V
Edu
Merge
txn +/+
txn -/-
D
ns
Fraction of Edu+ cells
1.0
0.8
0.6
0.4
0.2
0.0
txn +/+
txn -/-
Rac2D57N

Discussion

Throughout this study, we investigated the role of various factors on neutrophil recruitment to Ras^{G12V}-transformed epithelial cells. We observed $KRas^{G12V}$ expression in superficial keratinocytes stimulated the production of mitochondrial ROS (Fig. 2a-d). We then went on to demonstrate mROS mediates neutrophil recruitment to $KRas^{G12V}$-transformed cells as mROS scavenging with the mitochondrially-targeted antioxidant, mitoTEMPO, decreased neutrophil abundance around transformed cells and increased transformed cell-neutrophil distance (Fig. 2e-g). While the production of mROS by Ras-transformed cells has been described [121, 122], we provide the novel finding of its role *in vivo* in eliciting neutrophil recruitment. As mentioned in the introduction to this chapter, mROS may play a direct or indirect role in neutrophil recruitment - further studies would need to be conducted to delineate this mechanism.

Interestingly, apart from stimulating an inflammatory response, several reports indicate mROS can activate autocrine proliferative signaling. Treatment of rat vascular smooth muscle cells with the antioxidant *N*-acetylcysteine decreased MAPK phosphorylation in response to PDGF [124]. A similar report in human epidermoid carcinoma cells found inhibiting ROS accumulation via introduction of catalase decreased EGFR phosphorylation in response to EGF [125]. These findings suggest ROS is an important intermediate in transmitting mitogenic signals from a variety of growth factors. Thus, mROS appears to have both autocrine and paracrine methods of promoting proliferation, via stimulation of growth-factor signaling pathways and recruitment of proliferation-inducing neutrophils, respectively.

We continued our search for factors that influence neutrophil recruitment by conducting a tissue-specific RNA sequencing experiment outlined in Figure 3a-c. To reiterate, this method utilized GFP-tagged ribosomes expressed specifically within Ras-expressing keratinocytes, neutrophils, or macrophages in conjunction with immunoprecipitation and RNA-sequencing to generate gene expression profiles from these three cell types found in the transformed-cell microenvironment. Several inflammatory pathways including IL6-Jak-Stat3-signaling, Tnfα-signaling-via-NF-κB, and reactive-oxygen-species-pathways were enriched in the three cell types assessed in response to $HRas^{G12V}$ expression in keratinocytes (Fig. 4b). The concept of an inflammatory microenvironment in cancer is well established [138]. Tumor cells have been shown to upregulate inflammatory signaling pathways including NF-κB and Stat3 within infiltrating immune cells, thus augmenting cytokine production and exacerbating inflammation [33]. Our findings that several cell-types in the transformed cell microenvironment activate inflammatory pathways expand this principle and suggest the inflammatory microenvironment is established from the onset of transformation.

Among the 50 genes significantly upregulated in $HRas^{G12V}$-expressing keratinocytes, the antioxidant thioredoxin (*txn*) was upregulated roughly five-fold over control keratinocytes (Fig. 5b,c). This finding recapitulates observations *in vitro* in which Ras-induced transformation upregulates several antioxidant genes essential in providing protection from exogenous H_2O_2 [139]. The authors argued continuous proliferative signaling via Ras^{G12V} increases mitochondrial metabolic stress producing excess ROS as a result. Antioxidant gene upregulation in this context thus confers a protective function against transformation-induced ROS accumulation. Curiously, while many human tumors produce elevated levels of ROS [80], some express

antioxidants below normal levels. For instance, prostate cancers were shown to harbor reduced superoxide dismutase (SOD1 and SOD2) and catalase expression compared to normal prostate tissue [140]. One study supported these findings, showing decreased antioxidant expression in several cancers, but notably increased SOD and catalase expression in adenocarcinomas [141]. Thus, antioxidant gene expression may only be upregulated in certain cancer types, perhaps those of epithelial origin. Regardless, we believe our observation that elevated *txn* expression in Ras-transformed zebrafish keratinocytes reflects the human situation, as *txn* expression is elevated in many human carcinomas (Fig. 5d).

While the role of thioredoxin as an antioxidant is well established, its function in inflammatory signaling and tumor development is controversial, with pro- and anti-inflammatory and tumorigenic processes reported [111, 113, 142-144]. We therefore set out to ascertain the role of elevated *txn* in transformed cell growth and inflammation.

In pursuit of this goal, we first generated a global genetic *txn* knockout in zebrafish via CRISPR-Cas9 (Fig. 6a). *txn* mutant larvae did not express full-length Txn protein and displayed no noticeable basal increase in inflammatory gene expression (Fig. 6b,c). Mutants were also morphologically normal and developed similar neutrophil numbers compared to wildtype larvae (Fig. 6d,e).

In response to a wound, *txn* mutant larvae displayed elevated H_2O_2 and neutrophil abundance at the wound site (Fig. 7b-e). As discussed in the introduction, H_2O_2 is produced in response to tissue damage by the enzyme Duox [127]. As an antioxidant, thioredoxin is presumably catalyzing the turnover of H_2O_2. Indeed, thioredoxin can reduce peroxiredoxins,

enzymes capable of metabolizing H_2O_2, and could in this way limit the ROS burden generated at sites of injury [109]. Based on the well-established role of ROS as a neutrophil chemoattractant [92, 126, 127, 145], *txn* likely inhibits neutrophil recruitment to wounds by reducing the buildup of H_2O_2.

Seeing as *txn* inhibited neutrophil recruitment to a wound, we next sought to determine the role of *txn* in neutrophil recruitment to $KRas^{G12V}$-transformed basal keratinocytes. As in the context of a wound, we observed elevated neutrophil numbers in the transformed-cell microenvironment in *txn* mutant larvae (Fig. 9a,b). We also observed in *txn* mutants decreased neutrophil speed in the transformed cell microenvironment and increased *tnfa* expression within transformed cells, both of which indicate an enhanced inflammatory microenvironment in the absence of thioredoxin (Fig. 9c-e).

Thioredoxin may inhibit inflammatory signaling by directly reducing ROS accumulation or by dampening inflammatory signaling pathways. One study in mice depleted serum of *txn* and reported reduced neutrophil chemotaxis in response to LPS [146]. Due to technical limitations with the three ROS probes (pfbs-f, CellRox, and mitoSOX), we were unable to assess the relative abundance of ROS within basal transformed cells or the microenvironment in *txn* mutants, possibly due to minimal penetration of these compounds to the basal keratinocyte layer. As with wounding, *txn* may inhibit H_2O_2 accumulation in Ras-transformed cells and thereby directly limit levels of this known neutrophil chemoattractant. Alternatively, *txn* may inhibit inflammatory cytokine expression and subsequent leukocyte recruitment. Indeed, overexpression of thioredoxin in HeLa cells inhibited NF-κB activation, a transcription factor family commonly activated during inflammation [111]. Additionally, we observe increased *tnfa*

expression in transformed cells in *txn* mutants suggesting increased neutrophil recruitment in this context is not exclusively driven by direct H_2O_2 signaling.

While thioredoxin appears to have inhibitory effects on inflammation in the context of transformation, several studies conflict with this finding suggesting thioredoxin induces inflammatory gene expression, possibly by stimulating NF-κB DNA binding [143] or transactivation [142]. Additionally, exogenous thioredoxin upregulated *tnfa* expression *in vitro* [144] as well as neutrophil chemotaxis both *in vitro* and *in vivo* [113]. Nevertheless, our data suggest thioredoxin, in the context of Ras-induced transformation *in vivo* is inhibitory to neutrophil recruitment as well as inflammatory gene expression, possibly due to exclusive intracellular localization.

Additionally, a reduction in neutrophil speed is consistent with a heightened inflammatory response, as neutrophils migrate slower upon arrival at a wound [147]. This effect could be mediated by Tnfα, as Tnfα has been shown to promote neutrophil arrest [148]. Attempts to delineate the role of Tnfα in the increased neutrophil retention phenotype observed in *txn* mutants were conducted by treating with the Tnfα secretion inhibitor pentoxifylline (PTX) (data not shown). We observed no obvious difference in neutrophil behavior around transformed cells with treatment in the *txn* background suggesting *tnfa* may not play a role in the inflammatory phenotype; however, data were deliberately excluded due to lack of a positive control for PTX. Nevertheless, thioredoxin inhibits neutrophil homing and retention around transformed cells, mostly likely via a combination of direct and indirect mechanisms through ROS and cytokine expression, respectively.

Attempts to identify additional inflammatory changes within transformed cells in the *txn* background were inconclusive. NF-κB reporter activity within transformed cells was unchanged in the absence of *txn* (Fig. 11a,b). That said, EGFP expression levels were inherently highly variable within a given condition. This high intrinsic variability, relatively low sample size, and slight trend toward an increase in NF-κB activity in *txn* mutants warrant additional replicates.

Metabolic imaging of redox sensitive cofactors NAD(P)H and FAD was employed to assess intracellular redox status in transformed cells, in lieu of the alternative ROS probes discussed above. From the literature, $KRas^{G12V}$ expression has been shown to induce mitochondrial stress by decreasing transmembrane potential and increasing ROS production [149]. We hypothesized this increased mitochondrial stress and ROS production would oxidize the intracellular environment of transformed cells. Thus, we expected a higher proportion of the oxidized forms of NAD(P)H and FAD and therefore a reduced intracellular redox ratio (optical redox ratio = NAD(P)H/NAD(P)H + FAD) within *txn* mutant transformed cells. Our finding however indicated that *txn* did not significantly alter intracellular redox status in transformed cells (Fig. 11c,d). As with the NF-κB reporter experiments, sample size was low and a trend of slight reduction in redox status existed in *txn* mutant larvae. This finding, in conjunction with the negligible ROS signal observed with pfbs-f, CellRox, and mitoSOX, presents the interesting possibility that the enhanced inflammatory environment around basal transformed keratinocytes operates independent of ROS. Further experimentation is necessary to determine if ROS levels are indeed affected by constitutive Ras activation in basal keratinocytes and the role of ROS, if present, on neutrophil recruitment in this context.

We next assessed the role of thioredoxin in transformed apoptosis and discovered decreased active caspase-3 staining within transformed cells in the *txn* mutant background (Fig. 12a,b). This observation conflicts with reports *in vitro* in which thioredoxin has also been reported to inhibit apoptosis, likely through direct binding and inhibition of ASK1 [112, 150]. Clearly, thioredoxin has differing mechanisms of action *in vitro* and *in vivo* suggesting additional cell types play a role in thioredoxin function. However, we report thioredoxin appears to promote apoptosis in transformed cells early in tumorigenesis.

Lastly, we investigated the role of thioredoxin on transformed cell proliferation and observed increased Edu-incorporation frequency in *txn* mutant transformed cells (Fig. 13a,b). When neutrophil migration was inhibited via expression of dominant-negative $Rac2^{D57N}$, transformed cells proliferation was equivalent between *txn* wildtype and mutant larvae (Fig. 13c,d). Thus, neutrophils mediate increased transformed cell proliferation in the *txn* mutant background. Given the observation that neutrophils promote transformed cell growth [119, 123, 132], it follows that increased neutrophil abundance and prolonged time spent in the transformed cell microenvironment would presumably amplify any neutrophil-derived proliferative signals.

Curiously, these findings contradict many published results on the effect of thioredoxin on cell growth and survival. Exogenous thioredoxin overexpression *in vitro* promotes fibroblast growth [151, 152] whereas dominant-negative $Txn^{C32S/C35S}$ expression inhibits growth [151]. Thioredoxin has been shown to promote AP-1 transcription factor activity, important in cell-cycle progression, via the intermediate Ref-1 [153] likely by stimulating AP-1 DNA-binding [154]. Interestingly, these *in vitro* findings are only partially recapitulated *in vivo*, as thioredoxin

overexpression reduced tumor growth; however, not as severely as with dominant-negative expression [154].

In conclusion, thioredoxin appears to act as a tumor suppressor at early stages of tumorigenesis. Thioredoxin inhibits neutrophil recruitment and retention around $KRas^{G12V}$-transformed cells and impairs neutrophil-mediated proliferation. This result presents an interesting correlation between neutrophil migratory behavior and transformed cell growth.

In the next chapter, we address two unanswered facets of the role of thioredoxin in transformed cell growth and inflammation. The first aim is to identify the cell type within which thioredoxin affects transformed cell growth. The experiments conducted in this chapter utilize a global *txn* knockout which precludes identification of cell type-specific roles. The second aim is to determine the role of thioredoxin at later stages in tumorigenesis, beyond the initial transformation event. While we report a tumor suppressive role at early stages of transformation, several studies suggest thioredoxin is essential for tumor growth at later stages. We are therefore interested in discerning if thioredoxin switches from an anti- to pro-tumor function during the course of tumor development.

Methods

Zebrafish maintenance and $txn^{-/-}$ line generation

Zebrafish lines were maintained as previously described (Vincent *et al.* 2016). To generate $txn^{-/-}$ line, 400pg Cas9 protein (PNA Bio, CP01-50) and 200pg gRNA targeting *txn* exon II were microinjected into one-cell stage NHGRI-1 background. gRNA primers (table) and PCR was conducted according to CRISPRscan method [155] and gRNA was synthesized *in vitro* using HiScribe T7 kit (NEB, E2050S) and purified using *mir*Vana miRNA Isolation kit (ThermoFisher,

AM1561). CRISPR efficacy in 3dpf F_0 chimeras was assessed via Indel Detection and Amplicon Analysis (IDAA) using the gDNA extraction protocol described above. F_0 chimeras were raised to adulthood and a 1bp insertion was identified via IDAA in F_1 progeny indicating germline mutation of *txn* in the F_0 generation. The gRNA target region was cloned using the TOPO TA Cloning kit (Life Technologies, 450030) and sequenced via Sanger sequencing (Functional Biosciences) confirming a 1bp insertion in *txn* exon II. F_1 *txn* heterozygotes were genotyped via PCR followed by AlwNI restriction enzyme digestion (NEB, 101229-066) following gDNA extraction of adult fin-clips. *txn*$^{-/-}$ and *Tg(LyzC:H2B-mcherry) txn*$^{-/-}$ lines were generated via incrossing and screened using the *txn* genotyping protocol above.

To generate an anti-*txn* antibody, full-length zebrafish *txn* was cloned into pTrcHis and expressed in BL21 *E. coli*. His-tagged *txn* was extracted from bacterial lysates using nickel-nitrilotriacetic acid (Ni-NTA) resin (Qiagen, 30410) and subsequently used for anti-sera production in rabbits (Covance). Txn protein depletion was confirmed via Western blot using lysates from 30 *txn*$^{+/+}$ or *txn*$^{-/-}$ larvae 3dpf. Briefly, larvae were manually deyolked via pipette aspiration in Ca^{2+}-free Ringer's solution and lysate generated via sonication in lysis buffer (20mM Tris pH 7.6, 0.1% Triton X-100, 0.2mM phenylmethylsulfonyl fluoride (PMSF), 1µg/ml Pepstatin, 2µg/ml Aprotinin, 1µg/ml Leupeptin). Lysates were clarified via centrifugation and loaded on a 6-20% SDS-polyacrylamide gel prior to transfer to nitrocellulose and probing with anti-*txn* antisera.

<u>Plasmid construction and microinjection</u>

pTol2-krt4-RFP-HRas, pTol2-krt4-RFP-HRas^{G12V}, and pTol2-krt4-L10a-EGFP constructs used in TRAP RNA-sequencing experiment were generated as previously described [132]. PCR inserts containing the gene of interest and digested vector were fused using In-Fusion HD cloning kit (Clontech, 638911). All constructs microinjected contained Tol2 transposable elements thus allowing incorporation of the relevant promoter and gene-of-interest into the zebrafish genome.

Embryos at 1-cell stage were microinjected as previously described [132] with 3nl injection mix containing 37.5ng relevant plasmid, indicated in figure legend, and 52.5ng *tol2* mRNA. Injected embryos were incubated at 28.5°C in E3 media (5mM NaCl, 0.17mM KCl, 0.33mM $CaCl_2$, 0.33mM $MgSO_4$) containing 0.2mM N-phenylthiourea (PTU) to inhibit pigment formation (Sigma, P7629). Larvae were anesthetized with 0.2mg/ml Tricaine (Pentair, trs1) in E3 3dpf and screened for transgene expression using Zeiss Stereo Zoom Microscope.

Translating Ribosome Affinity Purification (TRAP)

Larvae were microinjected and screened 3dpf for transgene expression as described above. Microinjections for TRAP-RNA-sequencing included either control pTol2-krt4-RFP-HRas or oncogenic pTol2-krt4-RFP-HRas^{G12V} constructs injected with pTol2-krt4-GFP-L10a in wildtype larvae, or into *Tg(LyzC:EGFP-L10a)* or *Tg(mpeg1:EGFP-L10a)* larvae [156] for keratinocyte, neutrophil, or macrophage-specific expression profiling, respectively. For TRAP-qPCR experiments, control pTol2-krtt1c19e-mcherry-KRas or oncogenic pTol2-krtt1c19e-mcherry-KRas^{G12V} was injected into *txn*$^{+/+}$ or *txn*$^{-/-}$ larvae in conjunction with the TRAP construct pTol2-krtt1c19e-EGFP-L10a. Following microinjection, larvae were screened for transgene expression

3dpf and subsequently stored at -80°C in minimal residual media. The TRAP lysis and ribosome immunoprecipitation procedure was conducted as previously reported [156] using 50 larvae per condition per replicate. Immunoprecipitated mRNA was extracted from polysomes following Trizol (ThermoFisher, 15596026) manufacturer recommendations. 70% ethanol was added to the aqueous layer at 1:1 ratio and mRNA was purified using the RNAqueous Micro kit (ThermoFisher, AM1931).

RNA sequencing and analysis

cDNA libraries were generated from aforementioned TRAP samples as previously described [157] and sequenced on an Illumina HiSeq system. An average of 23 million single-end reads were generated and aligned to zebrafish reference genome GRCz10 using Bowtie v1.1.1. Transcript abundance was quantified using RSEM v1.2.20 and differential expression between conditions was assessed using DESeq2. Zebrafish genes were matched to human orthologs using BioMart and Hallmark gene set differences assessed via Gene Set Enrichment Analysis [158](Subramanian *et al.* 2015).

Txn transcript levels in human tumors samples from The Cancer Genome Atlas (TCGA) were assessed using Firebrowse (http://firebrowse.org/).

qPCR

mRNA isolated via TRAP was DNAse treated (Promega, M6101) for 30 min at 37°C. cDNA was synthesized using SuperScript III First-Strand Synthesis kit (ThermoFisher, 18080051) according to manufacturer specifications. Sybr green (check freezer for specs) qPCR master mix was used to quantify *il1b*, *cxcl8a*, *cxcl8b.1*, and *tnfa* gene expression in addition to *rps11*

expression as a normalization control (primer table). qPCR reactions were run on a Roche Lightcycler with the following reaction conditions:. Cq values were quantified from Lightcycler software and normalized to housekeeping gene *rps11*.

Live Imaging of neutrophil behavior and NAD(P)H/FAD abundance

Neutrophil behavior in response to basal transformation was carried out in LyzC-H2B-mcherry *txn* mutant lines. These lines were injected with pTol2-krtt1c19e-KRasG12V-GFP as described. Locations with 30-40 transformed cells within the FOV of 40x objective were selected. Timelapse images were taken at 90 second intervals for 2.5 hours on a Zeiss spinning disk confocal microscope. Neutrophils were tracked with Imaris and track speed was calculated.

Neutrophil random migration was assessed in unstimulated LyzC-H2B-mcherry *txn* wildtype and mutant lines. Timelapse images were taken at 90 second intervals for 2.5 hours using a 10x objective on a Zeiss spinning disk confocal microscope. Neutrophils were tracked with Imaris and mean track speed was calculated.

Analysis of NAD(P)H and FAD cofactor abundance was conducted as previously described using two-photon fluorescence microscopy [159].

Tail transection assays – pfbs-f ROS probe and neutrophil recruitment

Hydrogen peroxide abundance was assessed with the probe pentafluorobenzenesulfonyl fluorescein (pfbs-f) (Santa Cruz, sc-205429). Tail transection was conducted 3dpf as previously described (ref) in a solution of 1uM pfbs-f and 0.2mg/ml Tricaine

in E3. 30 minutes post-wound (mpw) and 4 hours post-wound (hpw), transected tails were imaged at 20x magnification via spinning disk confocal microscopy. Pfbs-f mean gray value was quantified from maximum intensity projections in an outlined region-of-interest posterior to the notochord extending to and encompassing the wound margin.

To assess neutrophil abundance, *Tg(LyzC:H2B-mcherry) txn*$^{+/+}$ and *Tg(LyzC:H2B-mcherry) txn*$^{-/-}$ larvae 3dpf were wounded as above in 0.2mg/ml Tricaine in E3. Neutrophil abundance posterior to the notochord was assessed 2hpw and 6hpw via spinning disk confocal microscopy at 20x magnification.

Edu proliferation assay and Immunofluorescence

pTol2-krtt1c19e-KRas^{G12V} injected *txn*$^{+/+}$ or *txn*$^{-/-}$ larvae were treated with 250uM Edu (ThermoFisher, C10338) for 6.5hrs at 28°C in E3 + PTU 3dpf. Larvae were fixed in formaldehyde buffer (100mM PIPES, 1mM $MgSO_4$, 2mM EGTA, 1.5% formaldehyde, 0.2mg/ml Tricaine) in E3 and stored at 4°C. Fixation buffer was exchanged for methanol and larvae were placed at -20°C overnight. Samples were rehydrated in a sequence of methanol dilutions (75% methanol:25% PBSTx (0.2% Triton X-100), 50% methanol:50% PBSTx, 25% methanol:75% PBSTx), washed in PBSTx, and blocked for 3 hours in blocking buffer (1.5% v/v sheep serum, 1% w/v BSA, 0.2% Triton X-100 in PBS) mixing via nutator. Alexa Fluor 555 azide conjugation was conducted according to Click-it manufacturer specifications (ThermoFisher, C10338) in 350µl at 4°C overnight on rocker. Samples were washed twice in PBSTx and blocked once in blocking buffer prior to primary rabbit α-GFP Ab treatment (ThermoFisher, A11122) in 350µl at 1:200 dilution in blocking buffer for 4 hours at room temperature. Antibody staining allowed for visualization

of GFP-KRas-expressing cells. Samples were washed twice in PBSTx and twice in blocking buffer and treated with secondary donkey α-rabbit AF488 (Jackson ImmunoResearch, 711-545-152) in 350ul at 1:250 dilution in blocking buffer overnight at 4°C. Samples were washed 6 times in PBSTx prior to imaging via confocal microscopy. Edu-positive cells were manually quantified in FIJI or Imaris.

Active caspase-3 staining was conducted as above, omitting Edu and Alexa Fluor 555 azide treatment. Primary antibody staining utilized rabbit α-active caspase-3 (BD Pharmingen, 559565) at 1:300 and secondary staining used donkey α-rabbit Dylight 405. Images were obtained via confocal microscopy and intracellular active caspase-3 mean gray value calculated in FIJI.

Statistical Analysis

Statistical analyses were performed on at least three independent experimental replicates, unless otherwise indicated in the figure legend. For all experiments except neutrophil speed assays, data points represent measurements from individual larvae. Replicate number is distinguished by differential data point color and shape, with the mean replicate value presented in bold. For neutrophil speed experiments, data points represent values from a given neutrophil, whereas bolded data points display the average neutrophil speed for a given larvae. Sample normality was assessed with Anderson-Darling and Shapiro-Wilk test ($p<0.05$). For normally and non-normally distributed data, statistical significance ($p<0.05$) was calculated by t-test or Mann-Whitney U test, respectively. Statistics were calculated in R version 3.6 and

graphed in GraphPad Prism version 9 using measurements from individual larvae as the sampling unit.

Chapter Three

Conclusions and Future Directions

Conclusions

Throughout this study, we have determined that thioredoxin (*txn*) acts as a tumor suppressor at early stages following Ras-induced transformation. In Figure 1, we present a model for the proposed mechanism of *txn*-mediated inhibition of transformed cell growth. From the TRAP-seq dataset in which we compared transcripts from HRas or $HRas^{G12V}$-expressing keratinocytes, we observed *txn* expression was upregulated roughly five-fold in response to constitutive HRas activation (Chapt. 2, Fig. 5b,c). We found a similar upregulation of *txn* in many human carcinomas indicating *txn* induction is not specific to zebrafish (Chapt. 2, Fig. 5d). After generating a *txn* knockout via CRISPR-Cas9 (Chapt. 2, Fig. 6a,b), we observed increased expression of the proinflammatory cytokine *tnfa* by $KRas^{G12V}$-transformed cells in the *txn* mutant (Chapt. 2, Fig. 9e). In accordance with increased cytokine expression, we found KRas-transformed cells recruited more neutrophils in the *txn* mutant background (Chapt. 2, Fig. 9a,b). Neutrophil retention around KRas-transformed cells was enhanced in the *txn* mutant, as their velocity remained low in the peri-transformed cell space (Chapt. 2, Fig. 9c,d). Thus, *txn* inhibits neutrophilic inflammation to transformed cells, possibly by inhibiting inflammatory cytokine expression within these cells.

We then showed transformed cells are more proliferative in the *txn*-mutant background (Chapt. 2, Fig. 13a,b). As neutrophils have been shown to enhance transformed cell growth in zebrafish [79, 119] and we observed increased neutrophil recruitment and retention in *txn* null larvae, we assessed the role of neutrophils in increased transformed cell growth in the *txn* mutant. Using $Rac2^{D57N}$ expressed in neutrophils to restrict their localization to the vasculature,

we found a rescue of transformed cell proliferation to wildtype levels (Chapt. 2, Fig. 13c,d). Therefore, neutrophils mediate increased transformed cell proliferation in *txn* mutants.

To delineate the role of transformed cell-specific expression of *txn* on neutrophil recruitment and proliferation, we used an exogenous melanoma (Zmel) injection model (Chapt. 3, Fig. 1). Zmel cells are sufficient for *txn*, and thus any observed differences between *txn* wildtype and null larvae must originate from a non-melanoma source. Using this model, we observed no change in neutrophil recruitment or melanoma mass volume 1dpi comparing *txn* wildtype and mutant larvae (Chapt. 3, Fig. 2a,b,c). This suggests *txn* produced by $KRas^{G12V}$-transformed cells is the primary source responsible for inhibiting neutrophil-mediated proliferation.

Lastly, and not summarized in the model figure (Fig. 1), we sought to determine the role of *txn* at later stages, as several reports indicate *txn* is essential for overt tumor growth [151, 154]. We used a model of β-catenin-driven hepatocellular carcinoma (HCC) (Chapt. 3, Fig. 4a,b) and observed *txn* inhibited liver growth at 6dpf but not 13dpf (Chapt. 3, Fig. 5a,b, Fig. 6. c,d). These results are preliminary, but they suggest *txn* may switch from a tumor-suppressive role early to a tumor-promoting role later in tumorigenesis.

Fig.1

Working model of *txn*-mediated growth inhibition of Ras-transformed cells

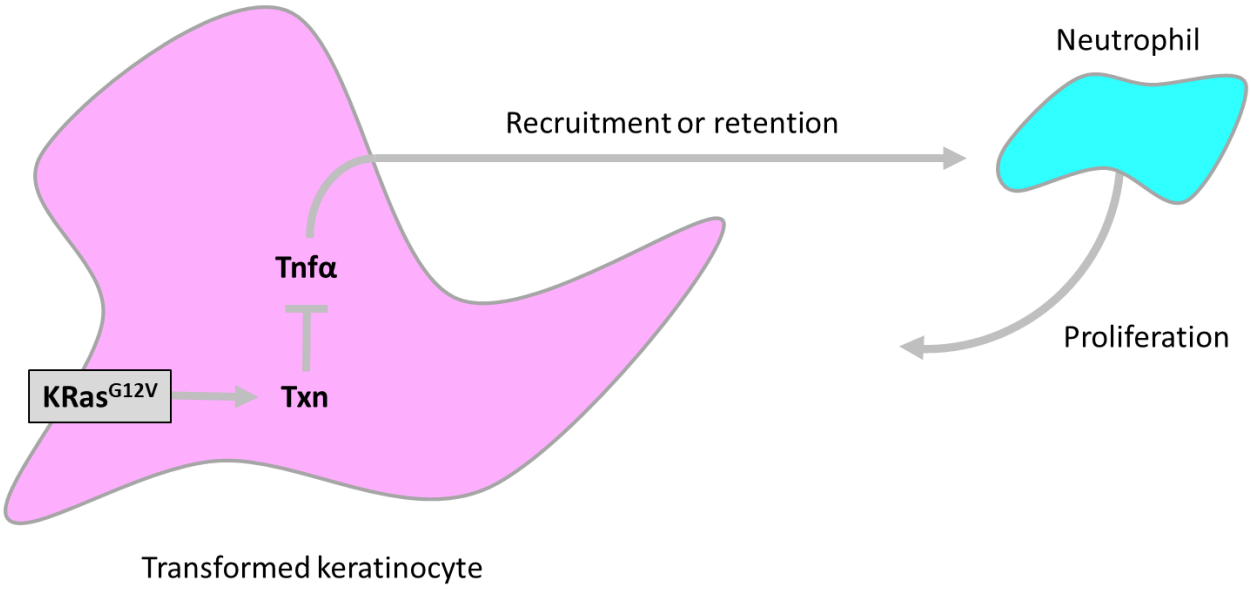

Future Directions

Does thioredoxin affect ROS production in transformed keratinocytes?

While we observed *txn* inhibited *tnfa* expression in transformed keratinocytes (Chapt. 2, Fig. 9e), its role in regulating transformed cell ROS and subsequent neutrophil recruitment has yet to be determined. We attempted to measure intracellular ROS using the panel of ROS probes discussed throughout this document including CellRox for intracellular ROS, mitoSOX for mitochondrial-localized ROS, and pfbs-f for intracellular H_2O_2. We failed to observe a detectable increase in either wildtype or *txn* mutant KRas^{G12V}-expressing basal keratinocytes over background (data not shown). While transformation in basal keratinocytes may not induce substantial ROS production, this seems unlikely as many cell types *in vitro* produce ROS

in response to constitutive Ras activation [120-122]. ROS production has also been observed in superficially transformed keratinocytes in zebrafish, both by us (Chapt. 2, Fig. 2a-d) and others [123]. One potential explanation for lack of a ROS signature could be limited penetration of ROS probes through the superficial to the basal keratinocyte layer. This scenario may be difficult to identify experimentally, but alternative measures could help delineate ROS levels in transformed cells. Repeating the metabolic characterization of NAD(P)H and FAD abundance in transformed keratinocytes may be informative as to the intracellular redox status within these cells. Indeed, we observed a trend toward decreased intracellular redox ratio within *txn* null transformed cells (Chapt. 2, Fig. 11c,d), suggesting the intracellular environment in the absence of *txn* may be more oxidized.

While ROS production may be difficult to assay in basal keratinocytes, the effect of ROS on neutrophil recruitment could still be addressed via treatment with antioxidants. For instance, mitoTEMPO could be used to inhibit accumulation of mitochondrial ROS (mROS). The most likely result would mimic that observed in the less-tractable superficial keratinocyte model in that mROS mediates neutrophil recruitment (Chapt. 2, Fig. 2e,f,g). Additional antioxidants such as *N*-acetylcysteine could also be used.

One final point, briefly discussed in Chapter two, is that ROS production could be leading to neutrophil recruitment directly by stimulating neutrophil migration [126] or indirectly by upregulating inflammatory cytokines [128, 129, 131, 174]. The relative contributions of direct versus indirect could be assessed by inhibiting inflammatory cytokine production, such as pentoxifylline to inhibit Tnfα secretion.

How does *txn* ablation increase transformed cell proliferation?

In Chapter two, I demonstrated that neutrophils mediate increased basal transformed cell proliferation in the *txn* mutant (Chapt. 2, Fig. 13a-d). While the role of neutrophils in promoting early neoplastic growth has been reported *in vivo* [79, 119], the mechanism by which they do so is poorly understood. The sole mechanistic observation showed prostaglandin E_2 (PGE_2), likely from a myeloid source, promoted transformed cell growth in zebrafish larvae [79]. Similar experiments could be implemented in *txn* wildtype or mutant larvae, we could similarly inhibit PGE_2 by antisense morpholino injection against myeloid-enriched PGE_2 synthase (mPGES).

As has been described previously, both elevated neutrophil elastase (NE) and elevated ROS levels can stimulate cancer cell growth [74, 75, 124]. The role of each of these in proliferation at early neoplastic stages has not been investigated. Neutrophil elastase inhibitor, Sivelestat, has been used in zebrafish and could be useful in this context [132]. Additionally, neutrophil-derived ROS could be detoxified by overexpression of *txn* specifically within neutrophils, and transformed cell proliferation could then subsequently be assessed.

While neutrophils undoubtedly influence transformed cell growth, we have yet to assess if transformed cells alter the neutrophil phenotype to enhance neoplastic cell growth. A mouse model of breast cancer demonstrated neutrophils acquire T cell inhibiting functions as disease progresses to the metastatic stage [175]. From the TRAP-seq dataset, we observed *p47phox* expression to be increased in neutrophils in response to oncogene transformation (data not shown). p47phox is a component of the phagocyte NADPH-oxidase (NOX2) complex [176] and

its upregulation could signify an increase in neutrophil ROS in response to transformation. Increased local ROS could then promote proliferation as discussed above.

Finally, neutrophils may be enhancing transformed cell growth in *txn* mutants simply due to their increased abundance and reduced proximity. These events may increase the local concentrations of transformed cell proliferative agents (NE or ROS) and thus activate proliferation pathways more robustly in *txn* null larvae. Neutrophil-induced proliferation may therefore be driven by changes in neutrophil migratory behavior and proximity and not a result of increased growth factor production by neutrophils.

Does transformed cell-derived *txn* drive anti-inflammatory signaling?

From the zebrafish melanoma (Zmel) injection experiments, we observed no change in melanoma growth, neutrophil recruitment, or neutrophil migratory behavior between *txn* wildtype and mutant larvae (Chapt. 3, Fig. 2,3). As Zmel are sufficient for *txn*, we believe these results suggest *txn* in the transformed-cell compartment is responsible for reduced neutrophilic inflammation and subsequent reduced neutrophil-dependent proliferation. To strengthen this conclusion, several additional experiments could be conducted.

First, thioredoxin activity could be impaired specifically within $KRas^{G12V}$-transformed cells via expression of a dominant-negative Txn isoform (DN-Txn). DN-Txn harbors two mutations in the active site cysteines to serine to eliminate its redox capabilities [177]. DN-Txn functions as a dominant-negative by binding thioredoxin reductase thus acting as a competitive inhibitor of wildtype Txn [177]. Attempts to synthesize DN-Txn plasmids for expression in transformed keratinocytes were conducted, but we experienced difficulties cloning and

fluorescently tagging DN-Txn. We believe covalent linkage of Txn (~12kDa) to GFP (~28kDa) at either terminus may inhibit activity by interfering with binding to thioredoxin reductase. We therefore planned to close DN-Txn upstream of an internal ribosome entry site (IRES), placing GFP downstream for visualizing expression, to generate untagged Txn expression constructs. Should future efforts succeed in generating the DN-Txn plasmid, a positive control for inhibition of wildtype Txn function could include measuring ROS production via pfbs-f in response to tail transection as in Chapter two.

Another means of determining the cellular source of Txn could entail deletion or knockdown of *txn* from Zmel cells *in vitro* and subsequent injection into wildtype, *txn*-sufficient zebrafish larvae. Deletion or knockdown could be conducted via CRISPR-Cas9 or siRNA, respectively, and assessed by Western blot to determine knockout and knockdown efficiency.

Does *txn* switch from a tumor-suppressive to tumor-promoting role during tumor progression?

Using the hyperactive β-catenin-driven hepatocellular carcinoma (HCC) model, we observed increased liver size in *txn* mutant larvae 6dpf and no change in liver size, with potential reduction, at 13dpf (Chapt. 3, Fig. 5,6). These results suggest *txn* may switch from a tumor-suppressive role early to a tumor-promoting role later in tumorigenesis. Indeed, several reports indicate *txn* is essential for overt tumor growth at later stages [151, 160].

To address this possibility, our HCC experiments at 6dpf and 13dpf should be repeated to increase sample size. Additionally, liver size and neutrophil recruitment could be assessed at later time points via fixing and histological analysis. Should we observe this switch in *txn*

function and subsequent growth inhibition in *txn* mutant livers at later stages, several factors could be influencing *txn*-mediated survival. ROS has been demonstrated to play growth-promoting effects at low doses and induce apoptosis at higher concentration [172, 178]. As tumors progress, the ROS burden reportedly increases at later stages [171]. This may explain reduced liver size observed at 13dpf, as *txn* null larvae may be unable to detoxify elevated levels of ROS at this stage. Future experiments could entail assaying ROS abundance within the liver at early and late stages, as well as apoptosis via active caspase-3 staining. Antioxidants such as *N*-acetylcysteine could also be supplied to assess the potentially detrimental role of ROS at later stages.

One final possible explanation for reduced liver size at later stages in *txn* mutant larvae could be elevated infiltration of CD8+ T cells. Zebrafish T cells have begun to mature by 13dpf [179] and could be infiltrating *txn* null livers at higher density than wildtype controls, possibly due to elevated ROS levels and inflammatory cytokine production. These T cells could be directly killing β-catenin-expressing hepatocytes in *txn* null larvae thereby reducing liver size. T cell ablation studies using □-irradiation or dexamethasone [179] could be implemented to address T cell effects on liver size at later stages.

Appendix

Tumor-cell specific effects of thioredoxin and effects during progression

Benjamin Korte, Gayathri Ramakrishnan, Anna Huttenlocher

Author contributions: BK designed and performed experiments and analyzed results. GR performed HCC experiments 6dpf. AH designed experiments and provided guidance.

Introduction

Previous reports have largely indicated that tumor-cell specific expression of thioredoxin is essential for tumor growth [151, 160], which stands in contrast to the anti-proliferative observation observed in chapter two. These studies were conducted in *txn* sufficient animal models, thus raising the possibility that *txn* in non-tumor cell types may be the primary contributor to the tumor-suppressive function we observe.

Little is currently understood concerning the effects of thioredoxin specifically on growth stimulation by immune or stromal cells. Interestingly, we found neutrophil-specific *txn* was elevated in response to $HRas^{G12V}$-induced transformation from the TRAP-seq experiment described in chapter two (data not shown). Pharmacological inhibition of ROS production in neutrophils with diphenyleneiodonium chloride (DPI) dramatically reduced chemotaxis to neutrophil chemokines fMLP, LTB_4, and IL-8 *in vitro*, suggesting ROS is essential for efficient neutrophil migration [145]. Thus, *txn* from the neutrophil compartment may influence transformed cell growth and survival.

While thioredoxin has a known intracellular localization, it is also reportedly secreted by a leaderless pathway from fibroblasts, airway epithelia, and B- and T-cells [161]. Extracellular human recombinant thioredoxin has been demonstrated to reduce expression of a number of cytokines including *il6*, *il1b*, *il23*, *il17a*, and *il22* in mouse skin cells (Sakurai 2016). Thioredoxin, secreted from cells in the tumor microenvironment, may therefore inhibit inflammatory signaling within transformed zebrafish keratinocytes.

In the stromal cell compartment, ROS has been demonstrated to promote DNA synthesis and growth factor secretion. Treatment of human endometrial stromal cells with the antioxidants vitamin E or *N*-acetylcysteine decreased thymidine incorporation into newly synthesized DNA, indicating stromal-derived ROS can promote proliferation [162]. Similarly, oxidative stress in breast cancer fibroblasts can induce differentiation into pro-tumor myofibroblasts, enhancing invasive phenotypes [163]. Additionally, tumor-associated myofibroblasts secrete growth factors including EGF, HGF-2, PDGF, and TGF-β [164]. Thus, ROS signaling in cell types present in the tumor microenvironment has the capacity to alter tumor cell growth. Thioredoxin produced by stromal or innate immune cells within the transformed cell microenvironment may therefore scavenge pro-tumor ROS.

To assess the role of tumor-derived thioredoxin on neutrophil-mediated growth, we exogenously introduced thioredoxin-sufficient zebrafish melanoma cells (Zmel) into *txn* wildtype or mutant larvae. Briefly, GFP-positive zebrafish melanoma cells expressing constitutively-active BRAF and devoid of p53 ($BRAF^{V600E}$, $p53^{-/-}$) were injected into the hindbrain ventricle of 2dpf larvae [165](Fig. 1). Hindbrain-injected melanoma cells recruit macrophages 1dpf indicating the melanoma cells elicit an inflammatory response and thus may recruit neutrophils [166]. Additionally, hindbrain-injected melanoma cells disseminate in ~40% of injected larvae by 4dpf and form large tumors by 30-days post intravascular injection [165, 166]. Thus, Zmel injection offers at least two advantages over the basal keratinocyte $KRas^{G12V}$ transformation model: the ability to determine tumor-cell specific effects in a whole-larvae genetic knockout, and the capacity to monitor tumor growth and inflammatory responses later in tumorigenesis in a bona fide tumor model. Due to time constraints, only the former point

was substantially pursued as we assessed the role of thioredoxin in the tumor microenvironment on melanoma growth and neutrophil recruitment 1 and 4 days-post injection (Fig. 1).

Fig.1

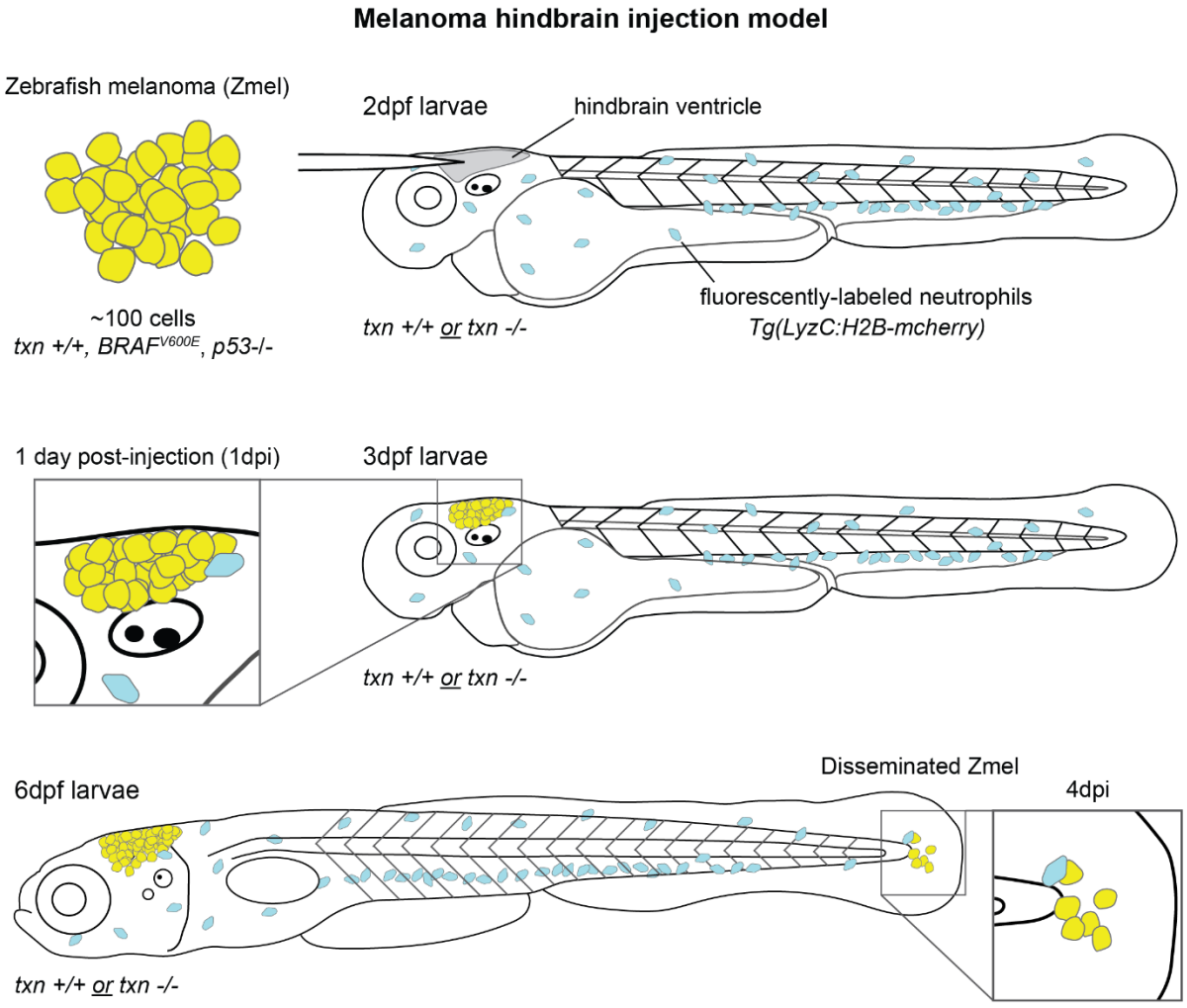

Fig. 1 – **Melanoma hindbrain injection model** Schematic of zebrafish melanoma (Zmel) injection into hindbrain ventricle of *txn*$^{+/+}$ Tg(*LyzC*:*H2B-mcherry*) or *txn*$^{-/-}$Tg(*LyzC*:*H2B-mcherry*) larvae 2dpf. Zmel injection site is imaged 1dpi (3dpf). Disseminated Zmel at posterior end of notochord are imaged 4dpi (6dpf)

In addition to identifying the cellular source of thioredoxin that regulates transformed cell fate, we are interested in determining its role at later stages in tumor development. Our reports of the effects of thioredoxin *in vivo* at early stages in tumorigenesis are unique and unstudied by other groups, to the best of our knowledge. The role of thioredoxin in tumor development however has been studied at later stages, where tumor cell-derived thioredoxin appears to be essential for tumor growth [151]. A recent study demonstrated that knockdown of thioredoxin in human gastric cancer cells reduced cell growth *in vitro* and tumor growth *in vivo* [167]. This report also identified elevated thioredoxin expression in gastric cancer was correlated with poor prognosis. Additionally, human carcinoma cells expressing low levels of thioredoxin grew more slowly when injected into mice [160]. This study also reported high levels of antioxidants such as glutathione are correlated with elevated aggressiveness. Indeed, prostate cancer cells with elevated levels of reduced glutathione, another cellular antioxidant, were more invasive than cells harboring a more oxidized environment, supporting the positive correlation between antioxidant abundance and tumor aggressiveness [168]. This finding suggests thioredoxin may play differential roles in tumor development depending upon stage, switching from an inhibitory role early to a pro-tumor role later.

To assess the role of thioredoxin in inflammatory processes and transformed cell growth at later stages in tumor development, a β-catenin-driven hepatocyte transformation model was employed. This model utilizes expression of a constitutively-active β-catenin mutant harboring four point mutations (S33A, S37A, T41A, and S45A) that render the protein insensitive to phosphorylation and subsequent degradation [169]. Constitutively-active β-catenin, hereafter referred to simply as β-cat, is expressed solely in hepatocytes along with EGFP via the liver-

specific promoter *fabp10a* in *txn* wildtype or mutant larvae (*txn*$^{+/+}$ or *txn*$^{-/-}$, *Tg(Fabp10:ptBcatenin, Fabp10:EGFP, Cryaa:venus, LyzC:H2B-mcherry)*(Fig. 4). By 13 days-post fertilization, livers of β-cat-expressing larvae are nearly twice as large as EGFP-expressing controls [170]. Additionally, β-cat expression increases neutrophil density within the liver. By two months-post fertilization, ~33% of juvenile fish expressing β-cat had developed hepatocellular carcinoma based on histological abnormalities with no HCC observed in controls [169]. β-cat-expression increased mortality substantially in adults with median survival reduced from ~393 days in controls to ~200 days in β-cat-expressing fish. Thus, constitutively active β-catenin expression in hepatocytes allows for the study of tumorigenesis from early transformation to malignant tumor formation.

We thus assessed the role of thioredoxin in β-cat-driven liver growth and neutrophil recruitment at 6dpf and 13dpf. For experiments conducted 13dpf, larvae were fed a high cholesterol diet previously shown to increase liver size and neutrophil density [170](Fig. 4b).

Results

Thioredoxin loss-of-function in the tumor microenvironment does not affect melanoma growth or neutrophil behavior

We first assessed the role of thioredoxin specifically within the tumor microenvironment on melanoma cell growth and neutrophil recruitment. 1 day-post injection (1dpi) of ~100 Zmel melanoma cells into the hindbrain ventricle, we observed no difference in the number of neutrophils recruited or in the melanoma mass size within the hindbrain between *txn* wildtype and mutant larvae (Fig. 2a-c). Similarly, we report no significant change

in average neutrophil speed around melanoma cells in the hindbrain with *txn* loss-of-function, though a trend toward decreased average speed in the *txn* mutant was observed (Fig. 2d,e). Thus, growth of injected melanoma cells and neutrophil recruitment and behavior in their vicinity is seemingly unaffected by thioredoxin from other, non-melanoma sources.

Thioredoxin in the tumor microenvironment does not affect invasive melanoma growth or neutrophil response

We next set out to identify a role for thioredoxin in the neutrophil response and growth of disseminated melanoma cells. By 4dpi, melanoma cells injected into the hindbrain ventricle have disseminated, most commonly to the distal end of the notochord in the tail (Fig. 1). We observed few neutrophils recruited to Zmel cells in this region, with no overt qualitative change in neutrophil behavior between *txn* wildtype and mutant larvae (Fig. 3a). Likewise, there was no observable difference in Edu-positive melanoma cell frequency or lesion volume 4dpi at the dissemination site with *txn* ablation in the microenvironment (Fig. 3b-d). Due to limited application of the Edu protocol, assessing proliferating melanoma cells in the hindbrain was impractical, though no obvious change in melanoma mass volume in the hindbrain was observed 4dpi (data not shown). Thus, as with melanoma cells in the hindbrain 1dpi, thioredoxin in the microenvironment does not appear to influence disseminated melanoma growth or neutrophil recruitment.

Fig.2

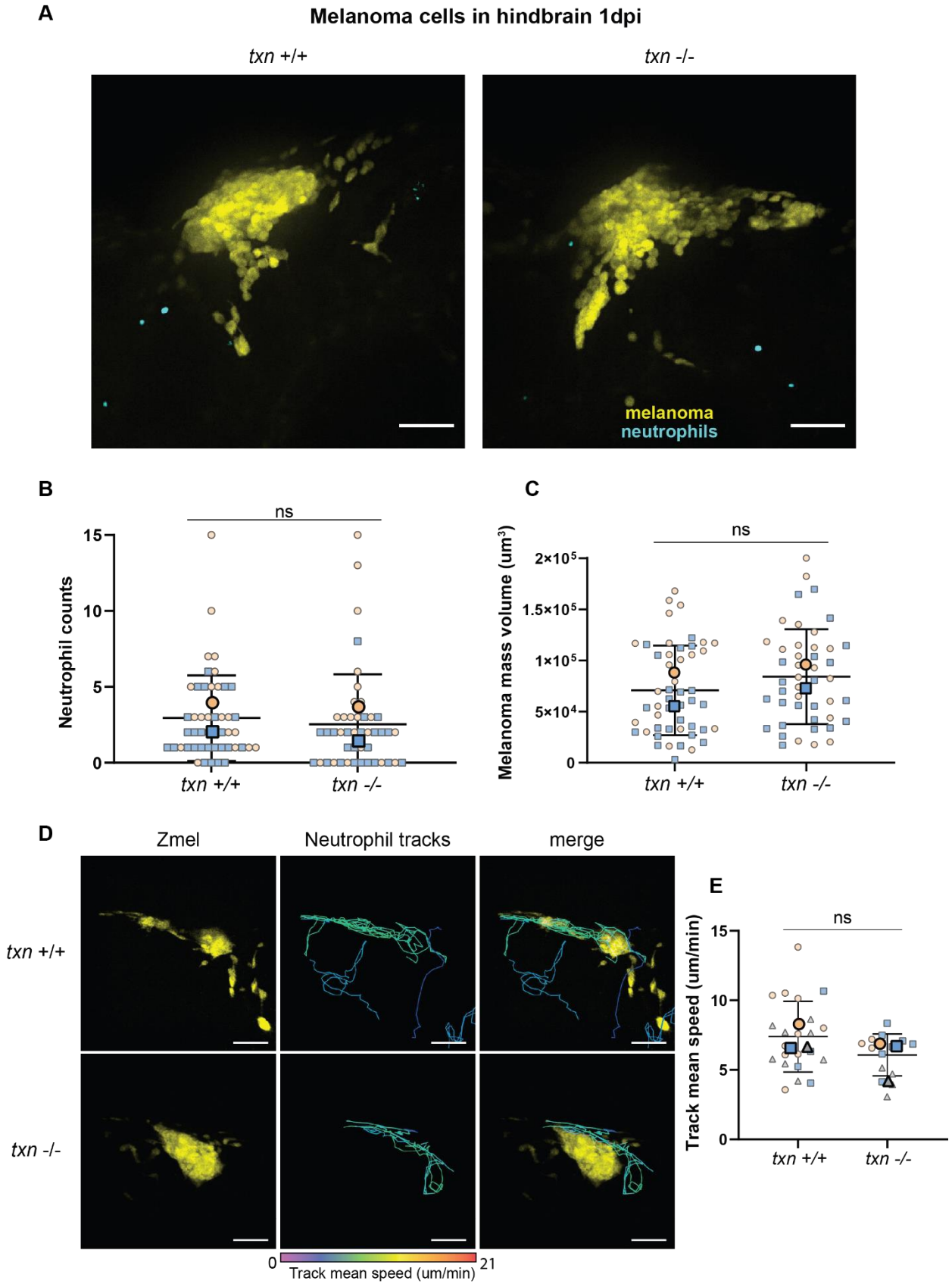
A
Melanoma cells in hindbrain 1dpi
txn +/+
txn -/-
melanoma
neutrophils
B
ns
Neutrophil counts
15
10
5
0
txn +/+
txn -/-
C
ns
Melanoma mass volume (um³)
2×10⁵
1.5×10⁵
1×10⁵
5×10⁴
0
txn +/+
txn -/-
D
Zmel
Neutrophil tracks
merge
txn +/+
txn -/-
0
Track mean speed (um/min)
21
E
ns
Track mean speed (um/min)
15
10
5
0
txn +/+
txn -/-

Fig. 2 – **Thioredoxin loss-of-function in the tumor microenvironment does not affect melanoma growth or neutrophil behavior** A) Zmel cells (yellow) and neutrophils (cyan) in hindbrain ventricle in *txn*$^{+/+}$ Tg(*LyzC*:*H2B-mcherry*) or *txn*$^{-/-}$Tg(*LyzC*:*H2B-mcherry*) larvae 1dpi. B) Quantification of neutrophil abundance in *txn* wt (n=49) and mutant (n=45) larvae. C) Quantification of melanoma mass volume in *txn* wt (n=49) and mutant (n=45) larvae. D) Neutrophil average migration speed around Zmel injection site in *txn*$^{+/+}$ Tg(*LyzC*:*H2B-mcherry*) or *txn*$^{-/-}$Tg(*LyzC*:*H2B-mcherry*) larvae 1dpi. Track color indicates average velocity per neutrophil tracked. E) Quantification neutrophil track mean speed from wt (n=3) and mutant (n=3) larvae. Scale bar, 50uM. Bolded shapes indicate average value per technical replicate, with shaded values representing data points from independent larvae. Samples were analyzed for statistical significance via Mann-Whitney U test.

Fig. 3 – **Thioredoxin in the tumor microenvironment does not affect invasive melanoma growth or neutrophil response** A) Zmel cells (yellow) disseminated to posterior end of the notochord and average neutrophil speed in *txn*$^{+/+}$ Tg(*LyzC*:*H2B-mcherry*) or *txn*$^{-/-}$ Tg(*LyzC*:*H2B-mcherry*) larvae 4dpi. Track color indicates average velocity per neutrophil tracked. B) Edu staining (white) of disseminated Zmel cells (yellow) in *txn*$^{+/+}$ Tg(*LyzC*:*H2B-mcherry*) or *txn*$^{-/-}$Tg(*LyzC*:*H2B-mcherry*) larvae 4dpi. C) Quantification of Edu-signal/melanoma-signal in *txn* wt (n=43) and mut (n=45) larvae. D) Quantification of disseminated melanoma cell volume in *txn* wt (n=43) and mut (n=45) larvae. Scale bar, 10uM. Bolded shapes indicate average value per technical replicate, with shaded values representing data points from independent larvae. Samples were analyzed for statistical significance via t-test.

Fig.3

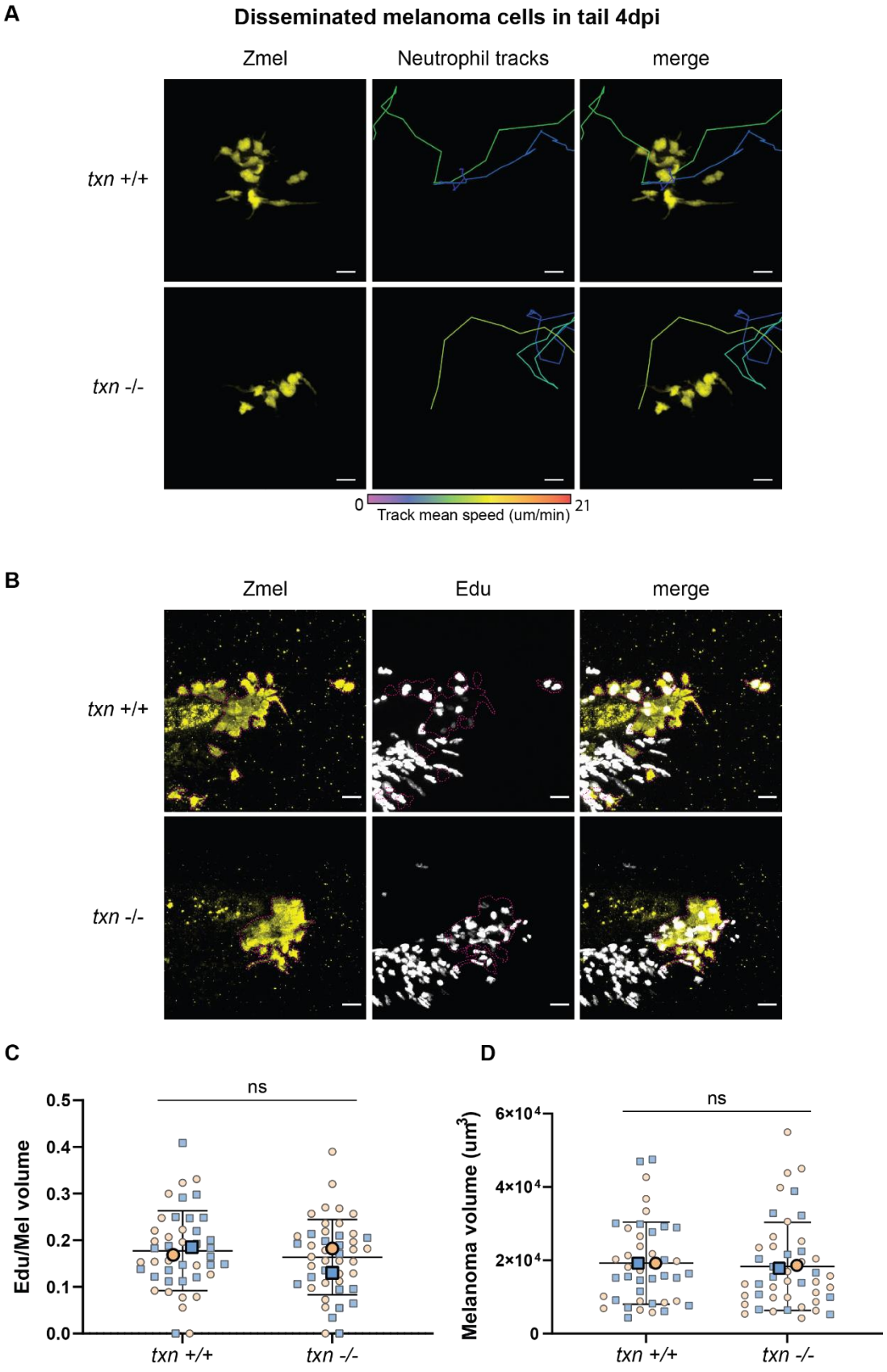
A
Disseminated melanoma cells in tail 4dpi
Zmel
Neutrophil tracks
merge
txn +/+
txn -/-
0
Track mean speed (um/min)
21
B
Zmel
Edu
merge
txn +/+
txn -/-
C
Edu/Mel volume
ns
0.5
0.4
0.3
0.2
0.1
0.0
txn +/+
txn -/-
D
Melanoma volume (um3)
ns
6×10⁴
4×10⁴
2×10⁴
0
txn +/+
txn -/-

Fig.4

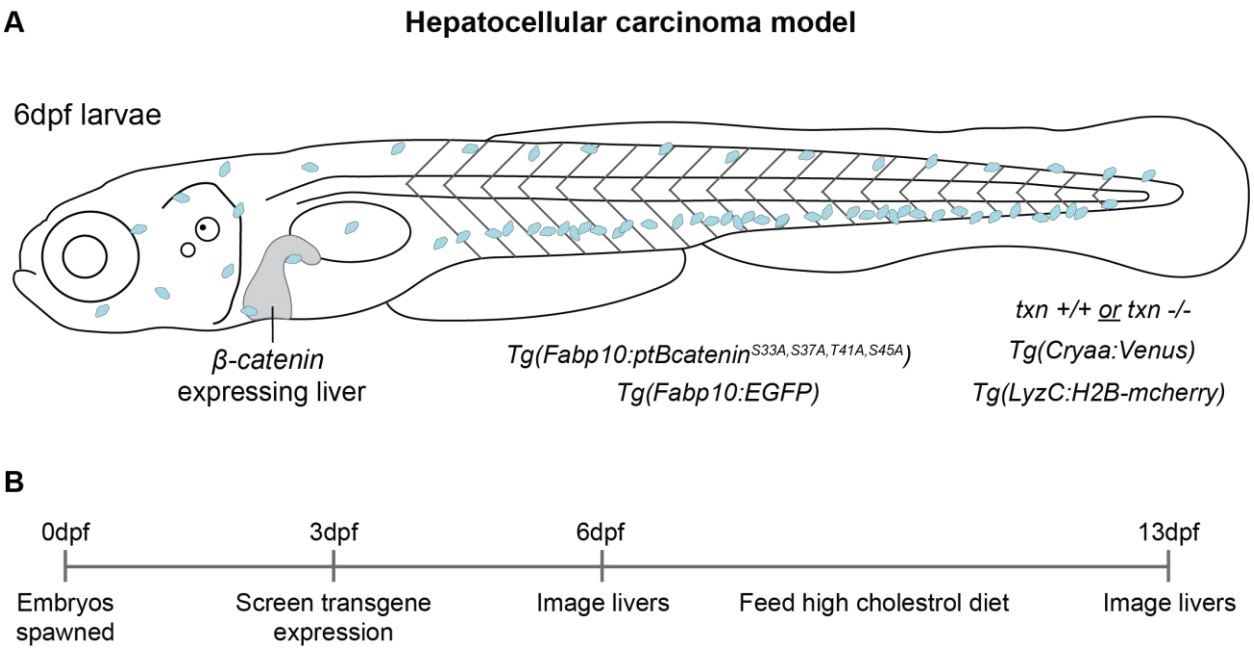

Fig. 4 – **Hepatocellular carcinoma model** A) Schematic of β-catenin-driven HCC model in *txn*$^{+/+}$ or *txn*$^{-/-}$ *Tg(Fabp10:ptBcatenin*^{S33A,S37A,T41A,S45A}*) Tg(Fabp10:EGFP) Tg(Cryaa:Venus) Tg(LyzC:H2B-mcherry)* 6dpf. B) Outline of HCC experimental time points

<u>Thioredoxin inhibits transformed hepatocyte growth 6dpf but does not affect neutrophil abundance</u>

We next pursued the role of thioredoxin in the growth of and neutrophil recruitment to constitutively-active β-catenin-expressing hepatocytes. We observed no change in neutrophil abundance in β-cat-expressing livers 6dpf (Fig. 5a, b). Interestingly however, livers were ~40% larger on average in *txn* mutant larvae (Fig. 5a,c). Neutrophil behavior at this time point was unfortunately not assessed. As with basal keratinocyte transformation, *txn* appears to be

inhibiting transformed hepatocyte growth at early stages, although possibly not by inhibiting neutrophils in some manner.

Thioredoxin inhibits neutrophil recruitment to transformed hepatocytes 13dpf but does not significantly alter growth

We then extended this experiment to 13dpf and introduced a high cholesterol diet to both control and *txn* mutant larvae. We observed no obvious effect on average neutrophil migration speed in *txn* deficient larvae, however neutrophil abundance appeared to be increased in *txn* mutant livers however (Fig. 6a-d). There was no significant effect of *txn* on liver size 13dpf, though a trend toward a slight reduction in size was observed in the mutant background (Fig. 6c,e). Thus, in the context of a high cholesterol diet at the later stage of 13dpf, β-cat-expressing livers in *txn* mutants appear to harbor more neutrophils than β-cat-expressing wildtype livers.

Fig. 5 – Thioredoxin inhibits transformed hepatocyte growth 6dpf but does not affect neutrophil abundance A) β-catenin-expressing livers (white) and neutrophils (cyan) in *txn*$^{+/+}$ or *txn*$^{-/-}$ *Tg(Fabp10:ptBcatenin*^{S33A,S37A,T41A,S45A}*) Tg(Fabp10:EGFP) Tg(Cryaa:Venus) Tg(LyzC:H2B-mcherry)* larvae 6dpf. B) Quantification of neutrophil abundance in livers of *txn* wt (n=42) and mut (n=35) larvae. C) Quantification of liver volume of *txn* wt (n=42) and mut (n=35) larvae. Scale bar, 50uM. Bolded shapes indicate average value per technical replicate, with shaded values representing data points from independent larvae. Samples were analyzed for statistical significance via t-test (p<0.0001****).

Fig.5

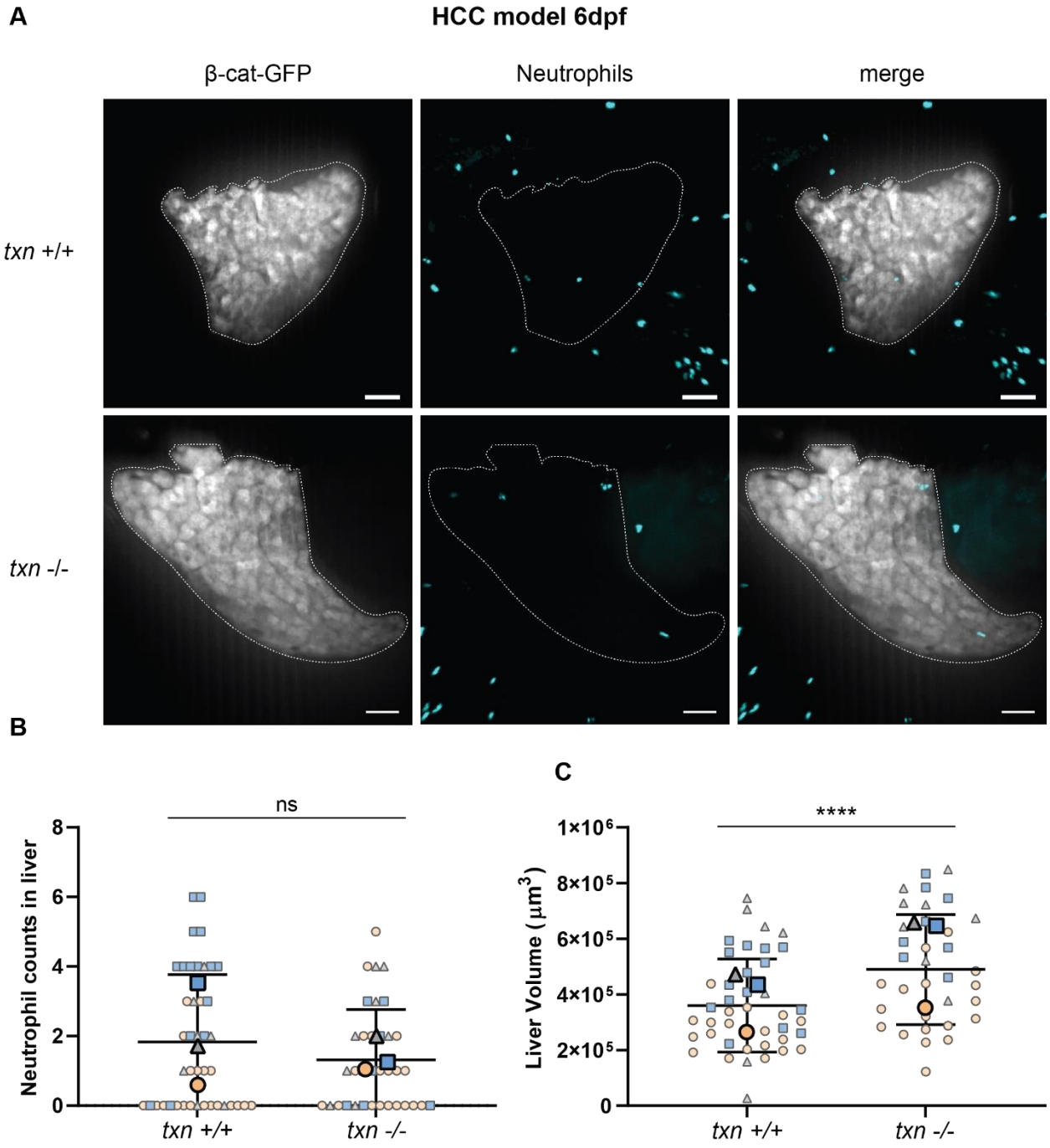
A
HCC model 6dpf
β-cat-GFP
Neutrophils
merge
txn +/+
txn -/-
B
ns
Neutrophil counts in liver
8
6
4
2
0
txn +/+
txn -/-
C
****
Liver Volume (μm3)
1×10⁶
8×10⁵
6×10⁵
4×10⁵
2×10⁵
0
txn +/+
txn -/-

Fig.6

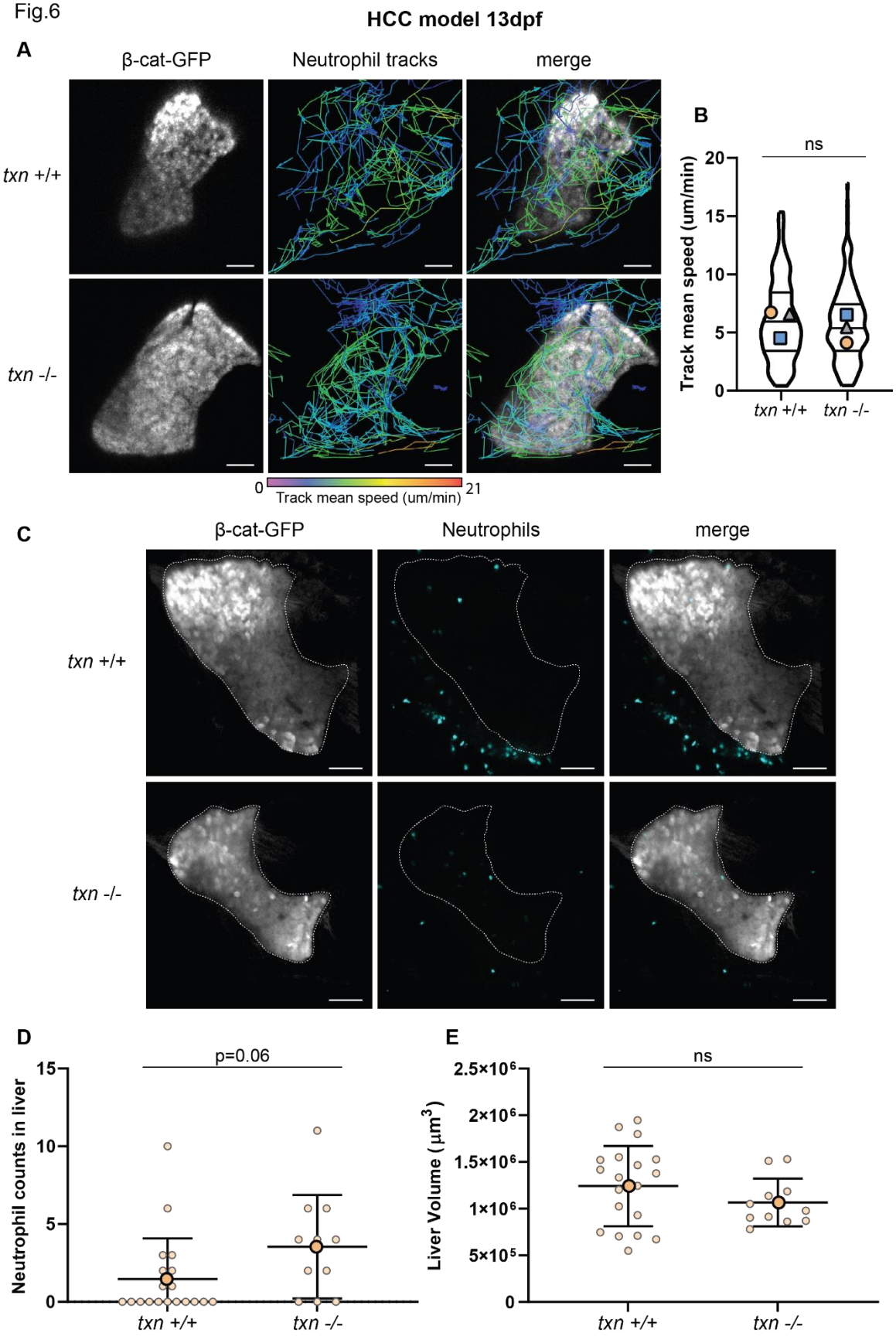
HCC model 13dpf
A
β-cat-GFP
Neutrophil tracks
merge
txn +/+
txn -/-
0
Track mean speed (um/min)
21
B
ns
Track mean speed (um/min)
20
15
10
5
0
txn +/+
txn -/-
C
β-cat-GFP
Neutrophils
merge
txn +/+
txn -/-
D
p=0.06
Neutrophil counts in liver
15
10
5
0
txn +/+
txn -/-
E
ns
Liver Volume (µm3)
2.5×10⁶
2×10⁶
1.5×10⁶
1×10⁶
5×10⁵
0
txn +/+
txn -/-

Fig. 6 – **Thioredoxin inhibits neutrophil recruitment to transformed hepatocytes 13dpf but does not significantly alter growth** A) β-catenin-expressing livers (white) and average neutrophil speed (tracks) in *txn*$^{+/+}$ or *txn*$^{-/-}$ *Tg(Fabp10:ptBcatenin*^{S33A,S37A,T41A,S45A}*) Tg(Fabp10:EGFP) Tg(Cryaa:Venus) Tg(LyzC:H2B-mcherry)* larvae 13dpf. Track color indicates average velocity per neutrophil tracked. B) Quantification of average neutrophil track speed in *txn* wt (n=3) and mut (n=3) larvae 13dpf. C) β-catenin-expressing livers (white) and neutrophils (cyan) in *txn*$^{+/+}$ or *txn*$^{-/-}$ *Tg(Fabp10:ptBcatenin*^{S33A,S37A,T41A,S45A}*) Tg(Fabp10:EGFP) Tg(Cryaa:Venus) Tg(LyzC:H2B-mcherry)* larvae 13dpf. D) Quantification of neutrophil abundance in livers of *txn* wt (n=19) and mut (n=11) larvae 13dpf. E) Quantification of liver volume in *txn* wt (n=19) and mut (n=11) larvae 13dpf. Scale bar, 50uM. Bolded shapes indicate average value per technical replicate, with shaded values representing data points from independent larvae. Samples were analyzed for statistical significance via t-test.

Discussion

In this section, we utilized the zebrafish melanoma hindbrain injection model (Fig. 1) to ascertain the tumor-cell intrinsic role of thioredoxin in promoting neutrophil inflammation and tumor cell growth. We observed no significant change in neutrophil abundance, melanoma mass size, or average neutrophil migration speed between *txn* wildtype and mutant larvae 1dpi in the hindbrain (Fig. 2a-e). Similarly at 4dpi, disseminated melanoma cells in the tail displayed no observable change in neutrophil migratory behavior or Edu-incorporation frequency between *txn* wildtype and mutant larvae (Fig. 3a-d).

The most straightforward interpretation of these findings suggest thioredoxin originating from within transformed or tumor cells inhibits neutrophil recruitment and growth,

and thioredoxin produced by the microenvironment does not affect these processes. Indeed, our TRAP-seq dataset indicated *txn* expression was increased in transformed cells roughly five-fold over wildtype-HRas-expressing cells. Constitutive Ras activation is known to induce mitochondrial stress and ROS production [121, 122, 149] and tumor cells, likely in response, produce increased levels of antioxidants including thioredoxin. It therefore seems likely that elevated thioredoxin expression in transformed cells would influence the inflammatory phenotype.

While the melanoma injection results strongly suggest *txn* derived from transformed cells drives neutrophil recruitment and enhanced proliferation, there was a slight trend toward increased melanoma mass volume and reduced average neutrophil migration speed in the vicinity in the *txn* mutant. Therefore, one possibility requiring further experimentation to confirm or refute is that thioredoxin produced by the microenvironment influences neutrophil recruitment and transformed cell growth.

In support of this notion, ROS in other cell types has been shown to elicit neutrophil recruitment and growth factor production. Inhibiting ROS production in neutrophils severely impaired their migration toward a chemoattractant *in vitro* [145]. Additionally, ROS produced by stromal fibroblasts has been shown to be essential in their production of growth factors [164]. Thioredoxin may therefore be acting in multiple cell types, including the transformed cell compartment, to synergistically inhibit neutrophil migration and transformed cell proliferation.

We next sought to determine the role of thioredoxin at later stages in tumor development, and so used the hyperactive β-catenin model of hepatocellular carcinoma

described above (Fig. 4). We observed at 6dpf, livers in *txn* null larvae were larger than control siblings (Fig. 5a,c). Interestingly, we did not observe a change in neutrophil abundance within the liver at this time point (Fig. 5a,b). Thus, the growth-promoting effect of *txn* loss-of-function may be independent of changes in neutrophil recruitment in this model. Neutrophil abundance data was however highly variable and warrants repetition, in conjunction with an analysis of neutrophil speed.

If future experiments determine a neutrophil-independent role of thioredoxin in liver growth, several studies suggest the effects could be specific to hepatocytes or the surrounding stroma. Thioredoxin null livers presumably produce elevated ROS which was previously demonstrated to be a necessary component for efficient signal transduction following growth factor stimulation [124, 125]. Additionally, as with the $KRas^{G12V}$ transformation model, stromal cells within livers of *txn* null hepatocytes may produce growth factors including hepatocyte growth factor in response to elevated ROS and thereby promote liver growth. While the underlying mechanism remains to be described, our results strengthen the conclusion that thioredoxin at early stages in tumorigenesis inhibits proliferation thus acting as a tumor suppressor.

As we carried experiments out to 13dpf and fed larvae a high cholesterol diet to enhance hepatic inflammation, we observed increased neutrophil abundance in *txn* null livers and no change in liver size comparing wildtype and mutant larvae (Fig. 6c-e). We similarly observed no change in average neutrophil speed in neutrophils within the liver or in the surrounding space (Fig. 6a,b). This data suggests an enhanced inflammatory environment in 13dpf livers in *txn* mutant larvae, yet perhaps even reduced hepatocyte growth in *txn* mutants.

Several published findings indicate thioredoxin is essential for overt tumor growth at later stages. Expression of dominant-negative thioredoxin in MCF-7 cells completely abolished tumor growth in injected mice [151]. Similarly, thioredoxin depletion by shRNA in gastric cancer cell lines decreased tumor growth *in vivo* [167]. Thus, thioredoxin appears to be necessary for tumor growth at more advanced stages. Indeed, tumor cells have been reported to produce elevated antioxidant levels at malignant stages compared to precancerous stages [171]. This is likely in response to increased metabolic stress and ROS production during progression, and could prevent tumor cell apoptosis by detoxifying cytotoxic levels of ROS [172]. Therefore, the effects of thioredoxin may indeed switch from tumor-suppressive at early stages to tumor-promoting later in tumor development.

In conclusion, while the data presented in this chapter is mostly preliminary, we believe they strongly suggest two findings that add to those presented in chapter two. First, thioredoxin derived from the transformed or tumor cells is likely the main contributor to the inhibitory effects observed on neutrophil recruitment and proliferation. Second, thioredoxin likely transitions from an anti-inflammatory role early to an essential antioxidant later in tumorigenesis.

Methods

Zebrafish maintenance and generation of transgenic zebrafish

Zebrafish lines were maintained as previously described (Vincent *et al.* 2016) and *txn* adults genotyped as described in chapter two. To generate the $txn^{-/-}$ line in the hyperactive β-catenin hepatocellular carcinoma background, $txn^{+/+}$ *Tg(LyzC:H2B-mcherry)* or $txn^{-/-}$

Tg(LyzC:H2B-mcherry) adults were crossed to *Tg(Fabp10:ptBcatenin, Fabp10:EGFP, Cryaa:venus)* fish generated previously [169]. Livers develop by 6dpf, but larvae can be screened 3dpf via venus expression in the eye.

Melanoma hindbrain injection model

Zebrafish melanoma cells (Zmel)(BRAF^{V600E}, *p53*$^{-/-}$) were isolated from adults and cultured *in vitro* [165]. Cells were trypsinized and resuspended in HBSS to 6x10^{7} cells/ml in 10ul and microinjected into hindbrain ventricle of 2dpf larvae as previously described [173]. Measurements of neutrophil abundance and migratory behavior and melanoma mass size or proliferation were taken 1dpi (3dpf) and 4dpi(6dpf) in the hindbrain and caudal tail locations respectively (Fig. 1).

Live Imaging and Edu proliferation assay

Melanoma cells in the hindbrain 1dpi and β-catenin-expressing hepatocytes 6dpf and 13dpf were imaged at 20x magnification on a Zeiss LSM 800 laser scanning confocal microscope. These specifications were used to collect images of melanoma size, neutrophil abundance, liver size, and neutrophil migration speed. Edu-positive melanoma cells in the tail were imaged 4dpi at 40x magnification using a Zeiss Spinning Disk confocal microscope. Edu staining was conducted as described in chapter two. All analyses reported in this chapter were conducted in the Imaris analysis software.

Statistical Analysis

Statistical analyses were performed on at least three independent experimental replicates, unless otherwise indicated in the figure legend. For all experiments except neutrophil speed assays, data points represent measurements from individual larvae. Replicate number is distinguished by differential data point color and shape, with the mean replicate value presented in bold. For neutrophil speed experiments, data points represent values from a given neutrophil, whereas bolded data points display the average neutrophil speed for a given larvae. Sample normality was assessed with Anderson-Darling and Shapiro-Wilk test ($p<0.05$). For normally and non-normally distributed data, statistical significance ($p<0.05$) was calculated by t-test or Mann-Whitney U test, respectively. Statistics were calculated in R version 3.6 and graphed in GraphPad Prism version 9 using measurements from individual larvae as the sampling unit.

References

1. Chen, L., et al., *Inflammatory responses and inflammation-associated diseases in organs.* Oncotarget, 2018. **9**(6): p. 7204-7218.
2. Bennett, J.M., et al., *Inflammation-Nature's Way to Efficiently Respond to All Types of Challenges: Implications for Understanding and Managing "the Epidemic" of Chronic Diseases.* Front Med (Lausanne), 2018. **5**: p. 316.
3. Coussens, L.M. and Z. Werb, *Inflammation and cancer.* Nature, 2002. **420**(6917): p. 860-867.
4. Grivennikov, S.I., F.R. Greten, and M. Karin, *Immunity, inflammation, and cancer.* Cell, 2010. **140**(6): p. 883-899.
5. Hanahan, D. and W.R.A. cell, *Hallmarks of cancer: the next generation.* Hallmarks of cancer: the next generation, 2011.
6. Balkwill, F. and A. Mantovani, *Inflammation and cancer: back to Virchow?* The Lancet, 2001. **357**(9255): p. 539-545.
7. Roder, D.M., *The epidemiology of gastric cancer.* Gastric Cancer, 2002. **5**(Suppl 1): p. 5-11.
8. Arzumanyan, A., H.M. Reis, and M.A. Feitelson, *Pathogenic mechanisms in HBV- and HCV-associated hepatocellular carcinoma.* Nat Rev Cancer, 2013. **13**(2): p. 123-35.
9. Wu, S., et al., *A human colonic commensal promotes colon tumorigenesis via activation of T helper type 17 T cell responses.* Nature Medicine, 2009. **15**(9): p. 1016-1022.
10. Waldner, M.J. and M.F. Neurath, *Colitis-associated cancer: the role of T cells in tumor development.* Seminars in Immunopathology, 2009. **31**(2): p. 249-256.
11. Takahashi, H., et al., *Tobacco Smoke Promotes Lung Tumorigenesis by Triggering IKKβ- and JNK1-Dependent Inflammation.* Cancer Cell, 2010. **17**(1): p. 89-97.
12. Dostert, C., et al., *Innate immune activation through Nalp3 inflammasome sensing of asbestos and silica.* Science, 2008. **320**(5876): p. 674-7.
13. Park, E., et al., *Dietary and Genetic Obesity Promote Liver Inflammation and Tumorigenesis by Enhancing IL-6 and TNF Expression.* Cell, 2010. **140**(2): p. 197-208.

14. Kune, G.A., S. Kune, and L.F. Watson, *Colorectal cancer risk, chronic illnesses, operations, and medications: case control results from the Melbourne Colorectal Cancer Study.* Cancer Res, 1988. **48**(15): p. 4399-404.
15. Corley, D.A., et al., *Protective association of aspirin/NSAIDs and esophageal cancer: a systematic review and meta-analysis.* Gastroenterology, 2003. **124**(1): p. 47-56.
16. Mahmud, S., E. Franco, and A. Aprikian, *Prostate cancer and use of nonsteroidal anti-inflammatory drugs: systematic review and meta-analysis.* Br J Cancer, 2004. **90**(1): p. 93-9.
17. Harris, R.E., et al., *Breast cancer and nonsteroidal anti-inflammatory drugs: prospective results from the Women's Health Initiative.* Cancer Res, 2003. **63**(18): p. 6096-101.
18. Wang, W.H., et al., *Non-steroidal anti-inflammatory drug use and the risk of gastric cancer: a systematic review and meta-analysis.* J Natl Cancer Inst, 2003. **95**(23): p. 1784-91.
19. Holick, C.N., et al., *Aspirin use and lung cancer in men.* Br J Cancer, 2003. **89**(9): p. 1705-8.
20. Brown, J.R. and R.N. DuBois, *COX-2: a molecular target for colorectal cancer prevention.* J Clin Oncol, 2005. **23**(12): p. 2840-55.
21. Sandler, R.S., et al., *A randomized trial of aspirin to prevent colorectal adenomas in patients with previous colorectal cancer.* N Engl J Med, 2003. **348**(10): p. 883-90.
22. Baron, J.A., et al., *A randomized trial of aspirin to prevent colorectal adenomas.* N Engl J Med, 2003. **348**(10): p. 891-9.
23. Dvorak, H.F., *Tumors: wounds that do not heal. Similarities between tumor stroma generation and wound healing.* N Engl J Med, 1986. **315**(26): p. 1650-9.
24. Senger, D.R., et al., *Tumor cells secrete a vascular permeability factor that promotes accumulation of ascites fluid.* Science, 1983. **219**(4587): p. 983-5.
25. Dvorak, H.F., et al., *Fibrin gel investment associated with line 1 and line 10 solid tumor growth, angiogenesis, and fibroplasia in guinea pigs. Role of cellular immunity, myofibroblasts, microvascular damage, and infarction in line 1 tumor regression.* J Natl Cancer Inst, 1979. **62**(6): p. 1459-72.

26. Dvorak, H.F., *Tumors: wounds that do not heal-redux.* Cancer Immunol Res, 2015. **3**(1): p. 1-11.
27. Silva, M.T. and M. Correia-Neves, *Neutrophils and macrophages: the main partners of phagocyte cell systems.* Front Immunol, 2012. **3**: p. 174.
28. Jones, H.R., et al., *The role of neutrophils in inflammation resolution.* Semin Immunol, 2016. **28**(2): p. 137-45.
29. Wang, J., *Neutrophils in tissue injury and repair.* Cell Tissue Res, 2018. **371**(3): p. 531-539.
30. Golpon, H.A., et al., *Life after corpse engulfment: phagocytosis of apoptotic cells leads to VEGF secretion and cell growth.* FASEB J, 2004. **18**(14): p. 1716-8.
31. Voll, R.E., et al., *Immunosuppressive effects of apoptotic cells.* Nature, 1997. **390**(6658): p. 350-1.
32. Gurtner, G.C., et al., *Wound repair and regeneration.* Nature, 2008. **453**(7193): p. 314-21.
33. Mantovani, A., et al., *Cancer-related inflammation.* Nature, 2008. **454**(7203): p. 436-444.
34. Guo, F.F. and J.W. Cui, *The Role of Tumor-Infiltrating B Cells in Tumor Immunity.* J Oncol, 2019. **2019**: p. 2592419.
35. Zhang, L., et al., *Intratumoral T cells, recurrence, and survival in epithelial ovarian cancer.* N Engl J Med, 2003. **348**(3): p. 203-13.
36. Hodi, F.S., et al., *Improved survival with ipilimumab in patients with metastatic melanoma.* The New England journal of medicine, 2010. **363**(8): p. 711-723.
37. Porter, D.L., et al., *Chimeric antigen receptor–modified T cells in chronic lymphoid leukemia.* New England Journal …, 2011.
38. Mantovani, A., et al., *The origin and function of tumor-associated macrophages.* Immunology today, 1992. **13**(7): p. 265-270.
39. Steidl, C., et al., *Tumor-associated macrophages and survival in classic Hodgkin's lymphoma.* N Engl J Med, 2010. **362**(10): p. 875-85.
40. Kurahara, H., et al., *Significance of M2-polarized tumor-associated macrophage in pancreatic cancer.* J Surg Res, 2011. **167**(2): p. e211-9.

41. Mantovani, A., et al., *Macrophage polarization: tumor-associated macrophages as a paradigm for polarized M2 mononuclear phagocytes.* Trends Immunol, 2002. **23**(11): p. 549-55.

42. Sica, A. and A. Mantovani, *Macrophage plasticity and polarization: in vivo veritas.* J Clin Invest, 2012. **122**(3): p. 787-95.

43. Bi, Y., et al., *M2 Macrophages as a Potential Target for Antiatherosclerosis Treatment.* Neural Plast, 2019. **2019**: p. 6724903.

44. Biswas, S.K., et al., *A distinct and unique transcriptional program expressed by tumor-associated macrophages (defective NF-kappaB and enhanced IRF-3/STAT1 activation).* Blood, 2006. **107**(5): p. 2112-22.

45. Lin, E.Y., et al., *Macrophages Regulate the Angiogenic Switch in a Mouse Model of Breast Cancer.* Cancer Research, 2006. **66**(23): p. 11238-11246.

46. Murdoch, C., et al., *The role of myeloid cells in the promotion of tumour angiogenesis.* Nat Rev Cancer, 2008. **8**(8): p. 618-31.

47. DeNardo, D.G., et al., *CD4(+) T cells regulate pulmonary metastasis of mammary carcinomas by enhancing protumor properties of macrophages.* Cancer Cell, 2009. **16**(2): p. 91-102.

48. Goswami, S., et al., *Macrophages promote the invasion of breast carcinoma cells via a colony-stimulating factor-1/epidermal growth factor paracrine loop.* Macrophages promote the invasion of breast carcinoma cells via a colony-stimulating factor-1/epidermal growth factor paracrine loop, 2005.

49. Vitiello, P.F., et al., *Impact of tumor-derived CCL2 on T cell effector function.* Immunol Lett, 2004. **91**(2-3): p. 239-45.

50. Loercher, A.E., et al., *Identification of an IL-10-producing HLA-DR-negative monocyte subset in the malignant ascites of patients with ovarian carcinoma that inhibits cytokine protein expression and proliferation of autologous T cells.* J Immunol, 1999. **163**(11): p. 6251-60.

51. Coussens, L.M., L. Zitvogel, and A.K. Palucka, *Neutralizing tumor-promoting chronic inflammation: a magic bullet?* Science (New York, N.Y.), 2013. **339**(6117): p. 286-291.

52. Coussens, L.M. and J.W. Pollard, *Leukocytes in mammary development and cancer.* Cold Spring Harbor perspectives in biology, 2011. **3**(3).

53. Shen, M., et al., *Tumor-Associated Neutrophils as a New Prognostic Factor in Cancer: A Systematic Review and Meta-Analysis.* PLoS ONE, 2014. **9**(6).

54. Jensen, T.O., et al., *Intratumoral neutrophils and plasmacytoid dendritic cells indicate poor prognosis and are associated with pSTAT3 expression in AJCC stage I/II melanoma.* Cancer, 2012. **118**(9): p. 2476-2485.

55. Fridlender, Z.G., et al., *Polarization of Tumor-Associated Neutrophil Phenotype by TGF-β: "N1" versus "N2" TAN.* Cancer Cell, 2009. **16**(3): p. 183-194.

56. Pickaver, A.H., et al., *Cytotoxic effects of peritoneal neutrophils on a syngeneic rat tumour.* Nat New Biol, 1972. **235**(58): p. 186-7.

57. Gerrard, T.L., D.J. Cohen, and A.M. Kaplan, *Human neutrophil-mediated cytotoxicity to tumor cells.* J Natl Cancer Inst, 1981. **66**(3): p. 483-8.

58. Katano, M. and M. Torisu, *Neutrophil-mediated tumor cell destruction in cancer ascites.* Cancer, 1982. **50**(1): p. 62-8.

59. van Egmond, M., *Neutrophils in antibody-based immunotherapy of cancer.* Expert Opin Biol Ther, 2008. **8**(1): p. 83-94.

60. Matlung, H.L., et al., *Neutrophils Kill Antibody-Opsonized Cancer Cells by Trogoptosis.* Cell Rep, 2018. **23**(13): p. 3946-3959 e6.

61. Fridlender, Z.G., et al., *Transcriptomic analysis comparing tumor-associated neutrophils with granulocytic myeloid-derived suppressor cells and normal neutrophils.* PloS one, 2012. **7**(2).

62. Cavallo, F., et al., *Role of neutrophils and CD4+ T lymphocytes in the primary and memory response to nonimmunogenic murine mammary adenocarcinoma made immunogenic by IL-2 gene.* J Immunol, 1992. **149**(11): p. 3627-35.

63. Beauvillain, C., et al., *Neutrophils efficiently cross-prime naive T cells in vivo.* Blood, 2007. **110**(8): p. 2965-73.

64. Ardi, V.C., et al., *Human neutrophils uniquely release TIMP-free MMP-9 to provide a potent catalytic stimulator of angiogenesis.* Proc Natl Acad Sci U S A, 2007. **104**(51): p. 20262-7.

65. Nozawa, H., C. Chiu, and D. Hanahan, *Infiltrating neutrophils mediate the initial angiogenic switch in a mouse model of multistage carcinogenesis.* Infiltrating neutrophils mediate the initial angiogenic switch in a mouse model of multistage carcinogenesis, 2006.

66. Jablonska, J., et al., *Neutrophils responsive to endogenous IFN-β regulate tumor angiogenesis and growth in a mouse tumor model.* Journal of Clinical Investigation, 2010. **120**(4): p. 1151-1164.

67. Das, A., et al., *MMP proteolytic activity regulates cancer invasiveness by modulating integrins.* Sci Rep, 2017. **7**(1): p. 14219.

68. Wislez, M., et al., *Hepatocyte growth factor production by neutrophils infiltrating bronchioloalveolar subtype pulmonary adenocarcinoma: role in tumor progression and death.* Cancer Res, 2003. **63**(6): p. 1405-12.

69. Dumitru, C.A., et al., *Tumor-derived macrophage migration inhibitory factor modulates the biology of head and neck cancer cells via neutrophil activation.* Int J Cancer, 2011. **129**(4): p. 859-69.

70. Strell, C., et al., *Neutrophil granulocytes promote the migratory activity of MDA-MB-468 human breast carcinoma cells via ICAM-1.* Exp Cell Res, 2010. **316**(1): p. 138-48.

71. Kowanetz, M., et al., *Granulocyte-colony stimulating factor promotes lung metastasis through mobilization of Ly6G+Ly6C+ granulocytes.* Proc Natl Acad Sci U S A, 2010. **107**(50): p. 21248-55.

72. Cools-Lartigue, J., et al., *Neutrophil extracellular traps sequester circulating tumor cells and promote metastasis.* J Clin Invest, 2013.

73. Tazzyman, S., et al., *Inhibition of neutrophil infiltration into A549 lung tumors in vitro and in vivo using a CXCR2-specific antagonist is associated with reduced tumor growth.* Int J Cancer, 2011. **129**(4): p. 847-58.

74. Wada, Y., et al., *Neutrophil elastase induces cell proliferation and migration by the release of TGF-alpha, PDGF and VEGF in esophageal cell lines.* Oncology Reports, 2007. **17**(1): p. 161-167.

75. Houghton, A.M., et al., *Neutrophil elastase-mediated degradation of IRS-1 accelerates lung tumor growth.* Nat Med, 2010. **16**(2): p. 219-23.

76. Zhou, S.L., et al., *Tumor-Associated Neutrophils Recruit Macrophages and T-Regulatory Cells to Promote Progression of Hepatocellular Carcinoma and Resistance to Sorafenib.* Gastroenterology, 2016. **150**(7): p. 1646-1658 e17.

77. Rotondo, R., et al., *IL-8 induces exocytosis of arginase 1 by neutrophil polymorphonuclears in nonsmall cell lung cancer.* Int J Cancer, 2009. **125**(4): p. 887-93.

78. Michaeli, J., et al., *Tumor-associated neutrophils induce apoptosis of non-activated CD8 T-cells in a TNFalpha and NO-dependent mechanism, promoting a tumor-supportive environment.* Oncoimmunology, 2017. **6**(11): p. e1356965.

79. Feng, Y., S. Renshaw, and P. Martin, *Live imaging of tumor initiation in zebrafish larvae reveals a trophic role for leukocyte-derived PGE 2.* Current Biology, 2012. **22**(13): p. 1253-1259.

80. Toyokuni, S., et al., *Persistent oxidative stress in cancer.* FEBS Lett, 1995. **358**(1): p. 1-3.

81. Zalewska-Ziob, M., et al., *Activity of Antioxidant Enzymes in the Tumor and Adjacent Noncancerous Tissues of Non-Small-Cell Lung Cancer.* Oxid Med Cell Longev, 2019. **2019**: p. 2901840.

82. Beno, I., et al., *Increased antioxidant enzyme activities in the colorectal adenoma and carcinoma.* Neoplasma, 1995. **42**(5): p. 265-9.

83. Han, D., E. Williams, and E. Cadenas, *Mitochondrial respiratory chain-dependent generation of superoxide anion and its release into the intermembrane space.* Biochem J, 2001. **353**(Pt 2): p. 411-6.

84. Crompton, M., *The mitochondrial permeability transition pore and its role in cell death.* Biochem J, 1999. **341 (Pt 2)**: p. 233-49.

85. Zorov, D.B., M. Juhaszova, and S.J. Sollott, *Mitochondrial reactive oxygen species (ROS) and ROS-induced ROS release.* Physiol Rev, 2014. **94**(3): p. 909-50.

86. Forman, H.J. and M.J. Thomas, *Oxidant production and bactericidal activity of phagocytes.* Annu Rev Physiol, 1986. **48**: p. 669-80.

87. Lambeth, D.J., *NOX enzymes and the biology of reactive oxygen.* Nature reviews. Immunology, 2004: p. 181-189.

88. Cachat, J., et al., *Phagocyte NADPH oxidase and specific immunity.* Clin Sci (Lond), 2015. **128**(10): p. 635-48.

89. Aratani, Y., *Myeloperoxidase: Its role for host defense, inflammation, and neutrophil function.* Arch Biochem Biophys, 2018. **640**: p. 47-52.

90. Donko, A., et al., *Dual oxidases.* Philos Trans R Soc Lond B Biol Sci, 2005. **360**(1464): p. 2301-8.

91. Geiszt, M., et al., *Dual oxidases represent novel hydrogen peroxide sources supporting mucosal surface host defense.* FASEB J, 2003. **17**(11): p. 1502-4.

92. Niethammer, P., et al., *A tissue-scale gradient of hydrogen peroxide mediates rapid wound detection in zebrafish.* Nature, 2009. **459**(7249): p. 996-999.

93. de Oliveira, S., et al., *ATP modulates acute inflammation in vivo through dual oxidase 1-derived H2O2 production and NF-kappaB activation.* J Immunol, 2014. **192**(12): p. 5710-9.

94. McCord, J.M. and I. Fridovich, *Superoxide dismutase: the first twenty years (1968-1988).* Free Radic Biol Med, 1988. **5**(5-6): p. 363-9.

95. Mondola, P., et al., *The Cu, Zn Superoxide Dismutase: Not Only a Dismutase Enzyme.* Front Physiol, 2016. **7**: p. 594.

96. Watanabe, K., et al., *Superoxide dismutase 1 loss disturbs intracellular redox signaling, resulting in global age-related pathological changes.* Biomed Res Int, 2014. **2014**: p. 140165.

97. Alfonso-Prieto, M., et al., *The molecular mechanism of the catalase reaction.* J Am Chem Soc, 2009. **131**(33): p. 11751-61.

98. O'Brien, P.J., *Peroxidases.* Chem Biol Interact, 2000. **129**(1-2): p. 113-39.

99. Hofmann, B., H.J. Hecht, and L. Flohe, *Peroxiredoxins.* Biol Chem, 2002. **383**(3-4): p. 347-64.

100. Hofmann, K., *The modular nature of apoptotic signaling proteins.* Cellular and Molecular Life Sciences, 1999. **55**(9): p. 1113.

101. Liou, G.Y. and S.-P. radical research, *Reactive oxygen species in cancer.* Free radical research, 2010.

102. Forman, H.J., H. Zhang, and A. Rinna, *Glutathione: overview of its protective roles, measurement, and biosynthesis.* Mol Aspects Med, 2009. **30**(1-2): p. 1-12.

103. Meister, A., *Glutathione metabolism and its selective modification.* J Biol Chem, 1988. **263**(33): p. 17205-8.

104. Brigelius-Flohe, R., *Tissue-specific functions of individual glutathione peroxidases.* Free Radic Biol Med, 1999. **27**(9-10): p. 951-65.

105. Boyland, E. and L.F. Chasseaud, *The role of glutathione and glutathione S-transferases in mercapturic acid biosynthesis.* Adv Enzymol Relat Areas Mol Biol, 1969. **32**: p. 173-219.

106. Holmgren, A., *Thioredoxin.* Annual review of biochemistry, 1985. **54**: p. 237-271.

107. Laurent, T.C., E.C. Moore, and P. Reichard, *Enzymatic Synthesis of Deoxyribonucleotides. Iv. Isolation and Characterization of Thioredoxin, the Hydrogen Donor from Escherichia Coli B.* J Biol Chem, 1964. **239**: p. 3436-44.

108. Thelander, L. and P. Reichard, *Reduction of ribonucleotides.* Annu Rev Biochem, 1979. **48**: p. 133-58.

109. Chae, H.Z., S.W. Kang, and S.G. Rhee, *Isoforms of mammalian peroxiredoxin that reduce peroxides in presence of thioredoxin.* Methods Enzymol, 1999. **300**: p. 219-26.

110. Brot, N., et al., *Reduction of N-acetyl methionine sulfoxide: a simple assay for peptide methionine sulfoxide reductase.* Anal Biochem, 1982. **122**(2): p. 291-4.

111. Schenk, H., et al., *Distinct effects of thioredoxin and antioxidants on the activation of transcription factors NF-kappa B and AP-1.* Proc Natl Acad Sci U S A, 1994. **91**(5): p. 1672-6.

112. Saitoh, M., et al., *Mammalian thioredoxin is a direct inhibitor of apoptosis signal-regulating kinase (ASK) 1.* EMBO J, 1998. **17**(9): p. 2596-606.

113. Bertini, R., et al., *Thioredoxin, a redox enzyme released in infection and inflammation, is a unique chemoattractant for neutrophils, monocytes, and T cells.* The Journal of experimental medicine, 1999. **189**(11): p. 1783-1789.

114. Prior, I.A., P.D. Lewis, and C. Mattos, *A Comprehensive Survey of Ras Mutations in Cancer.* Cancer Research, 2012. **72**(10): p. 2457-2467.

115. Lu, S., et al., *The Structural Basis of Oncogenic Mutations G12, G13 and Q61 in Small GTPase K-Ras4B.* Scientific Reports, 2016. **6**(1): p. 21949.

116. Downward, J., *Targeting RAS signalling pathways in cancer therapy.* Nature Reviews Cancer, 2003. **3**(1): p. 11-22.

117. Sparmann, A. and D. Bar-Sagi, *Ras-induced interleukin-8 expression plays a critical role in tumor growth and angiogenesis.* Cancer Cell, 2004. **6**(5): p. 447-458.

118. Liu, J., et al., *A Genetically Defined Model for Human Ovarian Cancer.* Cancer Research, 2004. **64**(5): p. 1655-1663.

119. Powell, D., et al., *Cxcr1 mediates recruitment of neutrophils and supports proliferation of tumor-initiating astrocytes in vivo.* Scientific Reports, 2018. **8**(1): p. 13285.

120. Szatrowski, T.P. and C.F. Nathan, *Production of large amounts of hydrogen peroxide by human tumor cells.* Cancer Res, 1991. **51**(3): p. 794-8.

121. Irani, K., et al., *Mitogenic Signaling Mediated by Oxidants in Ras-Transformed Fibroblasts.* Science, 1997. **275**(5306): p. 1649-1652.

122. Weinberg, F., et al., *Mitochondrial metabolism and ROS generation are essential for Kras-mediated tumorigenicity.* Proceedings of the National Academy of Sciences, 2010. **107**(19): p. 8788-8793.

123. Feng, Y., et al., *Live Imaging of Innate Immune Cell Sensing of Transformed Cells in Zebrafish Larvae: Parallels between Tumor Initiation and Wound Inflammation.* PLoS Biology, 2010. **8**(12).

124. Sundaresan, M., et al., *Requirement for generation of H2O2 for platelet-derived growth factor signal transduction.* Science, 1995. **270**(5234): p. 296-9.

125. Bae, Y.S., et al., *Epidermal growth factor (EGF)-induced generation of hydrogen peroxide. Role in EGF receptor-mediated tyrosine phosphorylation.* J Biol Chem, 1997. **272**(1): p. 217-21.

126. Yoo, S., et al., *Lyn is a redox sensor that mediates leukocyte wound attraction in vivo.* Nature, 2011. **480**(7375).

127. de Oliveira, S., et al., *Duox1-Derived H2O2 Modulates Cxcl8 Expression and Neutrophil Recruitment via JNK/c-JUN/AP-1 Signaling and Chromatin Modifications.* The Journal of Immunology, 2015. **194**(4): p. 1523-1533.

128. Mills, E.L., et al., *Succinate Dehydrogenase Supports Metabolic Repurposing of Mitochondria to Drive Inflammatory Macrophages.* Cell, 2016. **167**(2): p. 457-108118016.

129. Nakahira, K., et al., *Autophagy proteins regulate innate immune responses by inhibiting the release of mitochondrial DNA mediated by the NALP3 inflammasome.* Nature Immunology, 2011. **12**(3): p. 222-230.

130. Zhou, R., et al., *A role for mitochondria in NLRP3 inflammasome activation.* Nature, 2010. **469**(7329).

131. Bulua, A.C., et al., *Mitochondrial reactive oxygen species promote production of proinflammatory cytokines and are elevated in TNFR1-associated periodic syndrome (TRAPS).* J Exp Med, 2011. **208**(3): p. 519-33.

132. Freisinger, C.M. and A. Huttenlocher, *Live Imaging and Gene Expression Analysis in Zebrafish Identifies a Link between Neutrophils and Epithelial to Mesenchymal Transition.* PLoS ONE, 2014. **9**(11).

133. Patel, S., et al., *Unique pattern of neutrophil migration and function during tumor progression.* Nature …, 2018.

134. Heiman, M., et al., *Cell type–specific mRNA purification by translating ribosome affinity purification (TRAP).* Nature Protocols, 2014. **9**(6): p. 1282-1291.

135. Kanther, M., et al., *Microbial Colonization Induces Dynamic Temporal and Spatial Patterns of NF-κB Activation in the Zebrafish Digestive Tract.* Gastroenterology, 2011. **141**(1): p. 197-207.

136. Rosowski, E.E., et al., *Macrophages inhibit Aspergillus fumigatus germination and neutrophil-mediated fungal killing.* Macrophages inhibit Aspergillus fumigatus germination and neutrophil-mediated fungal killing, 2018.

137. Huang, S., A.A. Heikal, and W.W. Webb, *Two-Photon Fluorescence Spectroscopy and Microscopy of NAD(P)H and Flavoprotein.* Biophysical Journal, 2002. **82**(5): p. 2811-2825.

138. Balkwill, F.R., M. Capasso, and T. Hagemann, *The tumor microenvironment at a glance.* Journal of Cell Science, 2012. **125**(23): p. 5591-5596.

139. Young, T.W., et al., *Activation of antioxidant pathways in ras-mediated oncogenic transformation of human surface ovarian epithelial cells revealed by functional proteomics and mass spectrometry.* Cancer Res, 2004. **64**(13): p. 4577-84.

140. Bostwick, D.G., et al., *Antioxidant enzyme expression and reactive oxygen species damage in prostatic intraepithelial neoplasia and cancer.* Cancer, 2000. **89**(1): p. 123-34.

141. Oberley, T.D. and L.W. Oberley, *Antioxidant enzyme levels in cancer.* Histol Histopathol, 1997. **12**(2): p. 525-35.

142. Heilman, J.M., T.J. Burke, and M.-C.J. and …, *Transactivation of gene expression by NF-κB is dependent on thioredoxin reductase activity.* Free Radical Biology and …, 2011.

143. Matthews, J.R., et al., *Thiordoxin regulates the DNA binding activity of NF-χB by reduction of a disulphid bond involving cysteine 62.* Nucleic Acids Research, 1992. **20**(15): p. 3821-3830.

144. Schenk, H., M. Vogt, and D.-W. of …, *Thioredoxin as a potent costimulus of cytokine expression.* The Journal of …, 1996.

145. Hattori, H., et al., *Small-molecule screen identifies reactive oxygen species as key regulators of neutrophil chemotaxis.* Proceedings of the National Academy of Sciences, 2010. **107**(8): p. 3546-3551.

146. Nakamura, H., et al., *Circulating thioredoxin suppresses lipopolysaccharide-induced neutrophil chemotaxis.* Proc Natl Acad Sci U S A, 2001. **98**(26): p. 15143-8.

147. Qasaimeh, M.A., et al., *Neutrophil Chemotaxis in Moving Gradients.* Advanced Biosystems, 2018. **2**(7).

148. Lokuta, M.A. and A. Huttenlocher, *TNF-α promotes a stop signal that inhibits neutrophil polarization and migration via a p38 MAPK pathway.* Journal of Leukocyte Biology, 2005. **78**(1): p. 210-219.

149. Hu, Y., et al., *K-rasG12V transformation leads to mitochondrial dysfunction and a metabolic switch from oxidative phosphorylation to glycolysis.* K-rasG12V transformation leads to mitochondrial dysfunction and a metabolic switch from oxidative phosphorylation to glycolysis, 2012.

150. Baker, A., et al., *Thioredoxin, a gene found overexpressed in human cancer, inhibits apoptosis in vitro and in vivo.* Cancer Res, 1997. **57**(22): p. 5162-7.

151. Gallegos, A., et al., *Transfection with human thioredoxin increases cell proliferation and a dominant-negative mutant thioredoxin reverses the transformed phenotype of human breast cancer cells.* Cancer research, 1996. **56**(24): p. 5765-5770.

152. Lu, T., et al., *Thioredoxin 1 is associated with the proliferation and apoptosis of rheumatoid arthritis fibroblast-like synoviocytes.* Clin Rheumatol, 2018. **37**(1): p. 117-125.

153. Hirota, K., et al., *AP-1 transcriptional activity is regulated by a direct association between thioredoxin and Ref-1.* Proceedings of the National Academy of Sciences, 1997. **94**(8): p. 3633-3638.

154. Abate, C., et al., *Redox regulation of fos and jun DNA-binding activity in vitro.* Science (New York, N.Y.), 1990. **249**(4973): p. 1157-1161.

155. Moreno-Mateos, M.A., et al., *CRISPRscan: designing highly efficient sgRNAs for CRISPR-Cas9 targeting in vivo.* Nature Methods, 2015. **12**(10): p. 982-988.

156. Lam, P.Y., E.A. Harvie, and A. Huttenlocher, *Heat shock modulates neutrophil motility in zebrafish.* PLoS One, 2013. **8**(12): p. e84436.

157. Houseright, R.A., et al., *Cell type specific gene expression profiling reveals a role for complement component C3 in neutrophil responses to tissue damage.* Sci Rep, 2020. **10**(1): p. 15716.

158. Subramanian, A., et al., *Gene set enrichment analysis: a knowledge-based approach for interpreting genome-wide expression profiles.* Proceedings of the National Academy of Sciences of the United States of America, 2005. **102**(43): p. 15545-15550.

159. Miskolci, V., et al., *In vivo fluorescence lifetime imaging captures metabolic changes in macrophages during wound responses in zebrafish.* bioRxiv, 2020.

160. Ceccarelli, J., et al., *The redox state of the lung cancer microenvironment depends on the levels of thioredoxin expressed by tumor cells and affects tumor progression and response to prooxidants.* International Journal of Cancer, 2008. **123**(8): p. 1770-1778.

161. Rubartelli, A., et al., *Secretion of thioredoxin by normal and neoplastic cells through a leaderless secretory pathway.* Secretion of thioredoxin by normal and neoplastic cells through a leaderless secretory pathway., 1992.

162. Foyouzi, N., et al., *Effects of oxidants and antioxidants on proliferation of endometrial stromal cells.* Fertility and Sterility, 2004. **82**: p. 1019-1022.

163. Taddei, M., et al., *Mitochondrial Oxidative Stress due to Complex I Dysfunction Promotes Fibroblast Activation and Melanoma Cell Invasiveness.* Journal of Signal Transduction, 2012. **2012**: p. 684592.

164. Jezierska-Drutel, A., S.A. Rosenzweig, and C.A. Neumann, *Chapter Three Role of Oxidative Stress and the Microenvironment in Breast Cancer Development and Progression.* Advances in Cancer Research, 2013. **119**: p. 107-125.

165. Heilmann, S., et al., *A Quantitative System for Studying Metastasis Using Transparent Zebrafish.* Cancer Res, 2015. **75**(20): p. 4272-4282.

166. Roh-Johnson, M., et al., *Macrophage-Dependent Cytoplasmic Transfer during Melanoma Invasion In Vivo.* Dev Cell, 2017. **43**(5): p. 549-562 e6.

167. Shang, W., et al., *Increased Thioredoxin-1 Expression Promotes Cancer Progression and Predicts Poor Prognosis in Patients with Gastric Cancer.* Oxidative medicine and cellular longevity, 2019. **2019**: p. 9291683.

168. Chaiswing, L., et al., *Characterization of redox state of two human prostate carcinoma cell lines with different degrees of aggressiveness.* Free Radical Biology and Medicine, 2007. **43**(2): p. 202-215.

169. Evason, K.J., et al., *Identification of chemical inhibitors of β-catenin-driven liver tumorigenesis in zebrafish.* Identification of chemical inhibitors of β-catenin-driven liver tumorigenesis in zebrafish, 2015.

170. de Oliveira, S., et al., *Metformin modulates innate immune-mediated inflammation and early progression of NAFLD-associated hepatocellular carcinoma in zebrafish.* Journal of hepatology, 2019. **70**(4): p. 710-721.

171. Assi, M., *The differential role of reactive oxygen species in early and late stages of cancer.* American Journal of Physiology-Regulatory, Integrative and Comparative Physiology, 2017. **313**(6).

172. Aggarwal, V., et al., *Role of Reactive Oxygen Species in Cancer Progression: Molecular Mechanisms and Recent Advancements.* Biomolecules, 2019. **9**(11).

173. Knox, B.P., et al., *Distinct Innate Immune Phagocyte Responses to Aspergillus fumigatus Conidia and Hyphae in Zebrafish Larvae.* Eukaryotic Cell, 2014. **13**(10): p. 1266-1277.

174. Zhou, R., et al., *Thioredoxin-interacting protein links oxidative stress to inflammasome activation.* Nature immunology, 2010. **11**(2): p. 136-140.

175. Casbon, A.J., et al., *Invasive breast cancer reprograms early myeloid differentiation in the bone marrow to generate immunosuppressive neutrophils.* Proc Natl Acad Sci U S A, 2015. **112**(6): p. E566-75.

176. El-Benna, J., et al., *p47phox, the phagocyte NADPH oxidase/NOX2 organizer: structure, phosphorylation and implication in diseases.* Exp Mol Med, 2009. **41**(4): p. 217-25.

177. Oblong, J.E., M. Berggren, and G.P.Y. of Biological …, *Site-directed mutagenesis of active site cysteines in human thioredoxin produces competitive inhibitors of human thioredoxin reductase and elimination of mitogenic ….* Site-directed mutagenesis of active site cysteines in human thioredoxin produces competitive inhibitors of human thioredoxin reductase and elimination of mitogenic …, 1994.

178. Kumari, S., et al., *Reactive Oxygen Species: A Key Constituent in Cancer Survival.* Biomark Insights, 2018. **13**: p. 1177271918755391.

179. Langenau, D.M., et al., *In vivo tracking of T cell development, ablation, and engraftment in transgenic zebrafish.* Proc Natl Acad Sci U S A, 2004. **101**(19): p. 7369-74.